ON CYCLIC AND DYNAMIC PILE-BEARING BEHAVIOUR

Vom Promotionsausschuss der
Technischen Universität Hamburg

zur Erlangung des akademischen Grades

Doktor-Ingenieurin (Dr.-Ing.)

genehmigte Dissertation (Monografie)

von
Anne Hagemann

aus
Hamburg

2024

1. Gutachter: Univ.-Prof. Dr.-Ing. Jürgen Grabe
2. Gutachter: Prof. Dr.-Ing. habil. Ivo Herle
3. Gutachter: Prof. Dr.-Ing. Robert Seifried

Tag der mündlichen Prüfung: 25.06.2024

On cyclic and dynamic pile-bearing behaviour

von

Anne Hagemann

Herausgegeben von

J. Grabe

Technische Universität Hamburg
Institut für Geotechnik und Baubetrieb

Veröffentlichungen des Instituts für
Geotechnik und Baubetrieb

61

Herausgeber:

Univ.-Prof. Dr.-Ing. Jürgen Grabe
Technische Universität Hamburg
Institut für Geotechnik und Baubetrieb
Harburger Schloßstraße 36
D – 21079 Hamburg
e-mail: *grabe@tu-harburg.de*

ISBN-13: 978-3-936310-63-4 (Erstausgabe)

Druckerei

Druckzentrum Neumünster GmbH
Rungestraße 4
24537 Neumünster

In derselben Reihe erschienen:

1. J. Grabe (Hrsg.), 2000: Verbrennungsrückstände. Tagungsband, ISBN 3-936310-00-9
2. J. Grabe (Hrsg.), 2001: Schaden- und Risikomanagement im Tiefbau. Tagungsband, ISBN 3-936310-01-7
3. J. Grabe, 2003. Bodenmechanik und Grundbau. ISBN 3-936310-03-3
4. J. Grabe (Hrsg.), 2003: Euronormen in der Geotechnik – Was ändert sich? Tagungsband, ISBN 3-936310-04-1
5. J. Grabe (Hrsg.), 2003: Bodenverdichtung, Experimente - Modellierung - Geräteentwicklung - Baustellenberichte - F+E-Bedarf. Tagungsband, ISBN 3-936310-05-X
6. M. Kelm, 2004: Nummerische Simulation der Verdichtung rolliger Böden mittels Vibrationswalzen. Dissertation, ISBN 3-936310-06-8
7. J. Grabe (Hrsg.), 2004: Kaimauern - Messungen und Numerik. Tagungsband, ISBN 3-936310-07-6
8. J. Stein, 2005. Experimentelle und numerische Untersuchungen zum Düsenstrahlverfahren. Dissertation, ISBN 3-936310-09-2
9. J. Grabe (Hrsg.), 2005: Grenzschicht Wasser und Boden - Phänomene und Ansätze. Tagungsband, ISBN 3-936310-10-6
10. J. Grabe (Hrsg.), 2005: FEM in der Geotechnik - Qualität, Prüfung, Fallbeispiele. Tagungsband, ISBN 3-936310-11-4
11. B. Mardfeldt, 2006: Zum Tragverhalten von Kaikonstruktionen im Gebrauchszustand. Dissertation, ISBN 3-936310-12-2
12. J. Grabe (Hrsg.), 2006: Optimierung in der Geotechnik - Strategien und Fallbeispiele. Tagungsband, ISBN-13 978-3-936310-13-9
13. T. Bierer, 2007: Bodenschwingungen aus Straßenverkehr auf unebener Fahrbahn im Zeitbereich - experimentelle und theoretische Untersuchungen. Dissertation, ISBN-13 978-3-936310-14-6
14. J. Grabe (Hrsg.), 2007: Bemessen mit Finite-Elemente-Methoden. Tagungsband, ISBN-13 978-3-936310-15-3
15. K.-P. Mahutka, 2008: Zur Verdichtung von rolligen Böden infolge dynamischer Pfahleinbringung und durch Oberflächenrüttler. Dissertation, ISBN-13 978-3-936310-16-0
16. J. Grabe (Hrsg.), 2008: Seehäfen für Containerschiffe zukünftiger Generationen. Tagungsband, ISBN-13 978-3-936310-17-7
17. F. König, 2008: Zur zeitlichen Traglastentwicklung von Pfählen und der nachträglichen Erweiterung bestehender Pfahlgründungen. Dissertation, ISBN-13 978-3-936310-18-4
18. S. Henke, 2008: Herstellungseinflüsse aus Pfahlrammung im Kaimauerbau. Dissertation, ISBN-13 978-3-936310-19-1

19. J. Grabe (Hrsg.), 2009: Spundwände – Profile, Tragverhalten, Bemessung, Einbringung und Wiedergewinnung. Tagungsband, ISBN-13 978-3-936310-20-7
20. J. Dührkop, 2009: Zum Einfluss von Aufweitungen und zyklischen Lasten auf das Verformungsverhalten lateral beanspruchter Pfähle in Sand. Dissertation, ISBN-13 978-3-936310-21-4
21. O. Möller, 2009: Zum Langzeit-Kompressionsverhalten weicher organischer Sedimente. Dissertation, ISBN-13 978-3-936310-22-1
22. J. Grabe (Hrsg.), 2011: Ports of container ships of future generations. Tagungsband, ISBN-13 978-3-936310-23-8
23. S. Kinzler, 2011: Zur Parameteridentifikation, Entwurfs- und Strukturoptimierung in der Geotechnik mittels numerischer Verfahren. Dissertation, ISBN-13 978-3-936310-24-5
24. G. Qiu, 2012: Coupled Eulerian Lagrangian Simulations of Selected Soil-Structure Problems. Dissertation, ISBN-13 978-3-936310-25-2
25. X. Ma, 2013: Nutzung der oberflächennahen Geothermie mittels Energiepfählen und Erdwärmesonden. Dissertation, ISBN-13 978-3-936310-26-9
26. J. Grabe (Hrsg.), 2013: Proceedings of the Conference on Maritime Energy COME 2013. Tagungsband, ISBN-13 978-3-936310-28-3
27. J. Grabe (Hrsg.), 2013: Bemessen mit numerischen Methoden. Tagungsband, ISBN-13 978-3-936310-29-0
28. T. Pucker, 2013: Stoffmodell zur Modellierung von stetigen Materialübergängen im Rahmen der Optimierung geotechnischer Strukturen. Dissertation, ISBN-13 978-3-936310-30-6
29. S. Henke, 2013: Untersuchungen zur Pfropfenbildung infolge der Installation offener Profile in granularen Böden. Habilitation, ISBN-13 978-3-936310-31-3
30. J. Grabe (Hrsg.), 2014: Ports for Container Ships of Future Generations. Tagungsband, ISBN-13: 978-3-936310-32-0
31. J. Grabe (Hrsg.), 2014: Offshore Basishäfen. Tagungsband, ISBN-13: 978-3-936310-33-7
32. C. Rudolph, 2015. Untersuchungen zur Drift von Pfählen unter zyklischer, lateraler Last aus veränderlicher Richtung. Dissertation, ISBN-13: 978-3-936310-34-4
33. J. Grabe (Hrsg.), 2015: Morphodynamics 2015. Tagungsband, ISBN-13: 978-3-936310-35-1
34. T. Hamann, 2015: Zur Modellierung wassergesättigter Böden unter dynamischer Belastung und großen Bodenverformungen am Beispiel der Pfahleinbringung. Dissertation, ISBN-13: 978-3-936310-36-8
35. B. Schümann, 2015: Beitrag zum dynamischen Dreiphasenmodell für Boden auf Basis der Finite-Elemente-Methode. Dissertation, ISBN-13: 978-3-936310-37-5

36. M. Milatz, 2015: Untersuchungen zum Einfluss der Kapillarität auf das hydraulisch-mechanische Verhalten von granularer Tragschichten für Verkehrswege. Dissertation, ISBN-13: 978-3-936310-38-2
37. H. Kaya, 2016: Bodenverschleppung und Spaltbildung infolge der Einbringung von Profilen in Dichtungsschichten aus Ton. Dissertation, ISBN-13: 978-3-936310-39-9
38. J. Grabe (Hrsg.), 2017: Proceedings of the Conference on Maritime Energy COME 2017. Tagungsband, ISBN-13: 978-3-936310-40-5
39. B. Kocak, 2017: Zur numerischen Modellierung von hydraulisch-mechanisch gekoppelten Prozessen in gesättigten granularen Böden mittels Smoothed Particle Hydrodynamics. Dissertation, ISBN-13: 978-3-936310-41-2
40. K. Siegl, 2017: Zur Pfahldynamik von gerammten Großrohrpfählen und der daraus resultierenden Wellenausbreitung in Wasser und im Meeresboden. Dissertation, ISBN-13: 978-3-936310-42-9
41. J. Grabe (Hrsg.), 2017: Conference Proceedings of Workshop on Numerical Methods in Geotechnics 2017. Tagungsband, ISBN-13: 978-3-936310-43-6
42. J. Grabe (Hrsg.), 2018: Digitale Infrastruktur und Geotechnik (DIG 2018). Tagungsband, ISBN-13: 978-3-936310-44-3
43. D. Osthoff, 2018: Zur Ursache von Schlosssprengungen und zu einbringbedingten Lageabweichungen von Spundwänden. Dissertation, ISBN-13: 978-3-936310-45-0
44. E. Heins, 2018: Numerical based identification of the pile-soil interaction in terms of the axial pile bearing capacity. Dissertation, ISBN-13: 978-3-936310-46-7
45. K.-F. Seitz, 2021: Zur Topologieoptimierung von geotechnischen Strukturen und zur Tragfähigkeitssteigerung des Baugrunds durch Scherfugenverfestigung. Dissertation, ISBN-13: 978-3-936310-47-4
46. D. Plenker, 2021: Physical and numerical investigations of the dynamic interaction of saturated granulates and fluid. Dissertation, ISBN-13: 978-3-936310-48-1
47. J. Grabe, J. O. Backhaus, P. Vogel, 2021: Bauprojektmanagement. Skriptum, ISBN-13: 978-3-936310-49-8
48. M. Kanitz, 2021: Experimental and numerical investigations of particle-fluid systems in geotechnical engineering. Dissertation, ISBN-13: 978-3-936310-50-4
49. J. O. Backhaus, 2021: A methodology for the numeric time-cost forecast and paretro optimization of large injection projects in tunneling. Dissertation, ISBN-13: 978-3-936310-51-1
50. S. N. Sinduri, 2021: Optimisation of deep compaction as liquefaction mitigation measure. Dissertation, ISBN-13: 978-3-936310-52-8
51. J. Bubel, 2022: Zum Versagen von Unterwasserböschungen im Seegang. ISBN-13: 978-3-936310-53-5
52. J. Grabe (Hrsg.), 2022: Adaptive Structures At Shore 2022. ISBN-13: 978-3-936310-54-2

53. J. Grabe (Hrsg.), 2022: Numerische Methoden in der Geotechnik. ISBN-13: 978-3-936310-55-9
54. J. Grabe (Hrsg.), 2022: Processes in natural and technical Particle-Fluid Systems (PintPFS). DOI 10.15480/882.4640, ISBN-13: 978-3-936310-56-6
55. T. Törzs, 2022: Zum hydraulisch-mechanisch gekoppelten Verhalten teilgesättigter granularer Geomaterialien infolge hydraulischer und mechanischer Beanspruchungen. Dissertation, ISBN-13: 978-3-936310-57-3
56. M. Milatz, 2023: Investigation of capillary effects on the grain scale by means of in situ experiments, imaging and numerical simulations. Habilitation, ISBN-13: 978-3-936310-58-0
57. A. Chmelnizkij, 2023: Regularized MPM for porous media. Dissertation, ISBN-13: 978-3-936310-59-7
58. J. Grabe (Hrsg.), 2023: Herausforderungen in der Geotechnik - 25 Jahre Institut für Geotechnik und Baubetrieb, Technische Universität Hamburg. Tagungsband, ISBN-13: 978-3-936310-60-3
59. J. Beuße, 2023: Zur Einbringung und zum Tragverhalten von kombinierten Spundwänden von Ufereinfassungen. Dissertation, ISBN-13: 978-3-936310-61-0
60. D. Zobel, 2023: Zur Implementierung höherwertiger Stoffmodelle für Böden am Beispiel der Hypoplastizität. Dissertation, ISBN-13: 978-3-936310-62-7

Editor's preface

Der Ausbau der offshore Windenergie ist ein wesentliches Element, um aus fossilen Energieträgern auszusteigen und um zukünftig mit regenerativer Energie versorgt zu werden. Seit Beginn liegt ein besonderer Fokus auf der Gründung. Für die Dimensionierung der Monopiles ist das Tragverhalten unter zyklischen und dynamischen Einwirkungen aus Wind und Welle maßgebend. Es geht im Kern um die Frage, ob die Windenergieanlagen sich langfristig schief stellen, denn bereits bei einem Grad Schiefstellung ist mit einem erhöhten Verschleiß in der Turbine und einer reduzierten Leistung zu rechnen. Da die Einwirkungen aus Wind und Wellen in Richtung und Amplitude Schwankungen unterliegen, stellt sich insbesondere die Frage, welchen Einfluss die Lastrichtung und die Reihenfolge der Einwirkungen haben.

Es handelt sich um eine komplexe nicht lineare Struktur-Boden-Interaktion unter stochastischen Einwirkungen aus Wind und Wellen. Die Herausforderung für die Praxis besteht darin, anhand von einem besseren Verständnis der Zusammenhänge das System so zu vereinfachen, dass daraus abgesicherte Erkenntnisse zur Dimensionierung abgeleitet werden können. Die Thematik der Dissertation von Frau Hagemann hat daher für gegründete Offshore-Windenergieanlagen große Relevanz.

Die Arbeit ist zu wesentlichen Teilen im Rahmen des von der DFG geförderten Projektes GR 1024/37-1 und 37-2 „Holistic approach for the design of single piles and pile groups under cyclic loading“, welches in Kooperation mit der Ruhr Universität Bochum, Herrn Kollegen Wichtmann (WI 3810/5-1 und WI 3810/5-2) und der University Western Australia (UWA), Perth, Frau Kollegin Britta Bienen, bearbeitet wurde.

Zielsetzung der Arbeit von Frau Hagemann ist gemäß Kapitel 3 die Beantwortung folgender Fragen:

1. How can measurements with fibre optic strain gauges contribute to a comprehensive description of cyclic axial pile-bearing behaviour and pile-soil interaction and improve our understanding of pile response to axial cyclic loading?
2. Is Miner's rule valid for non-cohesive soils? How does the ordering of cycle packages influence cyclic deformation accumulation? Is it acceptable to simplify nonlinear wave-form load signals by means of classification methods?
3. Is it possible to describe the behaviour of pile and soil due to cyclic and dynamic loading using a p-y model? Which key aspects and mechanism are necessary and sufficient for this?

Frau Hagemann führt zur Beantwortung der Fragen

- Testreihen mit Modellpfählen unter zyklischer axialer Last unter ng-Bedingungen in der Groß-Zentrifuge der UWA in Perth,
- systematische Scherversuche in einem mehrdirektionalen Simple-Shear-Versuchsstand des Instituts und
- numerische Untersuchungen an einem selbst abgeleiteten und programmierten Ersatzschwingungssystem

durch. Die Wahl der Methoden wird vorbildlich im Abschnitt 3.1 begründet.

In Kapitel 1 führt sie zielstrebig in die Thematik ein. Der Stand der Technik und Wissenschaft ist in Kapitel 2 auf wenigen Seiten dargestellt. In Abschnitt 2.5 diskutiert sie beispielsweise die bisherigen Arbeiten zur Thematik und zeigt den Forschungsbedarf auf. Besonders gelungen ist der Zeitstrahl in Tabelle 2.1.

Das Tragverhalten von Pfählen unter zyklischen axialen Lasten wird in Kapitel 4 behandelt. Diese Untersuchungen erweitern das Wissen für den Einzelpfahl innerhalb einer Pfahlgruppe, beispielsweise von Jacket- und Tripilegründungen. Das laterale Verhalten eines Einzelpfahls unter zyklischer Last wurde u. a. bereits von Dührkop (2010), Rudolph (2015) und anderen untersucht. Zum axialen Verhalten unter zyklischer Last liegen dagegen weniger Untersuchungen vor. In Abschnitt 4.1 behandelt sie die zu beachtenden Modellgesetze in der Zentrifuge mit n-facher Beschleunigung. Die Versuche wurden von Frau Hagemann in der Zentrifuge der UWA in Perth durchgeführt. Neu ist die Nutzung von Glasfasern unter ng-Bedingungen. Das Testprogramm ist in Tabelle 4.2 aufgetragen. Die Ergebnisse werden im Abschnitt 4.7 zusammengefasst. Interessant ist, dass die zyklische Belastung das axiale Tragverhalten insbesondere der Mantelreibung positiv beeinflusst, solange die Zugbelastung kleiner ist als die über die Einbindelänge integrierte Mantelreibung. Aus den Versuchen folgert sie, dass Glasfasermessungen auch unter ng-Bedingungen geeignet sind, zusätzliche Kenntnisse zu gewinnen. Damit ist ihre erste Forschungsfrage beantwortet.

In Kapitel 5 beschreibt sie die von ihr durchgeführten zyklischen Scherversuche bei Variation der Scherrichtung (Polarisation). Die Abbildungen 5.2, 5.3 und 5.4 geben einen Überblick über ihre Testreihen. Sie untersucht, ob und unter welchen Bedingungen die akkumulierten Verformungen weitestgehend unabhängig von der Reihenfolge der Lastpakete ist. Gemäß Miner (1945) kann bei Stahl eine Unabhängigkeit von der Reihenfolge der Lastpakete angenommen werden. Bei Boden ist das offen. Abbildung 5.7 und 5.8 zeigen, dass die Abweichungen bei Sand nach 100 000 Zyklen bis zu 20 % groß sein können. Frau Hagemann untersucht zusätzlich die Verformungsakkumulation unter stochastischen Scherspannungen, was eher der Realität entspricht, siehe Abbildung 5.9 und folgende, und stellt eine Abweichung von 44 % fest. Des Weiteren untersucht sie in Abschnitt 5.6 den Einfluss der stufenweisen Richtungsänderung. Abbildung 5.14 und folgende zeigen ihre Ergebnisse. Das Kapitel endet mit der Beantwortung der zweiten Forschungsfrage. Wesentlich sind für die akkumulierten Verformungen demzufolge die Extremlasten. Besonders interessant ist ihre Feststellung, dass bei Änderung der Lastrichtung eine Umlagerung der Partikel eintritt.

Sie leitet in Kapitel 6 ein dynamisches p-y Modell mit nicht linearen Federkennlinien und Dämpfern ab, siehe Abbildung 6.2. Das zu lösende Differentialgleichungssystem ist in Gleichung 6.2 dargestellt. Die Bettung wird ratenabhängig definiert, siehe Gleichung 6.4, was sicherlich als außergewöhnlich anzusehen ist. Sie kann hierzu Vorarbeiten von Carstensen, Pucker, Grabe (2018) nutzen. Die Programmierung hat Frau Hagemann selbst durchgeführt. Besonders spannend ist m. E. der Abschnitt 6.1.4, in dem sie auf ihren Ansatz der Dämpfung eingeht. In Abschnitt 6.2 untersucht sie die Sensitivität ihres Models, siehe Abbildung 6.8 und folgende, und vergleicht die horizontale Auslenkung mit dem Ansatz nach API (2000).

In Kapitel 7 wendet sie ihr Modell zur Untersuchung der Verformungsakkumulation infolge zyklischer Einwirkungen an. Die Ergebnisse sind in den Abbildung 7.1 und folgende

dargestellt. Mir ist kein vergleichbares numerisches Modell der Pfahl-Boden-Interaktion bekannt. Der große Vorteil ist, dass das dynamische Verhalten des Pfahls bei hohen Zyklenzahlen berechenbar ist, was bei Finite Elemente Simulationen aufgrund der Rechenzeit und Genauigkeit nicht gelingt. Das HCA-Modell nach Niemunis et al. (2005) und darauf aufbauende sind meines Wissens nach nicht für dynamische Berechnungen geeignet. In Abschnitt 7.3 behandelt sie das dynamische Verhalten unter stochastischen Welleneinwirkungen. Es zeigen sich Eigenmoden, siehe Abbildung 7.5, die bedingt durch die Dämpfung abklingen.

Die Arbeit schließt mit einem Fazit und einem Ausblick.

Die von Frau Hagemann vorgelegte Arbeit besticht durch ihre systematische Vorgehensweise und methodische Breite. Ihre Ergebnisse liefern einen wesentlichen Beitrag zum besseren Verständnis des dynamischen und akkumulierten Verhaltens von Monopiles unter in Amplitude und Richtung hochzyklisch variierenden Einwirkungen. Sie hat mit ihren Untersuchungen einen wesentlichen Beitrag zum Stand der Wissenschaft in der Marinen Geotechnik geleistet. Durch ihre Dissertationsschrift hat sie ihre Befähigung zur selbstständigen wissenschaftlichen Arbeit ausdrücklich nachgewiesen.

Ich bin mir sicher, dass Frau Hagemann ihren Weg zielstrebig weitergehen wird. Hierfür wünsche ich ihr alles Gute.

Hamburg, Juli 2024

Jürgen Grabe

Author's preface

This thesis summarises parts of my research done at the Institute of Geotechnical Engineering and Construction Management of Hamburg University of Technology, Hamburg, Germany (2018 - to date) and the Centre for Offshore Foundation Systems, University of Western Australia, Perth, Australia (March - April 2022). This research was funded by the German Research Council (DFG) within the project 'Holistic approach for the design of single piles and pile groups under cyclic loading' (GR 1024/37-1 and 37-2). This financial support is gratefully acknowledged.

First and foremost, I would like to thank my supervisor, Prof. Jürgen Grabe, for his continuous support and scientific advice over the last years. Further, I would like to show my gratitude to Prof. Ivo Herle, Prof. Robert Seifried, and Prof. Benedikt Kriegesmann for their interest in my work and for their participation in my doctoral committee.

Furthermore, I thank Prof. Torsten Wichtmann and Dr. Felipe Prada for the fruitful discussions and collaboration within our joint research project. Thank you for your continuous advice and for welcoming me to the Institute of Foundation Engineering and Soil Mechanics of Ruhr-University Bochum several times.

I want to acknowledge the invaluable help and guidance of Prof. Britta Bienen and Prof. Conleth O'Loughlin. I appreciate learning from your experience and your scientific advice. I would also like to thank the National Geotechnical Centrifuge Facility team for their support and expertise in planning and conducting the centrifuge experiments. I highly appreciate the teamwork and atmosphere in the lab. Thank you!

Next, I want to express my gratitude to all my present and past colleagues at the institute. I want to give special thanks to Dr. Hans Stanford for his valuable input and scientific discussions, to Göta Bürkner and Marek Banduch for supporting my experimental work over the past few years and to Angelika Prahl. I would like to express my gratitude to Dr. Manuela Kanitz, Dr. Marc Stapelfeldt, and Dr. Dominik Zobel for your valuable help, discussions, and critical proofreading of this thesis. I would also like to thank my friends and colleagues Pauline Kaminski and Dr. Jannik Beuße. I am very grateful to have you as a peer who critically reviews my research and as a friend. Thank you for your always open ear, weekend trips, and daily coffee breaks.

I thank all my students involved in this or my related research. Working with you is always a great pleasure. Amongst all others, I appreciate the contributions of Andrés Cortez and Sebastian Breidenstein.

Finally, I want to express my heartfelt gratitude to my partner, Alex, for his invaluable support, your love, and the joy you bring into my life every day.

My PhD would not have been possible without the unwavering support and love of my dear parents, Regina and Jens, my sister, Rieke, and my brother, Fynn. You taught me empathy and kindness. Thank you.

Hamburg, July 2024

Anne Hagemann
to my parents

Schlagwörter:

Zentrifugenversuche, numerische Modellierung, Pfahl-Boden-Interaktion, zyklische Belastung, Wellenbelastung, Dämpfung, Ermüdung

Keywords:

centrifuge experiments, numerical modelling, pile-soil interaction, cyclic loading, wave-type loading, damping, fatigue

Abstract

Global warming due to climate change is altering marine ecosystems and thus having a striking impact on the world's oceans. Technical solutions in offshore wind for future sustainable energy can contribute to alleviating this situation. To develop representative tools for cyclic loading analysis of offshore structures, it is essential to understand the cyclic and dynamic soil response, such as the bearing behaviour of pile foundations.

Therefore, the general objective of this thesis is to analyse the pile-bearing behaviour due to cyclic and dynamic loading in sand and to derive further a p-y model which combines the analysis of cyclic deformation accumulation and dynamic analysis of offshore monopiles in a reliable and simple model.

First, this thesis investigates the pile response to cyclic axial loading in centrifuge experiments with the aim to gain a deeper understanding of the cyclic axial pile-bearing behaviour and pile-soil interaction (chapter 4). The successful application of fibre optic strain gauges in cyclic axial centrifuge experiments at 200 g on typical offshore piles into water-saturated sand is shown. The experiments indicate that partial two-way cyclic loading leads to greater ratcheting than one-way cyclic loading to the same maximum load. Following cyclic loading, the pile capacity increases in compression and is maintained or increased in tension, enhancing the confidence in the post-cyclic bearing capacity of axial loaded piles.

Second, relevant aspects of cyclic soil behaviour in the near field of the pile are investigated in direct simple shear tests (chapter 5). This includes a study on the validity of Miner's rule investigating the effect of the ordering of cycle packages on the total cyclic strain accumulation such as irregular cyclic load tests. An evident effect of the ordering of cycle packages on the accumulated volumetric strain is found from the experimental data. In addition, both the high cyclic multi-amplitude tests and the irregular cyclic load tests highlight the impact of the loading history – specifically of the maximum load, applied to the soil – on the ratcheting response. Based on the experimental data, the application of classification methods in current offshore design practice is discussed (section 5.7).

Conclusively, a dynamic p-y model for lateral loading in sand, which combines relevant aspects of cyclic and dynamic pile-soil interaction, is developed (chapter 6 and 7). The model depicts key aspects of cyclic soil response and describes the interaction at the model interfaces, i.e. wave-pile, pile-soil.

Thus, this thesis presents new knowledge about the cyclic and dynamic pile-bearing behaviour and pile-soil interaction and provides a promising and efficient approach to combine the analysis of cyclic deformation accumulation and dynamic structural analysis of a monopile supporting offshore wind turbine.

Contents

1 Motivation

Nowadays, any mention of climate change turns on all the warning lights, with global warming affecting marine ecosystems and thus strikingly impacting the world's oceans. Further consequences are storms, bushfires and droughts, to the extent of which they were (partly) caused by climate change (IPCC, 2019). To alleviate the situation, reducing CO_2 emissions is crucial. Technical solutions can add to this. The offshore industry is constantly expanding and is seen as a primary sustainable energy source for the future. The high demand for renewable energy requires effective and accurate design methods for the foundation design of offshore wind parks. This thesis focuses on monopile foundations, which are currently the preferred type for coastal waters.

Thereby, one urgent task for engineers and researchers in geotechnical engineering is to provide simple and representative tools for cyclic loading analysis during the wind turbine lifetime and to ensure that appropriate design methods are applied in the design process (Jardine, 2020). First, this implies an accurate prediction of accumulated displacements due to wind, wave and currents, and second, it relates to a reliable estimate of foundation stiffness to allow for the derivation of natural frequencies of the offshore structure (Byrne, Houlsby et al., 2020). Sophisticated numerical models can contribute to this but require significant computation power and time. These factors are crucial in designing offshore wind parks. One way of making advanced numerical models useful for the designer is to apply p-y models. This involves creating spring and dashpot elements that reflect the soil behaviour. The simplicity of the p-y model greatly reduces computational complexity.

The current approach to foundation modelling in design practice is the p-y method, which utilises the API p-y curves recommended by API (2000). This approach has proven itself in practical applications for many years, but is widely known to have significant limitations. Literature indicates discrepancies between the response predicted by the API p-y curves and the actual monopile behaviour (Doherty and Gavin, 2012; Jardine, 2020) and questions their applicability to the soil-pile response of large diameter monopiles (Byrne et al., 2017; Kallehave, Byrne, et al., 2015; Page et al., 2018).

Various advanced numerical models are available that either concentrate on describing cyclic deformation accumulation, e.g. Niemunis et al. (2005), or focus on aspects of fatigue analysis of offshore wind turbines (OWTs) (Page et al., 2018). Certain models, for example, consider damping effects and assess natural frequencies. However, cyclic pile response and dynamic loading analysis are viewed as separate problems, and conventional models are constrained to monotonic loading. Consequently, the research objective should be to understand and model the cyclic and dynamic pile-bearing behaviour.

The general objective of this thesis is to analyse the soil-pile interaction during cyclic and dynamic loading and to derive further a p-y model which combines the analysis of cyclic

deformation accumulation and the dynamic analysis of the wind turbine support structure in one model. To specify this general objective, the theory and state-of-the-art research for cyclic and dynamic pile-bearing behaviour is evaluated in the next chapter.

Reviewing existing knowledge about the bearing behaviour of piles will reveal if the cyclic soil behaviour is understood in sufficient detail, if the pile response due to cyclic and dynamic loading can be modelled precisely and if the resulting system response is understood comprehensively. Based on the state-of-the-art review, a research aim and an approach for the scope of work will be formulated.

2 State of the art and research

This thesis focuses on understanding the cyclic and dynamic soil response and the bearing behaviour of pile foundations. Further, the general objective is to derive a simple p-y model that combines cyclic and dynamic analysis of piles, considering relevant mechanisms of soil-pile interaction. Hence, the following sections concentrate on cyclic and dynamic pile-bearing behaviour.

In this thesis, the term *dynamics* will be considered to describe the time-dependent behaviour of a soil or a structure. This encompasses time-dependent effects such as inertia, damping, wave radiation and time-dependent material behaviour. At low frequencies ($f \leq 1$ Hz), the load velocity does not significantly affect the mechanical properties of the soil, resulting in a purely *cyclic* response. In this particular case, inertia forces can be neglected.

Analogously, this thesis uses the terms cyclic and irregular cyclic loading to characterise the kind of impact. Specifically, irregular cyclic loading is presumed to involve fast load changes, which results in a dynamic structural response. Cyclic loads are characterised by slow, repetitive sinusoidal regular load sequences with constant amplitude and mean load.

The cyclic load characteristics will be explained in detail in section 2.1. Subsequently, section 2.2 summarises relevant aspects of cyclic soil response. Section 2.3 explains axial and lateral pile-bearing behaviour mechanisms, focusing on the global pile response during cyclic loading. In section 2.4, a timeline summarises relevant approaches for analysing pile-soil response to cyclic and dynamic loading. Section 2.5 concludes the review of existing research.

2.1 Cyclic load characteristics

Due to wind, waves and currents, offshore structures experience severe loads from varying directions. For this reason, the cyclic soil response is essential in the design of offshore structures. Cyclic loading can generate excess pore water pressures, cyclic strains, resulting displacements and finally, cause permanent strains in the soil. Although storms, wind and waves have irregular amplitude and frequency (refer to figure 2.1a), investigating the cyclic soil response primarily applies cyclic loading scenarios with constant mean load, stress amplitude and frequency, as shown in figure 2.1b (Randolph and Gourvenec, 2011).

Cyclic loads are characterised by their average or mean load H_{av}, amplitude H_{cyc} and frequency f. The cyclic amplitude is applied around the average load, resulting in a load sequence which oscillates periodically between the minimum H_{min} and the maximum H_{max} value of the applied load. Literature distinguishes four different modes of cyclic loading, depending on the magnitude of the average load in relation to the cyclic amplitude, compare

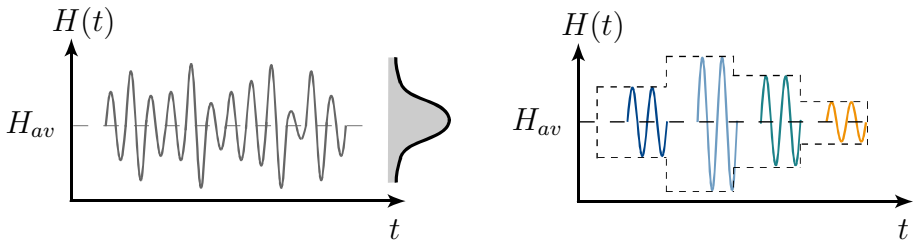

(a) Changes in amplitude and frequency.

(b) Constant mean load, stress amplitude and frequency.

Figure 2.1: Cyclic loading characterised by frequency and amplitude: (a) a typical offshore irregular load sequence and (b) cyclic loading scenario for laboratory investigations and the design of offshore structures.

Randolph and Gourvenec (2011). Figure 2.2 illustrates the modes of cyclic loading and clarifies the nomenclature of cyclic loading and total strain accumulation. One-way cyclic loading is defined as a load sequence without zero-crossing (figure 2.2a and d). Two-way cyclic loading denotes cycles with positive and negative values (figure 2.2b and c). A cyclic load can either be symmetric, in a particular case of two-way cyclic loading, including a zero mean load (figure 2.2 b) or unsymmetric with a mean load unequal to zero (figure 2.2a, c and d).

Within this thesis, the load characteristics are denoted according to LeBlanc, Byrne, et al. (2010) using the dimensionless ratios ζ_b and ζ_c which are defined as:

$$\zeta_b = \frac{H_{max}}{H_{ult}} \qquad \text{and} \tag{2.1}$$

$$\zeta_c = \frac{H_{min}}{H_{max}} \tag{2.2}$$

and involve H_{min} and H_{max}, i.e. the minimum and maximum force, and H_{ult} which is the ultimate capacity.

2.2 Cyclic soil response

The cyclic soil response is characterised by a gradual accumulation of plastic strains, also known as *ratcheting* behaviour. Figure 2.3c) shows the typical load-unload-reload response (ABCD) during cyclic loading. Very small loads result in a linear soil response. However, a nonlinear soil behaviour is observed when loads beyond the linear-elastic strain range are applied to the soil (path AB). The soil response due to cyclic loading depicts a hysteresis loop (BCD), which does not close in points B and D. During unloading, the soil stiffness increases, and a plastic displacement can be observed, which means that point C is separate from point A. Hence, permanent displacements accumulate with the number of cycles. Also, the shape of the hysteresis loop changes due to energy dissipation during a load cycle (Houlsby et al., 2017). Three different modes of long-term ratcheting behaviour describe the

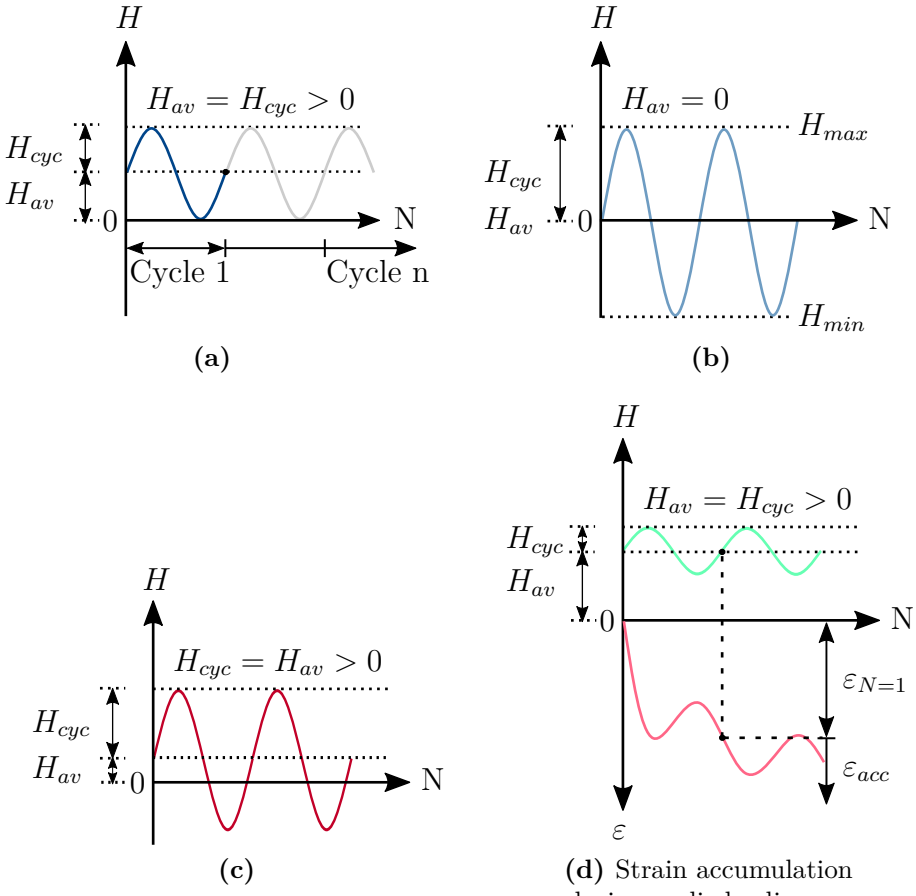

Figure 2.2: Cyclic loading and strain accumulation nomenclature: (a) one-way, $H_{av} = H_{cyc}$ (b) two-way (symmetric), $H_{av} = 0$ (c) two-way (unsymmetric), $H_{cyc} > H_{av}$ and (d) one-way, $H_{av} > H_{cyc}$ cyclic loading.

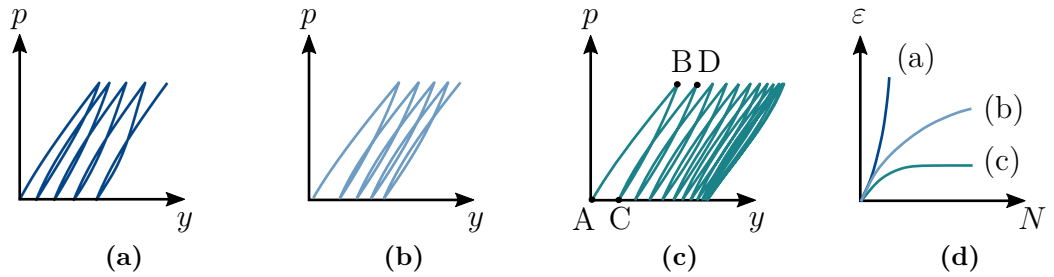

Figure 2.3: Cyclic soil response: (a) progressive failure, (b) gradual accumulation of plastic strains, (c) shakedown and (d) modes of long-term ratcheting behaviour under many load cycles.

accumulation of ratcheting displacement. Those are shown in figure 2.3d. First, a gradually increasing accumulation rate can be observed, resulting in a progressive failure, compare figure 2.3a. Second, cyclic loading gradually accumulates plastic strains, illustrated in figure 2.3b. Third, the rate of accumulation of ratcheting displacement decreases over the number of load cyclic (figure 2.3c) which is also known as *shakedown* (Goldscheider and Gudehus, 1976).

2.2.1 Key aspects of cyclic soil response

The cyclic ratcheting behaviour is influenced by specific parameters which can be identified based on existing research, e.g. Wichtmann (2005) and Wichtmann (2016). The most frequently investigated parameters are the initial confining stress and relative density, the cyclic amplitude and load characteristics, and the applied load frequency. The typical soil response is shown in figure 2.4a-d, indicating the influence of those key aspects from the results of cyclic direct simple shear tests for very fine silica sand. The main conclusions from this experimental data are summarized below.

Influence of initial stress

Various experimental studies (Silver and Seed, 1971; Youd, 1972; Sawicki and Swidzinski, 1989) concluded a minor influence of the vertical axial stress on the cyclic ratcheting behaviour in strain-controlled direct simple shear experiments for a limited number of load cycles. Later works report an increasing strain accumulation at higher confining pressures (Le, 2015; Wichtmann, 2016), which corresponds to the results displayed in figure 2.4a. Hence, higher confining pressures lead to higher compaction during cyclic loading with identical load amplitude and similar relative densities.

Influence of relative density

The initial relative density strongly influences the accumulated strain due to cyclic loading (Silver and Seed, 1971). Figure 2.4b indicates an accelerated ratcheting behaviour involving three different soil states at lower relative densities.

Influence of amplitude and cyclic load scenario

Figure 2.4c shows the influence of the magnitude of the cyclic load scenario on the accumulated volumetric strain. It can be observed that the strain accumulation increases as the cyclic amplitude increases. Several authors reported this behaviour earlier, respectively Silver and Seed (1971), Youd (1972), and Sawicki and Swidzinski (1989).

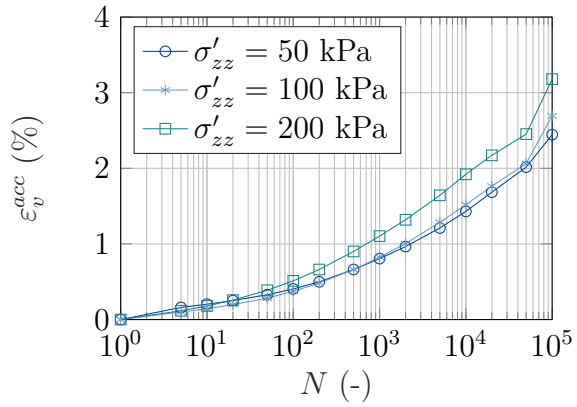

(a) Axial stress σ'_{zz}.

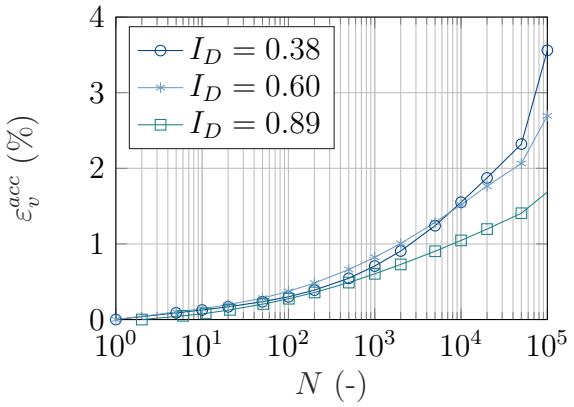

(b) Initial relative density I_D.

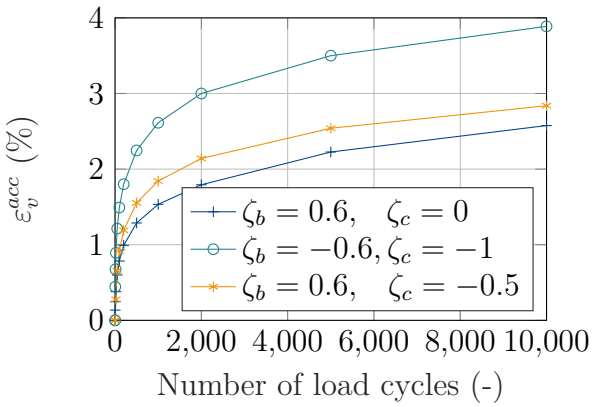

(c) Load scenario characterised by ζ_b and ζ_c.

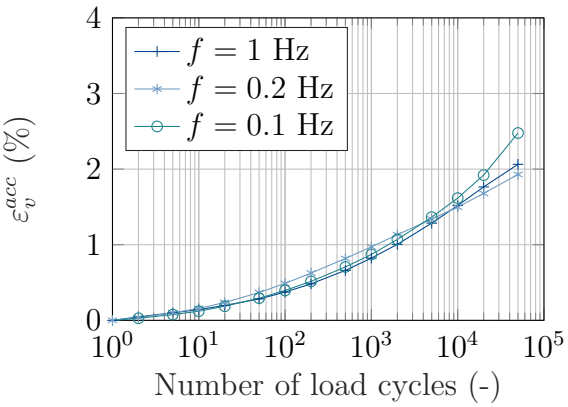

(d) Load frequency f.

Figure 2.4: Key aspects of cyclic soil response derived from results of cyclic direct simple shear tests for very fine silica sand with three different (a) axial stresses, (b) relative densities, (c) load scenarios and (d) load frequencies.

Frequency effects

Figure 2.4d depicts the results of cyclic direct simple shear tests with three different load frequencies $0.1 \leq f \leq 1$ Hz with identical initial stress and similar relative density. The results suggest that the magnitude of ratcheting may be considered independent of the cyclic frequency in low-frequency range. This is in good agreement with, e.g. Peacock and Seed (1968), Yoshimi and Oh-oka (1975), Tatsuoka, Maeda, et al. (1986), and Tatsuoka, Toki, et al. (1986).

2.2.2 Polarisation effects and multidirectional loading

Offshore structures are subjected to multi-component cyclic loads from varying directions. Much research has been dedicated to one-directional strain accumulation and tilting of offshore piles, while less attention was given to complex multidirectional cyclic loading. Dührkop and Grabe (2008) and Rudolph (2015) reported an increased ratcheting magnitude of piles resulting from a variable loading direction compared to one-dimensional loading. This observation was manifested from multidirectional direct simple shear tests by Wichtmann (2005), Rudolph, Grabe, et al. (2014), and Le (2015), after that

a) the strain accumulation is aligned to the direction of the average load,

b) a stepwise or continuous change in loading direction reinforces the displacement accumulation in granular materials.

2.2.3 Ordering effects and the applicability of Miner's rule

Offshore structures experience a high number of load cycles resulting from wind and wave conditions offshore. The design procedure facilitates these complex and time-dependent loading histories by means of classification methods. Thus, load sequences composed of idealised regular cycle packages with constant cyclic properties (i.e. frequency, amplitude and mean load) result, compare figure 2.1. This method adopts the concept of Miner's rule, a linear damage accumulation hypothesis according to Miner (1945). Miner's rule describes a linear relation between cycle packages/ load and structure fatigue/ partial damage of a structure. Hence, the ordering of cycle packages does not affect the total damage. Miner's rule was initially developed to describe the fatigue behaviour of metals due to cyclic loading but is a widely used concept to adopt the loading history for offshore geotechnical engineering design purpose on monopiles (LeBlanc, Byrne, et al., 2010; Abadie et al., 2015). However, the applicability of Miner's rule in soil mechanics is relevant to recent research (Liu et al., 2022; Tafili et al., 2023) and still needs to be fully confirmed for cohesionless and fine-grained materials. Wichtmann, Niemunis, et al. (2006) and Wichtmann, Niemunis, et al. (2010) applied the idea of Miner's rule to cohesionless soils and concluded its validity for variations of cycle packages with constant mean load based on a series of cyclic triaxial tests performed on Karlsruhe sand. This conclusion was confirmed later in Glasenapp (2016) and extended by further investigations on preloading effects and self-healing (Wichtmann, Niemunis, et al., 2010; Wichtmann and Triantafyllidis, 2017). Staubach and Wichtmann

(2020), Liu et al. (2022), and Tafili et al. (2023) assessed sequence effects numerically, investigating capabilities and limitations of the respective constitutive models. The majority of these contributions have in common that they solely involve cycle packages with constant mean load whereas Luo et al. (2020) investigate the effect of the ordering of cycle packages on the response of suction caissons subjected to multi-amplitude cyclic loading and a variation of the cyclic load magnitude. The results indicate a significant influence of the ordering of the cyclic loads on the accumulated rotation. Hence, sequence effects with varying mean loads deserve further research.

2.2.4 Constitutive models

To develop constitutive models for cyclic loading, it is necessary to account for the significantly different soil responses under repeated loading. Several constitutive models reproduce the mechanical behaviour of the soil during drained or undrained cyclic loading, which differs entirely from that during monotonic loading. By now, no all-embracing model exists that captures all key aspects of cyclic soil response in a simple formulation for practical purposes (Randolph and Gourvenec, 2011). Wichtmann et al. (2019) inspected three sophisticated constitutive models for their capability to estimate the cyclic behaviour of granular soils:

- the hypoplastic model with intergranular strain (Niemunis and Herle, 1997; Von Wolffersdorff, 1996),
- SANISAND, an elastoplastic implicit constitutive model which was initially proposed by Dafalias and Manzari (2004) and Dafalias et al. (2004) and later improved by adopting an additional memory surface to enhance the model for cyclic strain accumulation (Liu et al., 2019; Liu and Pisanó, 2019; Liu et al., 2020) and
- ISA (intergranular strain anisotropy) developed as an extension for hypoplastic models to account for small strain effects and improve modelling cyclic soil behaviour (Fuentes, 2014; Fuentes et al., 2020).

Following on from that Duque et al. (2021) identified certain limitations of these models, such as stress overshooting and one-way ratcheting in cyclic strain accumulation, to name just some of the investigated key aspects. Simultaneously, the authors highlighted the potential for future soil model development. The high-cycle accumulation (HCA) model originally published by Niemunis et al. (2005) adopts the aspect of cyclic strain accumulation. The model is an explicit accumulation model for high cyclic loading and one of the most sophisticated models for predicting long-term pile displacements (Zachert and Wichtmann, 2020; Staubach, Machaček, Bienen, et al., 2022).

2.3 Response of piles to cyclic axial and lateral loading

This thesis divides the loads acting on the pile head into vertical F and horizontal H components. Thereby, vertical loads imply purely cyclic loading. Horizontal loads can involve either cyclic or dynamic loading. The pile response nomenclature is shown in figure 2.5.

2.3.1 Pile response to axial loading

The axial pile resistance Q_t is decomposed of the base resistance Q_b, and the shaft resistance Q_s. Thus,

$$Q_t = Q_b + Q_s = q_b \cdot A_b + \tau_s \cdot A_s \quad , \tag{2.3}$$

wherein τ_s denotes the skin friction along the pile shaft area A_s and q_b is the bearing pressure at the area of the pile tip A_b. Both the shaft and base resistance are mobilised due to relative displacements between pile and soil. The shaft resistance is mobilised even at small pile displacements (around 0.5 to 2% of the pile diameter) due to shearing at the pile-soil interface. Full mobilisation of the base resistance requires larger pile displacements, typically 5 to 10% of the pile diameter (Fleming et al., 2008). Once the ultimate shaft capacity is reached, pile displacements increase, followed by a load transfer to the lower part of the pile (Randolph, 2003).

Cyclic axial loading can lead to an immense degradation of shaft resistance compared to monotonic loading and, thus, enhance this effect. During cyclic loading, the soil adjacent to the pile densifies, i.e. shows a contractile shearing response, which leads to a stress relief and a softer response of the pile-soil system. The shaft resistance degrades with the number of load cycles, especially for larger cycles. Under one-way cyclic loading, the degradation is caused by increasing settlements. In contrast, two-way cyclic loading rapidly reduces the soil stiffness, which increases the cyclic amplitude, followed by failure (Randolph and Gourvenec, 2011).

Considering offshore applications, axial loads on monopiles are small relative to the lateral load magnitude and, more importantly, to the bearing behaviour of jacket foundations.

2.3.2 Pile response to lateral loading

The mobilised soil resistance due to lateral loading of monopiles results from a horizontal pressure on the pile. Various components contribute to the total soil resistance. Those are the front resistance resulting from normal radial stresses, the friction resistance from normal and tangential shear stresses along the pile and the base moment resistance (Briaud et al., 1984). The radial stresses around the pile are uniformly distributed in an unloaded state. When the pile is loaded laterally, normal stresses increase in front of the pile, resulting in soil densification at the pile front. Behind the pile, normal stresses decrease to the magnitude of active earth pressure. At a particular loading stage, gap opening behind the

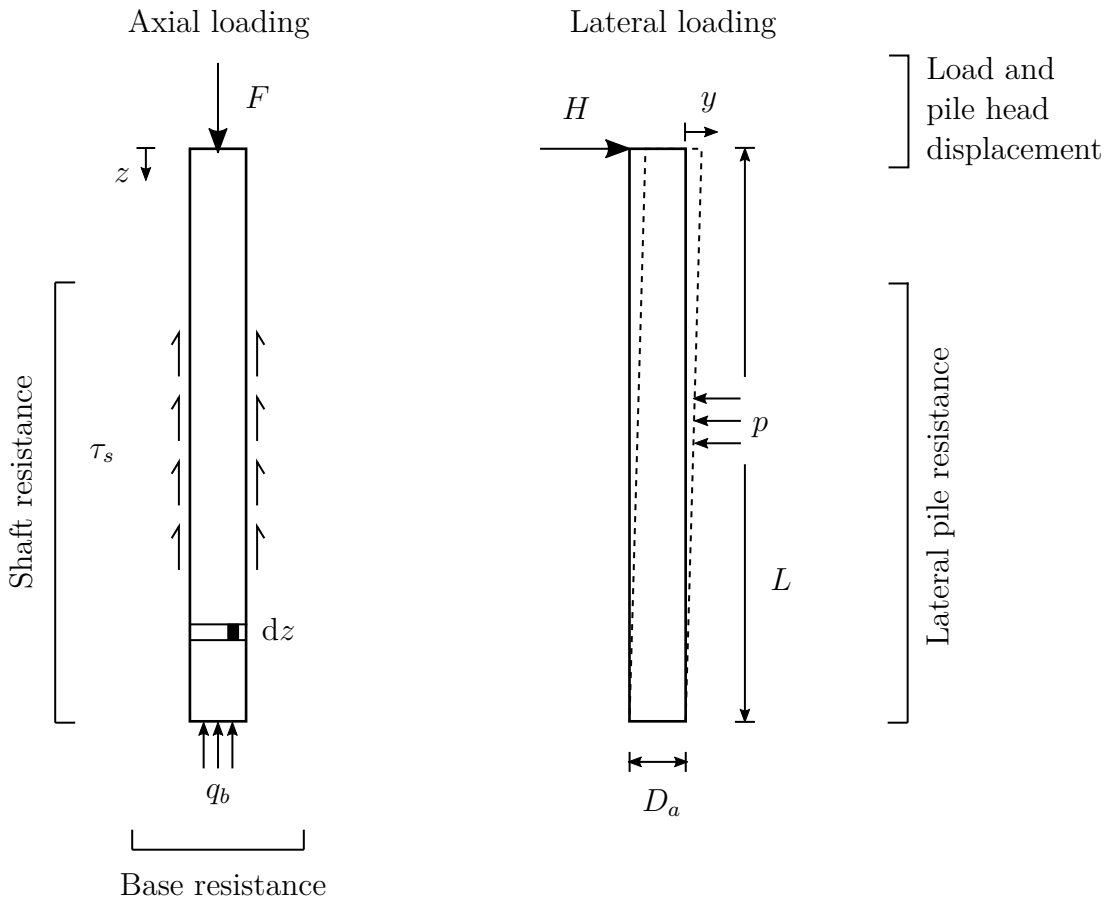

Figure 2.5: Pile response to axial and lateral loading: notation for loads, displacements and resistance according to Randolph and Gourvenec (2011).

pile might occur near the soil surface, which involves the failure of a wedge of soil at the pile front. This effect is also called *postholing*.

Failure modes for laterally loaded piles mainly depend on the flexibility and bending stiffness of the pile. Short piles or piles with significant flexure rigidity will rotate as a rigid body without being subjected to bending. Long flexible piles bend around a centre of rotation. Hence, passive earth pressures develop in front of the pile above the point of rotation and behind the pile below the point of rotation (Fleming et al., 2008).

The magnitude of mobilised soil resistance mainly depends on the stiffness of the adjacent soil. Cyclic loading can significantly reduce soil stiffness due to postholing, which results in a low resistance during the first load cycles (Randolph and Gourvenec, 2011). Long-term cyclic failure is induced by accumulating displacements and a decreasing soil stiffness (Jardine et al., 2012). Research on cyclic lateral loading on monopiles has successfully adopted physical model tests at 1g (LeBlanc, Byrne, et al., 2010; Nicolai and Ibsen, 2014; Arshad and O'Kelly, 2017) and ng level (Klinkvort and Hededal, 2010; Rudolph, 2015; Bayton et al., 2018; Truong et al., 2019). However, understanding the monopile response to long-term lateral loading still gets a lot of attention, refer to section 2.4.

2.4 Approaches to analysis of pile-soil response to cyclic and dynamic loading

This section briefly overviews current industry design practice and captures recent approaches to assess the pile-soil response to cyclic and dynamic loading. Table 2.1 summarises the most relevant contributions within this field in the last years, indicating the increasing research dedicated to offshore geotechnics and pile foundations. It includes design approaches, experimental works on cyclic soil/pile response, and constitutive and accumulation models for cyclic soil behaviour, such as cyclic and dynamic models for numerical assessment of pile response.

The foundation model used in current industry design practice applies the p-y method, i.e. the API p-y curves following API (2000). The p-y method, initially developed by Reese and Matlock (1956), is based on Winkler beam theory, modelling the monopile and the surrounding soil as a beam on elastic foundation (Winkler, 1867). Thereby, a set of uncoupled spring elements describes the soil response. The resulting load-deflection curves are commonly known as p-y curves. Following this, the original p-y approach for piles in cohesionless soils was suggested by Reese et al. (1974).

Although the API p-y curves have been successfully applied in the offshore industry for several years, the literature indicates discrepancies between the response predicted by the API p-y curves and the actual monopile behaviour (Doherty and Gavin, 2012; Jardine, 2020) and questions their applicability to the soil-pile response of large diameter monopiles (Kallehave, Byrne, et al., 2015; Byrne et al., 2017; Page et al., 2018). To overcome these deficiencies, several authors modified the original p-y curves, i.e. by improving the foundation stiffness formulation or extending the approach for large diameter piles (Sørensen et al., 2010; Kallehave, LeBlanc Thilsted, and Liingaard, 2012) and Sørensen (2012).

The recent PISA project addressed the deficiencies mentioned previously to gain a deeper understanding of the monopile response to monotonic lateral loading and to develop better methods to predict the pile response (Richards et al., 2020). The PISA project included field testing (Burd et al., 2020; Byrne, McAdam et al., 2020; McAdam et al., 2020; Zdravković, Jardine et al., 2020) and three-dimensional finite-element modelling (Zdravković, Taborda et al., 2020; Taborda et al., 2020). The implications of these investigations for design practice were discussed and applied to develop new design methods (Byrne et al., 2015; Byrne et al., 2017). As an outcome of the project, a one-dimensional computational model was developed to analyse and design laterally loaded monopile foundations in offshore wind turbine applications. The PISA model employs the p-y method but enhances the soil model by further soil reaction components. The current PISA model can be applied to homogenous soils and is now restricted to monotonic loading (Byrne, Houlsby et al., 2020).

While PISA combined field testing and numerical modelling, various approaches exist to assess the cyclic pile and soil behaviour experimentally or based on further advanced numerical models. In this context, besides field tests (Long and Reese, 1984; Little and Briaud, 1988; Long and Vanneste, 1994; Lin and Liao, 1999), small-scale model tests (Hettler, 1981; Achmus, Abdel-Rahman, et al., 2007), element tests (Wichtmann, 2005) and centrifuge experiments (Rudolph, Bienen, et al., 2014; Truong et al., 2019) provided valuable insights on an experimental basis. Additionally, various numerical models attempt to improve individual aspects of foundation modelling and, respectively, the design process. Some of those address high cyclic pile response and strain accumulation (Achmus, Kuo, et al., 2008; Dührkop, 2010; Taşan et al., 2011; Niemunis et al., 2005; Triantafyllidis and Chrisopoulos, 2016) while others concentrate on integrated analysis of offshore structures (Kementzetzidis, Corciulo, et al., 2019; Page et al., 2018), fatigue (Aasen et al., 2017; Katsikogiannis et al., 2019) and frequency effects (Kementzetzidis, Metrikine, et al., 2021).

2.5 Discussion on existing research

Global warming due to climate change is altering marine ecosystems and thus having a striking impact on the world's oceans. Technical solutions in offshore wind for future sustainable energy can contribute to alleviating this situation. In order to develop representative tools for cyclic loading analysis of offshore structures, it is essential to understand the cyclic soil response and the bearing behaviour of pile foundations.

To gain further insights into the underlying mechanisms of cyclic axial pile-bearing behaviour, it is necessary to study the deformation behaviour of piles at different cyclic loading scenarios, including cyclic axial loading in tension and compression and the pile response in layered soils.

While the key aspects of one-directional cyclic soil behaviour are well investigated, multi-directional cyclic loading and the effect of continuous polarisation changes are not fully understood. Existing research manifests an increased strain accumulation resulting from stepwise polarisation changes and continuous multidirectional cyclic loading compared to one-directional loading.

TABLE 2.1 Timeline: Approaches to analysis of pile-soil response to cyclic and dynamic loading.

Year	Advances in recent research on monopile response in offshore applications
1956	P-y method initially developed by Reese and Matlock (1956)
1974	P-y approach for piles in cohesionsless soils Reese et al. (1974)
1996	Hypoplastic constitutive model according to Von Wolffersdorff (1996)
1997	Hypoplastic model for cohesionless soils with elastic strain range Niemunis and Herle (1997)
2004	SANISAND sand plasticity model e.g. by Dafalias and Manzari (2004) and Dafalias et al. (2004)
2005	High Cycle Accumulation Model (HCA) (Niemunis et al., 2005)
2010	Modified p-y method (Dührkop, 2010)
2014	Intergranular strain anisotropy (ISA) (Fuentes, 2014)
2015	Cyclic soil/ pile response and strain accumulation due to cyclic loading from varying direction (Le, 2015; Rudolph, 2015)
2018	Macro-element pile foundation model for integrated analysis of monopile-based offshore wind turbines (Page et al., 2018)
2019	Memory enhancement for cyclic ratcheting accumulation, SANISAND-MS (Liu et al., 2019; Liu and Pisanó, 2019)
2020	ISA-Hypoplasticity accounting for cyclic mobility effects (Fuentes et al., 2020)
2020	Monopile application in renewable offshore wind energy (Jardine, 2020)
2020	PISA project (Burd et al., 2020; Byrne, Houlsby et al., 2020; Byrne, McAdam et al., 2020; McAdam et al., 2020; Richards et al., 2020; Taborda et al., 2020; Zdravković, Jardine et al., 2020; Zdravković, Taborda et al., 2020)
2020	Assessment of monopile installation effects (Staubach, Machaček, Moscoso, et al., 2020; Bienen et al., 2021; Fan et al., 2021)
2021	Standard for support structures of wind turbines (Standard DNV-ST-0126, 2021)

The design procedure for offshore monopiles decomposes irregular cyclic loading caused by wind and wave conditions into regular cyclic load packages with constant cyclic properties. This is done by means of counting methods, i.e. the ordering of load parcels by their magnitude, including an equivalent number of load cycles. This approach assumes the validity of Miner's rule, which postulates that the strain accumulation in the soil is independent of ordering effects. By now, the approach of Miner's rule is not fully confirmed in existing literature but is reported to lead to conservative predictions in the design. Nevertheless, sequence effects, especially when involving a varying mean stress state in the soil, deserve further attention.

In literature, various numerical models, methods and soil models exist - all aiming to predict monopile displacements or capture fatigue behaviour and dynamic loading effects. A reliable and simple model is necessary to combine both aspects of cyclic and dynamic pile-bearing behaviour. This model needs to depict the key aspects of cyclic soil response and describe the interaction at the model interfaces, i.e. wave-pile, pile-soil.

3 Aim of research and methodology

Today's high demand for renewable energy requires effective and accurate design methods for offshore wind parks. On the one hand, the design process demands an accurate prediction of accumulated displacements and, on the other hand, a reliable estimate of foundation stiffness.

In order to develop representative tools for cyclic loading analysis of offshore structures, it is essential to understand the cyclic bearing behaviour of pile foundations. In a literature review, the lateral pile response due to cyclic loading was found to be well-investigated experimentally. In contrast, reviewing existing knowledge about cyclic axially loaded piles was identified to be less complete (compare section 2.3).

Distributed fibre optic sensing is suitable for monitoring long linear structures, like pile foundations. The fibres can be laid in continuous lines along the structure and thus provide a logged strain profile over depth. In addition, the fibres marginally increase the surface of the pile and, therefore, are expected to have a minor influence on the pile-bearing behaviour and pile-soil interaction. The application of fibre optic sensing in civil engineering and especially in geotechnics is a recent technique that still requires further understanding and experience in different applications (Künzel, 2016; Möller et al., 2022). However, the incorporation of fibre optic strain gauges could improve our understanding of pile response to axial cyclic loading and is thus applied to record the profile along the pile.

Generally, offshore structures are exposed to variable and highly cyclic loads from continuously changing directions due to wind and wave conditions. In the design process, these complex dynamic loading scenarios are simplified by means of classification methods to purely cyclic load packages with constant frequency, mean load and amplitude. This procedure assumes the resulting accumulated strain in the soil to be independent of the ordering of these cycle packages, i.e. the validity of Miner's rule (compare section 2.2). Reviewing existing literature does not finally confirm the validity of Miner's rule for non-cohesive soils, which leads to the question of whether it is acceptable to apply this concept in the context of (offshore) geotechnical engineering.

In the design process, the API p-y curves, according to API (2000), have successfully been applied for several years. Regardless, literature questions their applicability to depict the soil-pile response of large diameter monopiles and indicates certain limitations (compare section 2.4). In recent research, the PISA project addressed these deficiencies experimentally and numerically (Byrne et al., 2017); contributing to a better understanding of high cyclic pile response. These works are complemented by research addressing the dynamic structural analysis of monopile-supporting OWTs (e.g. Page et al. (2018)). Conclusively, various models exist in the literature that either focus on accurately describing deformation accumulation or concentrate on aspects of dynamic analysis, i.e. fatigue, damping effects and evaluation of natural frequencies.

Therefore, this thesis aims to gain a deeper understanding of the pile-bearing behaviour during cyclic and dynamic loading. Specifically, this thesis seeks to improve the understanding of the pile response to axial cyclic loading in sand, to address the knowledge gap in terms of the validity of Miner's rule for non-cohesive soils and to derive further a p-y model, which combines the analysis of cyclic deformation accumulation and dynamic analysis of laterally loaded offshore monopiles. Based on this widely formulated aim, the following research questions for this thesis are formulated:

- How can measurements with fibre optic strain gauges contribute to a comprehensive description of cyclic axial pile-bearing behaviour and pile-soil interaction and improve our understanding of pile response to axial cyclic loading?
- Is Miner's rule valid for non-cohesive soils? How does the ordering of cycle packages influence cyclic deformation accumulation? Is it acceptable to simplify nonlinear waveform load signals by means of classification methods?
- Is it possible to describe the behaviour of pile and soil due to cyclic and dynamic loading using a p-y model? Which key aspects and mechanisms are necessary and sufficient for this?

These research questions will be answered throughout this thesis, focusing on open-ended piles installed into granular soil, even though the formulated research questions are relevant to other types of piles and soils, e.g. clay or chalk.

3.1 Methodology

Generally, four different research methods exist to achieve the formulated goals. These are:

- numerical modeling,
- physical model tests either as
  - 1g-laboratory or as
  - ng-centrifuge tests at model scale and
- field tests at prototype scale.

Field tests have the advantage of representing a realistic stress state during testing and, therefore, depict the real pile-soil interaction very well. However, this method involves a lot of time and high costs, while the tests are usually not reproducible due to inhomogeneous soil conditions. In physical model tests, scaling laws apply. In ng-model tests, a realistic stress state can be realised due to the increased acceleration in a centrifuge. In this way, a comparable stress level for in situ test conditions can be realised. In 1g-laboratory tests, the stress level is decreased compared to in-situ conditions. However, testing procedures and soil conditions are reproducible and require low time and costs. Therefore, this method is routinely applied in research and for soil characterisation in design practice. With numerical simulations, the effect of specific parameters on the actual pile-bearing behaviour can be investigated more effectively. These can be applied on different scales, assuming realistic

conditions regarding the stress state. The results depend on the chosen modelling technique, constitutive model and material parameter.

Within this thesis, 1g-laboratory tests, ng-centrifuge experiments and numerical simulations are conducted.

3.2 Structure of the thesis

This thesis is structured according to the formulated research questions. First, the pile response due to cyclic axial loading is investigated in centrifuge experiments with the aim of gaining a better understanding of axial pile bearing behaviour and pile-soil interaction. The centrifuge experiments are explained in detail in chapter 4. In the subsequent chapter 5, relevant aspects of cyclic soil behaviour in the nearfield of the pile are investigated in direct simple shear tests. This includes a study on the validity of Miner's rule that investigates the effect of ordering of cycle packages on the resulting cyclic deformation accumulation in tests with varying mean and cyclic load levels (section 5.4). The experimental program is supplemented by dynamic tests, including waveform streaming (section 5.5). Hence, the load sequences during testing vary constantly while the underlying energy spectrum stays constant. This method enables capturing natural conditions offshore during testing. It allows for comparing individual loading scenarios as the wave spectrum in the frequency domain defines the distribution of wave amplitudes. Section 5.7 contrasts the experimental findings from hydrodynamic loading scenarios with design load cases. Based on the experimental data, the application of classification methods in current offshore design practice is discussed.

Addressing the third research question, a p-y model for lateral loading in sand, which combines relevant aspects of cyclic and dynamic soil-pile interaction, is presented in chapter 6. The model follows the subgrade reaction approach using hypoplasticity to reproduce key characteristics of the surrounding soil and includes geometric and material damping. The concept and basic features of the model are described, and its limitations are discussed. The performance of the subgrade reaction model is demonstrated for selected load cases and verified against current standards. The main idea of the model is to create a simple but accurate model for cyclic and dynamic loading analysis. Consequently, the model can be applied to several offshore-related questions, i.e. determination of eigenfrequencies, model pile response due to cyclic and hydrodynamic loading, and calculating design storm scenarios. These applications of the model related to OWT design practice are described in chapter 7.

Conclusively, chapter 8 summarises the findings of the presented work, discusses future potentials in offshore wind turbine design practice and provides an outlook on future research in offshore geotechnical engineering.

Appendix A includes all applied symbols and notation.

4 Pile response to cyclic axial loading in centrifuge experiments

Centrifuge modelling is of major importance to investigating geotechnical engineering problems since it enables studying complex large-scale field situations at model scale. This chapter presents a series of centrifuge experiments conducted to investigate the load-displacement behaviour of piles in sand due to cyclic axial loading. The test series aims to comprehensively describe the cyclic axial pile-bearing behaviour and pile-soil interaction and to improve the understanding of pile response to axial cyclic loading. First, the test program comprises different cyclic loading scenarios and investigates pile displacements through measurements with fibre optic strain gauges at different cyclic load ratios. This includes the pile response due to cyclic axial loading in tension and compression. Second, the pile response in layered soils, i.e. loose over dense sand, is investigated in addition to a medium dense homogenous soil layer. Possible mechanisms involve friction fatigue and cyclic strain accumulation in terms of the mobilized shaft resistance and a stiffness degradation or beneficial compaction at the pile tip (ref. section 2.3).

4.1 Scaling laws

Physical modelling requires scaling of the prototype situation closely similar to the actual event and replicating the soil behaviour in terms of strength and stiffness. In a centrifuge experiment, the model is placed in a strongbox at the end of the centrifuge beam and accelerated to an inertial radial acceleration, which acts as an increased gravitational acceleration, that is n times higher than the earth's gravity. The surface of the soil sample in the strongbox is usually stress-free. The magnitude of vertical stress increases with depth depending on the soil density and the strength of the acceleration field. Hence, the vertical stress σ_v in a certain depth of the strongbox h_m corresponds to a prototype depth h_p, where

$$\sigma_v = \gamma_p h_p = \gamma_m n h_m \quad , \quad \gamma_p = \gamma_m \quad . \tag{4.1}$$

From this basic law of centrifugal modelling, the scaling factors for relevant parameters within the scope of testing are derived and summarised in Table 4.1.

With this, the results gained in a physical model test can be extrapolated to the prototype scale. The following limitations play a role in this experiment: on the one hand, the acceleration field in a centrifuge is not uniformly distributed over the depth of the soil sample, i.e. a slight variation occurs through the model. This is due to the varying radius at different depths in a soil sample. According to Taylor (2018) minor attention can be given

Table 4.1: Scaling laws of centrifuge modelling.

Quantity	Prototype	Physical model test
radial acceleration	g	ng
effective stress	σ'	σ'
strain	ε	ε
density	ρ	ρ
length	nL	L
area	n^2A	A
force	n^2F	F
frequency	f	nf
axial stiffness	n^2EA	EA

to this problem if the inertial acceleration is applied to a depth of $h_m/3$, wherein h_m is the height of the sample in the centrifuge model. On the other hand, potential errors can occur due to particle size effects. In centrifuge modelling, the particle size can hardly be scaled realistically. Extrapolating the model dimensions to the prototype scale requires similar scaling of the particle size, which means that a fine sand used in a modelling exercise would represent the size of a gravel in the prototype situation. As the stress-strain behaviour of a granular material is closely related to its mechanical properties, limited options exist to adjust the particle size of the granular material.

4.2 Outline of testing

The centrifuge experiments are conducted in a geotechnical centrifuge of the Centre for Offshore Foundation Systems (COFS) at the University of Western Australia. The fixed beam centrifuge of type Acutronic 661 is illustrated in figure 4, including descriptions of its main parts. A detailed description can be found in Randolph, Jewell, et al. (1991). The centrifuge has a platform radius of 1.8 m and can reach a maximum acceleration of 200g at

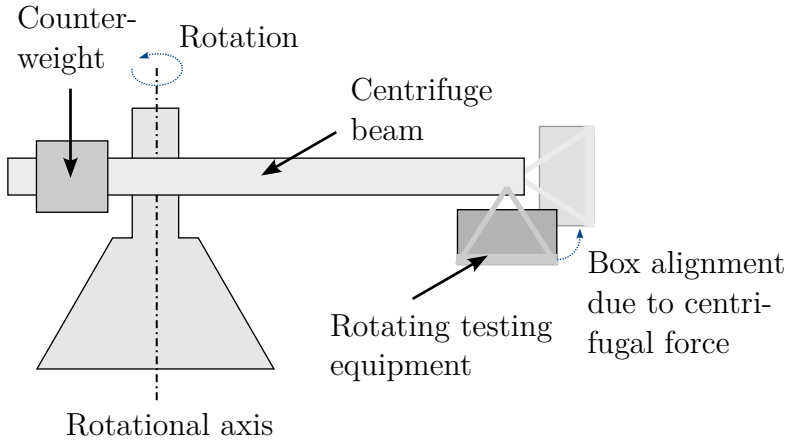

Figure 4.1: Illustration of a geotechnical centrifuge modified from Heins (2018).

a maximum load of 200 kg. The tests are performed in a strongbox with an inner width of 0.39 m, an inside length of 0.65 m and a height of 0.325 m. The height of the soil sample inside the strongbox is 0.230 m.

The centrifuge tests are carried out at a g-level of 200. Hence, a scaling factor of $n = 200$ applies for the tests. The exact scaling of the lengths ensures geometric similarity between the model test and the prototype scale. The centrifuge model dimensions represent a typical offshore pile for a jacket foundation considering natural conditions and are summarised in figure 4.2a.

To meet a realistic flexure rigidity and axial stiffness, i.e. a typical effective ratio of D_a/t_w for offshore piles, scaling leads to a wall thickness of $t_w = 0.3$ mm at model scale. Such a thin wall thickness requires precise manufacturing processes and was realised using 3D printing. The mechanical properties of the 3D printed tubular stainless steel pile are an ultimate tensile strength of $550-650$ MPa, a yield strength of $450-550$ MPa and a Young's modulus of 180 GPa. The 3D printing process leads to a normalised surface roughness of the material in the range of $0.28-0.33$, which is higher than the typical normalised surface roughness of an offshore pile (De Nicola and Randolph, 1997). The surface roughness directly impacts the pile's skin friction. However, among the centrifuge tests, comparability is guaranteed, and therefore, an increased surface roughness is accepted. Besides, exact scaling of wall thickness enables to depict the mobilized pile toe resistance and plugging behaviour realistically during testing.

4.3 Soil sample

The soil samples are created of fine silica sand. A detailed characterisation of the material can be found in Chow et al. (2019). Supplementary laboratory test results are shown in figure A.2 in appendix A.

The samples of fine silica sand are created by dry sand pluviation. The pluviation parameters are adjusted to achieve soil layers of three different relative densities, specified in figure 4.2c. At the end of sand pluviation the samples are vacuum levelled, and a measurement of the global density of the sample is made. A total sample height of 230 mm is targeted in order to minimise boundary effects (Tran and Randolph, 2008). The layered sample consists of a representative soil profile of typical North Sea sands. The dense sand bottom layer is targeted to a total sample height of 220 mm above the base of the strongbox. The height of the loose sand top layer is 10 mm, compare figure 4.2b. The sand samples are saturated with water, as drained conditions are expected during low-frequency cyclic axial loading. To ensure that the sample is fully saturated, the fluid height is kept a few centimeters above the soil during testing.

A series of cone penetration tests (CPTs) is conducted using a 6.3 and a 7 mm diameter miniature cone penetrometer in each centrifuge sample to characterise the properties of the sand and ensure homogenous testing conditions. Figure 4.3 shows the cone tip resistance profiles. All CPT results for the medium dense and the loose over dense samples are each within a relatively narrow range. The relative density of the soil can be derived

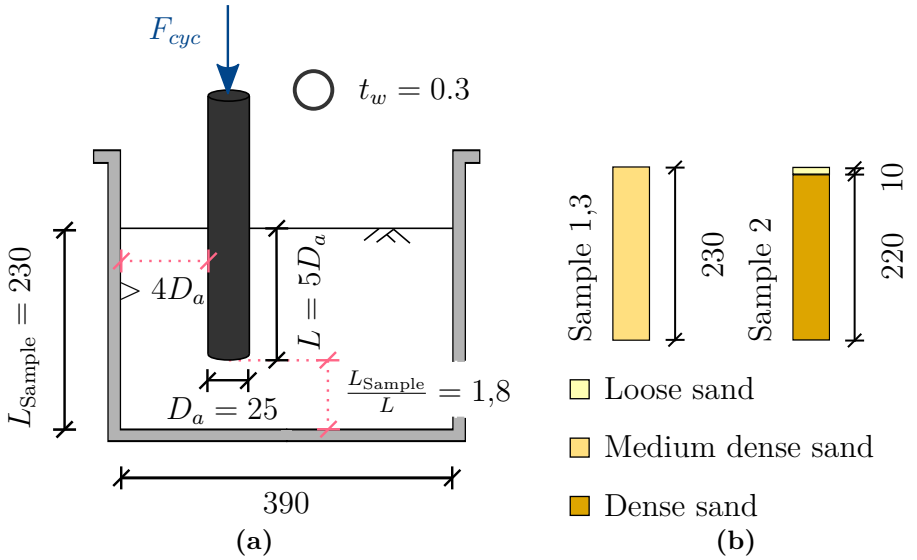

Silica sand	D_r (%)
Loose	33
Medium dense	55
Dense	87

(c)

Figure 4.2: Model dimensions and sample characteristics for physical model tests within the centrifuge facility in cyclic axial loading in sand: (a) pile dimensions and boundary distances chosen in accordance with Tran and Randolph (2008) (b) soil profiles (c) relative densities. (All values are given in mm unless stated otherwise.)

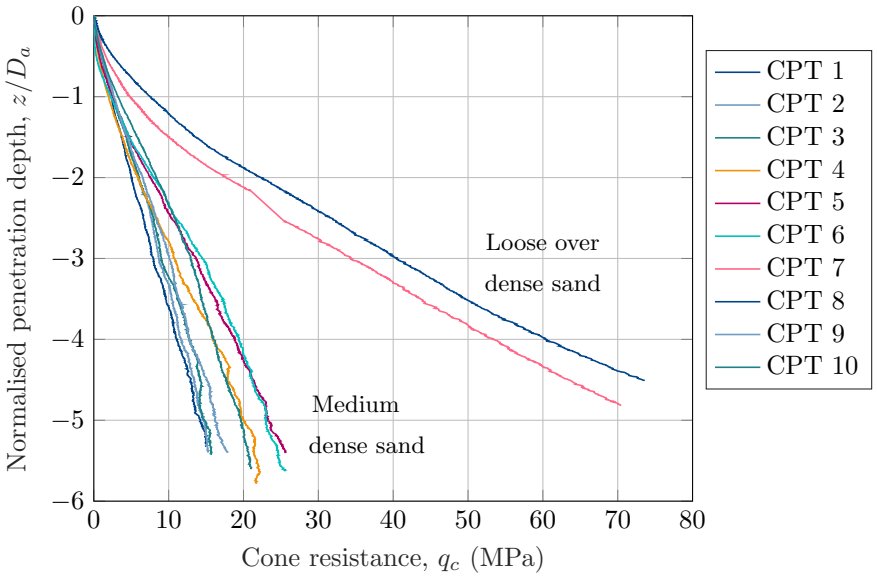

Figure 4.3: Cone penetration test results from sample no. 1 (CPT 1-6), sample no. 2 (CPT 7 & 8) and sample no. 3 (CPT 9 & 10): cone resistance q_c over normalised penetration depth z/D_a.

from the cone resistance using the correlation after Schneider and Lehane (2006) given in equation (4.2):

$$D_r = \sqrt{\frac{q_c}{250\sigma'_v}} \quad . \tag{4.2}$$

For the medium dense sample, the estimated relative density is $D_r = 48\% \pm 4$. The cone resistance in the dense soil layer indicates a relative density of $D_r = 93\% \pm 2.5$. The slight deviation between estimated and targeted relative densities is acceptable within the scope of testing. The results prove the soil samples' homogeneity and comparability, see figure 4.3.

4.4 Testing arrangement

The test setup used within the physical model tests is illustrated in figure 4.4a. A maximum of six tests are performed within each sample. The position of the test setup on the strongbox is adjusted in order to perform six tests with the same soil conditions. The pile is located at a minimum distance of $4D_a$ to the strongbox wall and previous test locations. Additionally, a sufficient sand layer thickness in the target position of the pile is ensured between the pile tip and the bottom of the strongbox in order to minimize boundary effects like wave reflections. This distance is chosen in accordance with Tran and Randolph, 2008.

Manipulation of the pile is achieved with a two-degree-of-freedom robotic actuator. A photograph of the experimental arrangement with the pile being attached to the actuator prior to pile installation can be seen in figure 4.4b. The actuator can be moved vertically and horizontally along the short axis of the strongbox.

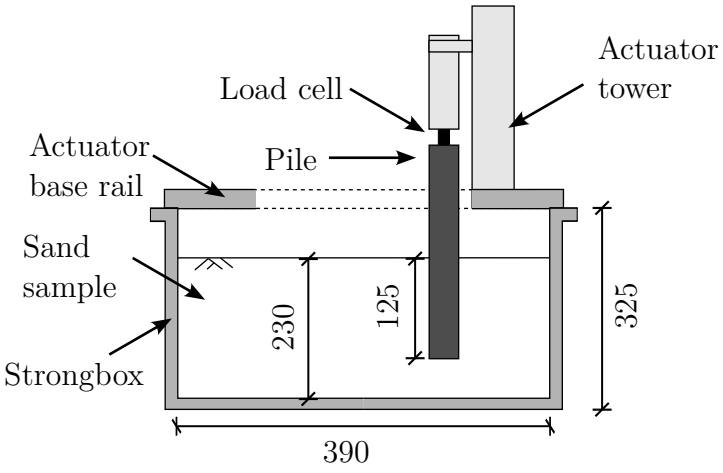

(a)

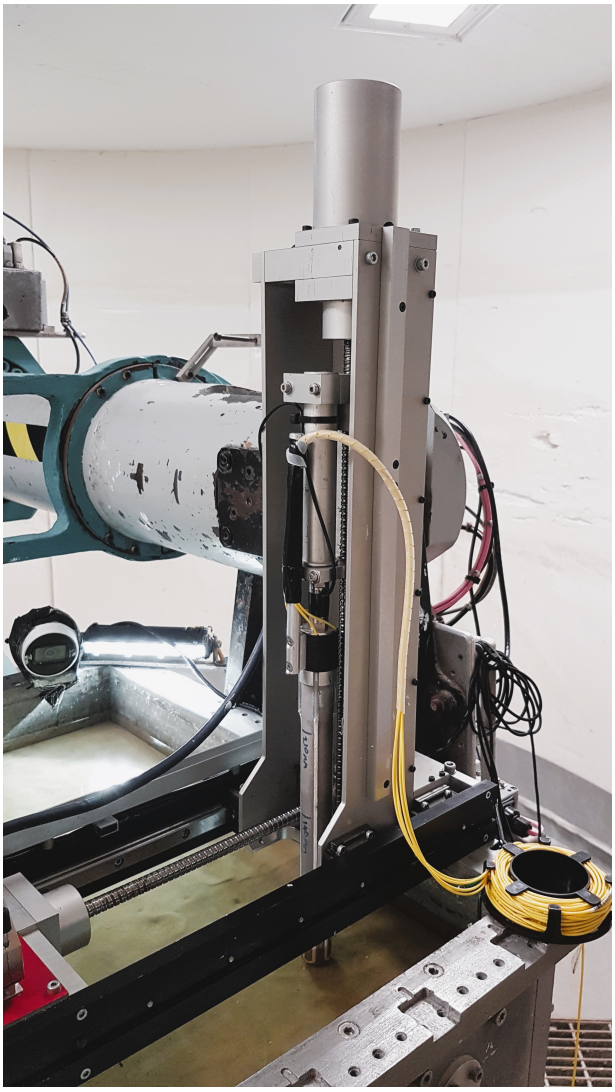

(b)

Figure 4.4: Setup for physical model tests within the centrifuge facility in cyclic axial loading in sand: (a) schematic setup and (b) photograph of the setup.

To capture the axial pile-bearing behavior and pile-soil interaction during testing, the pile is instrumented with a load cell and fibre optic strain gauges. The applied load, the pile head displacement and displacements along the pile are measured during testing. The load cell is attached to the pile head. The maximum achievable axial force limited by the load cell's capacity and by the actuator's integrity is around $F_{max} = 6$ kN. The pile's deformation is measured using fibre optic strain gauges. Here, fibre optics are beneficial compared to conventional strain gauges, as they marginally increase the wall thickness of the pile and maintain the pile tip area and external surface.

Four fibre optic strain gauges of type LBL-1550-125 are attached to the outer pile surface. This fibre has a cladding diameter of 125 μm and is optimized for operation in the 1550 nm wavelength window. The fibres are covered by a protective coating of X60, consisting of methylmetacrylate. The sensing distance starts 50 mm from the top of the pile and ends 7 mm from the bottom of the pile. An excess fibre is led around the pile tip in order to reduce back reflections in the output signal. Figure 4.5 illustrates the fibre optics pile instrumentation in detail. Thereby, figure 4.5a and b show 3D and 2D drawings of the fibre line, while the photograph in figure 4.5c shows the instrumented pile.

4.5 Test programme and procedure

The pile is installed at 1g with a constant velocity of the vertical actuator of 1 mm/s to a target embedded length of 125 mm. After pile installation, the soil sample is accelerated to 200g, acting at 1/3 of pile embedment. To ensure that no pore pressure build-up occurs during testing, an equalisation time between ramping up and application of the prescribed loading regime is provided. Subsequently, either a monotonic load test in axial compression or a cyclic load test is executed.

During a quasi-static monotonic test, the pile is pushed into the soil with the actuator at a constant velocity of $v_p = 0.1$ mm/s, which ensures drained conditions. The ultimate axial capacity is defined as the axial load at a vertical displacement of $0.1D_a$ at the pile head. A quasi-static monotonic test is terminated when the vertical pile displacement of $0.1D_a$ or the capacity of the actuator is reached.

The cyclic load tests are characterised by the dimensionless ratios ζ_b and ζ_c and were selected to maintain consistency with LeBlanc, Houlsby, et al. (2010). Hence, ζ_b takes values $0 < \zeta_b < 0.6$ and $\zeta_c \in [-1; 0]$. This includes one-way (load scenario a and b) and two-way symmetric (load scenario c) and unsymmetric (load scenario d) cyclic loading. A cyclic load test with either 1,000 or 10,000 load cycles is executed by applying a cyclic axial load with constant mean load and amplitude with the actuator to the pile head. This is done at a frequency of 0.2 Hz. Table 4.2 provides an overview of the performed centrifuge experiments and specifies sample and load characteristics.

Following the cyclic load test, the post-cyclic capacity and mobilized skin friction after cyclic loading are determined by a subsequent monotonic load test in compression and subsequently in tension following the same procedure as indicated before.

The tests are conducted within one box following each other. Hence, the test setup, illustrated in figure 4.4, is moved to both sides of and along the strongbox. A total of two

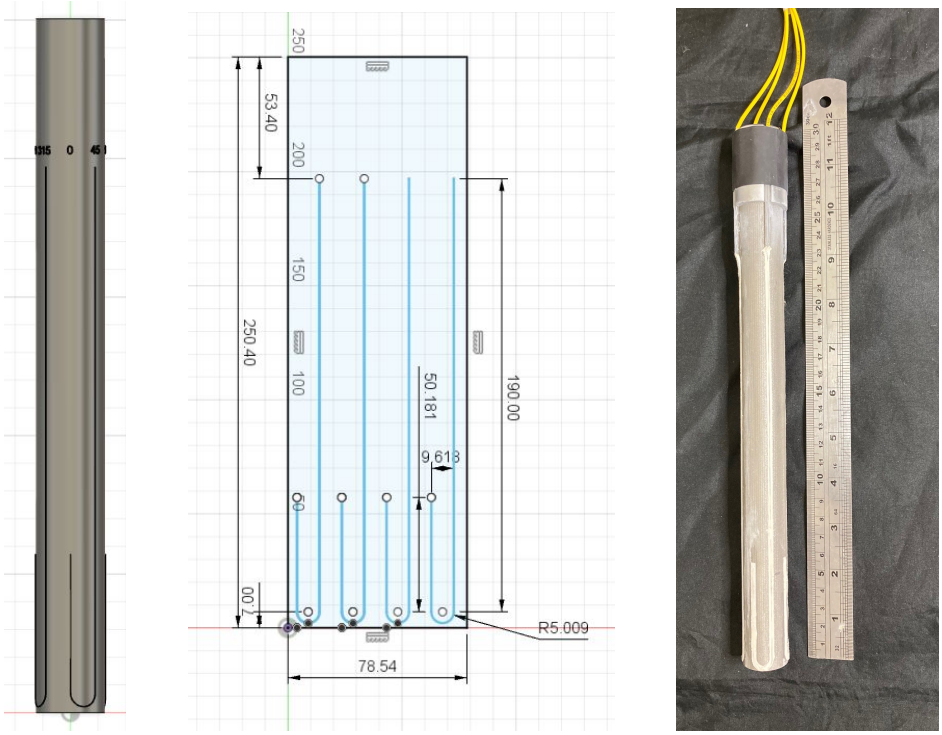

(a) **(b)** **(c)**

Figure 4.5: Fibre optics pile instrumentation for physical model tests within the centrifuge facility in cyclic axial loading in sand: (a) 3D drawing of fiberline, (b) 2D drawing of fiberline including dimensions and (c) photograph of pile instrumented with fibre optics.

Table 4.2: Characteristics of the performed cyclic centrifuge tests. The table differentiates the tested scenarios by relative density of the sample and indicates the number of load cycles, cyclic load ratios, mean load and load amplitude for each test.

Medium dense sand	Loose over dense sand
Load scenario a) 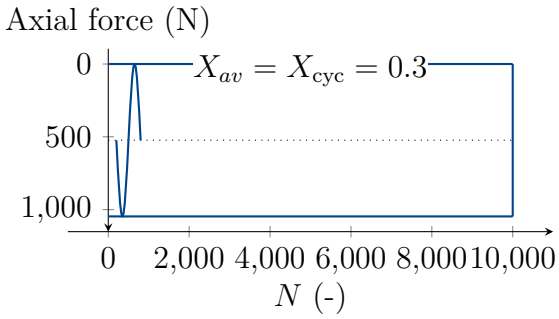	Load scenario a) 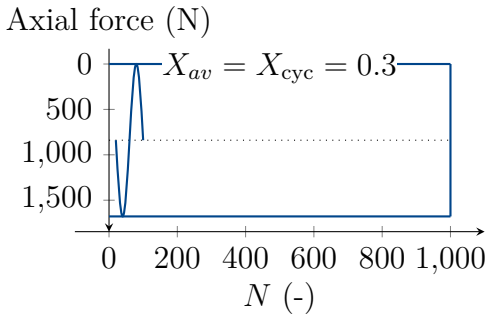
Load scenario b) 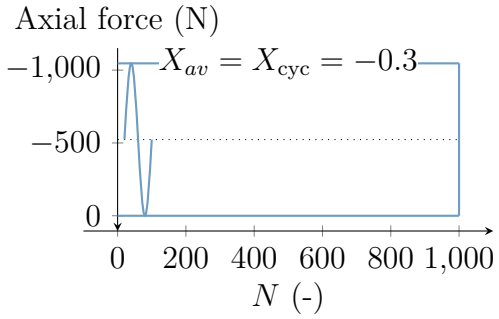	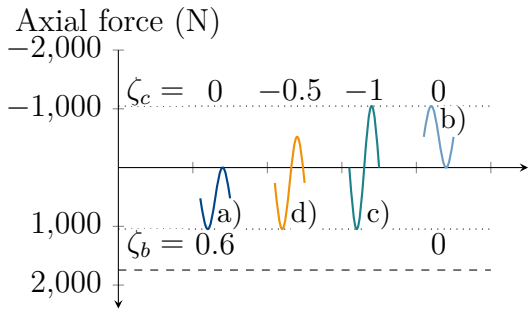
Load scenario c) 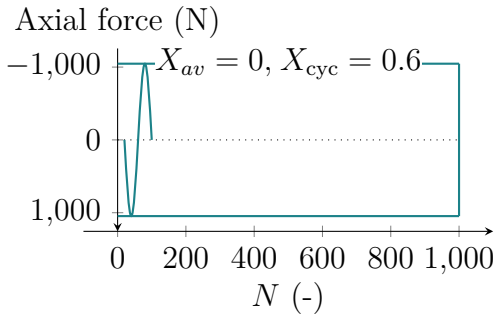	
Load scenario d) 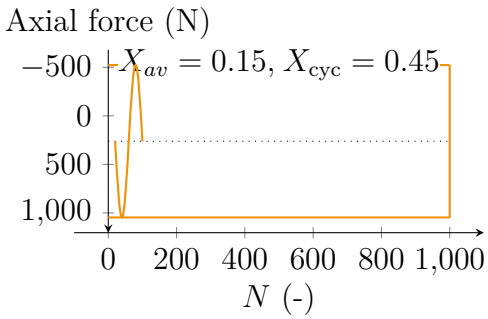	Load scenario d) 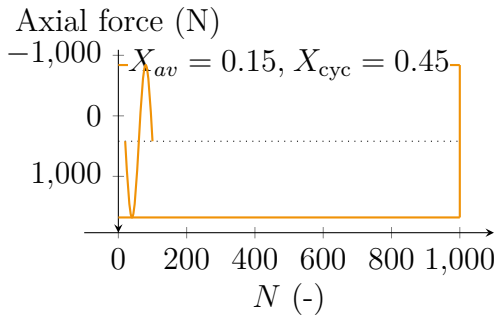

$X_{av} = \frac{F_{av}}{F_{ult}}$ and $X_{cyc} = \frac{F_{cyc}}{F_{ult}}$

monotonic tests and six cyclic tests were performed. Table 4.3 summarises the centrifuge testing program.

To achieve the aim of gaining a better understanding of axial pile-bearing behaviour and pile-soil interaction during cyclic axial loading, a series of centrifuge experiments is performed at 200g considering different initial relative densities of the sand (medium dense and loose over dense sand) and different cyclic loading scenarios (one-way, two-way, symmetric and unsymmetric cyclic loads).

4.6 Results of the axial load tests

Each pile test was carried out following the procedure outlined in section 4.5. The test results presented in this section are given in model scale. Positive values denote compression and downward displacements, while negative values indicate tension and upward displacements.

4.6.1 Axial monotonic response

Figure 4.6a and b visualise the pile-head load-settlement response of the monotonic tests MON-1-MS and MON-2-LoDS in axial compression and tension in medium dense and loose over dense sand. The penetration depth displayed at the vertical axis is normalised by the outer pile diameter.

The monotonic test results reveal an increasing axial force with increasing pile penetration when subjected to axial compression (ref. figure 4.6a). Compared to the medium dense sand sample, a significantly stiffer pile response is observed in the loose over dense sand sample, corresponding to a higher ultimate bearing capacity. Hence, the influence of the relatively thin, loose sand layer on the response of the pile-soil system is considered marginal based on the monotonic test results (compare section 4.3). The densely packed bottom sand layer mainly contributes to the overall mobilized capacity and to the stiffer response of the pile in the layered sample. The ultimate axial capacity in compression is defined at a normalised

Table 4.3: Centrifuge testing program.

Test name	Sand sample	Test type	Number of load cycles	Load scenario
MON-1-MS	medium dense (no. 1)	monotonic	-	-
CYC-3-A-MS	medium dense (no. 3)	cyclic	10,000	a
CYC-1-B-MS	medium dense (no. 1)	cyclic	1,000	b
CYC-1-C-MS	medium dense (no. 1)	cyclic	1,000	c
CYC-1-D-MS	medium dense (no. 1)	cyclic	1,000	d
MON-2-LoDS	loose over dense (no. 2)	monotonic	-	-
CYC-2-A-LoDS	loose over dense (no. 2)	cyclic	1,000	a
CYC-2-D-LoDS	loose over dense (no. 2)	cyclic	1,000	d

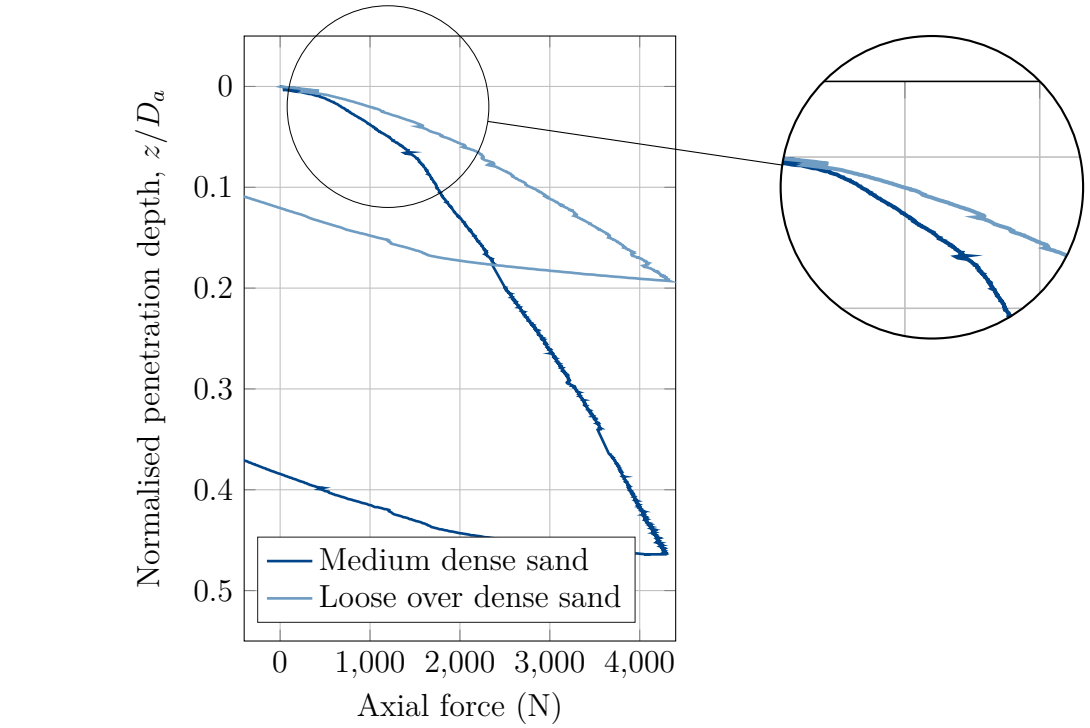

(a)

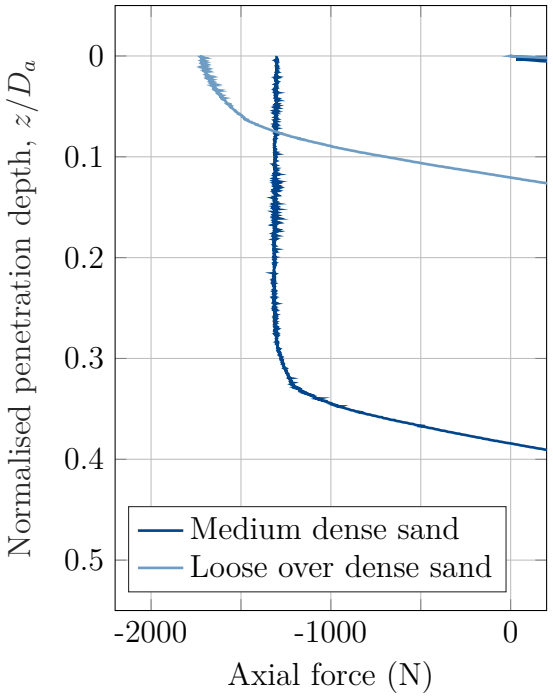

(b)

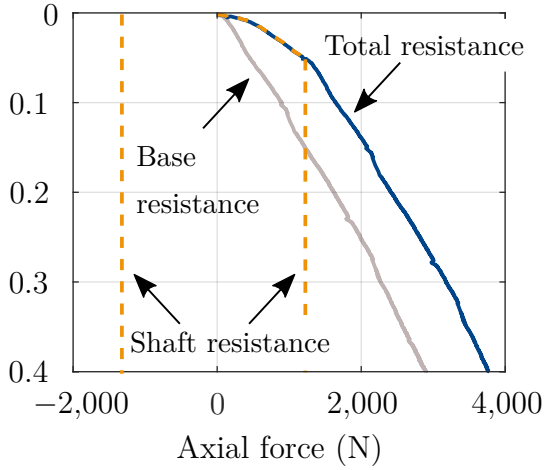

(c) Components of axial pile resistance in medium dense sand.

Figure 4.6: Comparison of pile-head load–settlement behavior in axial (a) compression and (b) tension in medium dense (test MON-1-MS) and loose over dense sand (test MON-2-LoDS), and (c) components of axial pile resistance.

penetration depth of $z/D_a = 0.1$, compare section 4.5, which is $F_{ult} = 1{,}744.2$ N in the medium dense sample and $F_{ult} = 2{,}797.6$ N in the loose over dense sample.

Subsequently, an axial monotonic load test into tension was conducted (ref. section 4.5). The test results are shown in figure 4.6b and reveal a significantly higher tensional capacity in the layered sample.

Figure 4.6c illustrates the components of axial pile resistance, i.e. base and shaft resistance, derived from the quasi-static monotonic test in medium dense sand. The shaft resistance, $F_s = 1{,}300$ N, is found as the tensional capacity of the pile (compare figure 4.6b) and is mobilized even at small pile displacements. With the increasing settlement of the pile, the base resistance is fully mobilized, resulting in a load transfer to the lower part of the pile (ref. section 2.3.1).

4.6.2 Axial cyclic response

The centrifuge experiments aim to investigate the behaviour of piles under cyclic axial loads. The following aspects are evaluated and discussed: repeatability of the cyclic axial load tests, the influence of the cyclic load ratio, relative density and the ratcheting evolution.

Repeatability of the cyclic axial load tests

To compare the results of cyclic axial load tests between different soil samples, comparability and repeatability of the test results must be ensured. The repeatability of the testing procedure can be shown by comparing the axial force and the pile head displacement of the cyclic tests on the initial loading path. The tests were conducted in the same soil conditions but in different boxes. Since no direct comparability is given between two tests, the repeatability is studied by comparing the initial loading path of the tests CYC-3-A-MS, CYC-1-C-MS and CYC-1-D-MS. The results of the cyclic axial load tests of these three tests are compared in Figure 4.7. On the initial loading path, the results differ only marginally. This proves comparable and repeatable testing conditions for the cyclic load tests.

Influence of cyclic load ratio

The influence of the cyclic load ratio on the cyclic axial pile-bearing behaviour is studied using centrifuge test results from the tests CYC-3-A-MS, CYC-1-B-MS, CYC-1-C-MS and CYC-1-D-MS. The piles are tested in a medium dense, $D_r = 55\%$, water-saturated sand sample at an embedment length of $L_e = 125$ mm. Figures 4.8a-d show the pile-head load-settlement behaviour for the load scenarios a), b), c) and d). Please note that a total of 10,000 load cycles was envisaged for load scenario a) while the other three tests involved 1,000 load cycles.

The force-displacement plots in figure 4.8 show the hysteretic pile response. In general, an increase in vertical pile displacement by the number of load cycles can be observed. The ratcheting rate decreases with an increasing number of load cycles. The impact of the cyclic load scenario is clear, with greater ratcheting recorded for load scenario c) than for

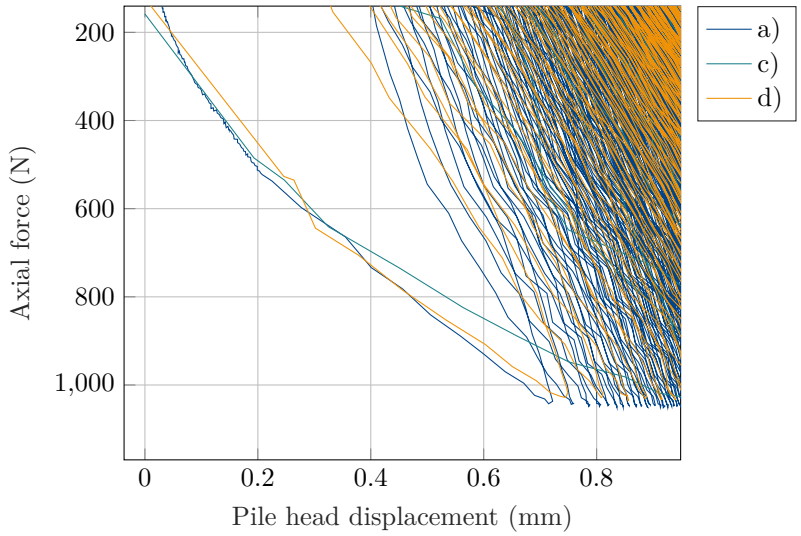

Figure 4.7: Repeatability of the cyclic axial load tests in medium dense sand: initial pile-head load-settlement response due to cyclic loading scenarios a), c) and d).

load scenario d) and a), respectively. Since load scenario a) involved 10,000 load cycles, the overall magnitude of pile head displacement cannot be compared directly but is discussed later as part of the ratcheting evolution. The shape of the hysteresis loops becomes less expanded during cycling, indicating a stiffer pile response.

Tensile cyclic loads – as applied in load scenario b) – uplift the pile with subsequent ratcheting. Contrasting load scenarios a), c) and d), this test shows a narrow hysteretic response. The system behaviour due to cyclic loading into tension differs compared to the behaviour of both one-way and partial two-way cyclic loading in compression, mainly relying on the mobilized skin friction along the pile shaft. Although the pile was subjected to cyclic tensile loads, the pile settles and accumulates permanent displacements directed downwards, following an initial uplift (figure 4.8b). Hence, the skin friction counteracting the applied tensile loads has significant influence on the pile-bearing behaviour and aids stabilizing. This is considered to apply only if the maximum tensile load is below the cyclic frictional pile capacity.

Influence of relative density

The influence of the relative density on the cyclic axial pile-bearing behaviour is studied using centrifuge test results from test CYC-1-D-MS in a homogenous medium dense sand sample and tests CYC-2-A-LoDS and CYC-2-D-LoDS in a layered sample, which consisted of a loose sand layer ($D_r = 33\%$) on top of a dense sand layer ($D_r = 87\%$). Figure 4.9 shows the pile-head load-settlement response for load scenarios a) and d). The tests involved 1,000 load cycles.

The effect of the cyclic load ratio, i.e. the magnitude of load amplitude, is evident from the comparison in figure 4.9. Although the maximum load remains constant in both tests,

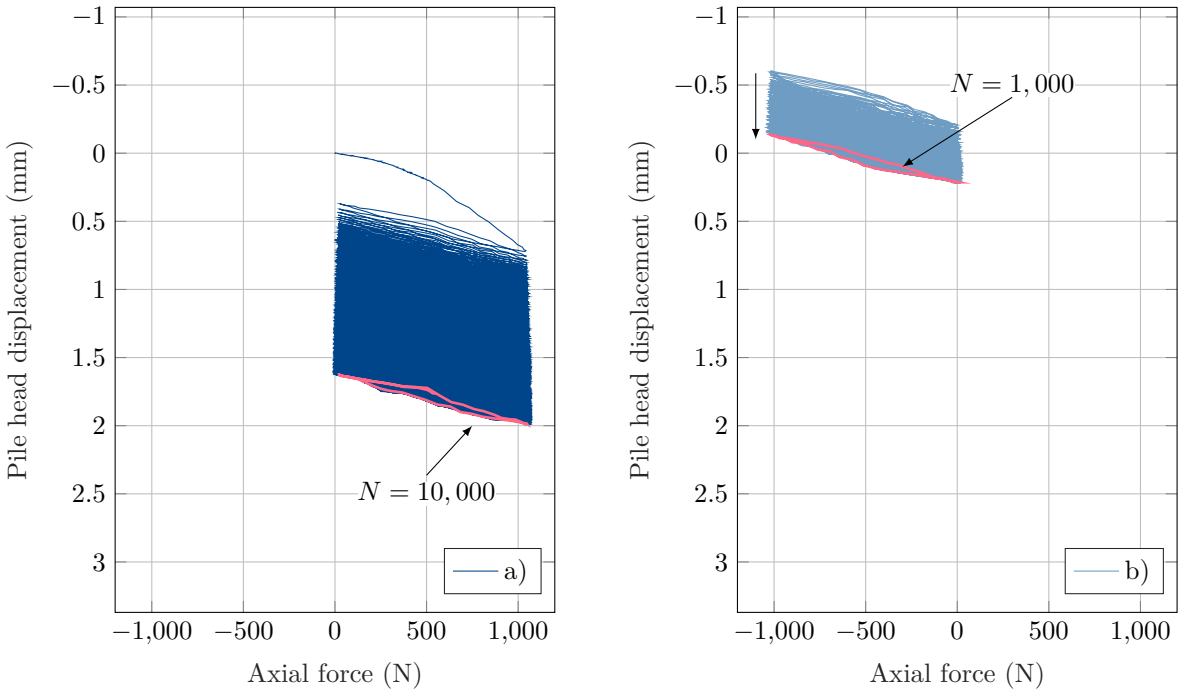

(a) Test CYC-3-A-MS.

(b) Test CYC-1-B-MS.

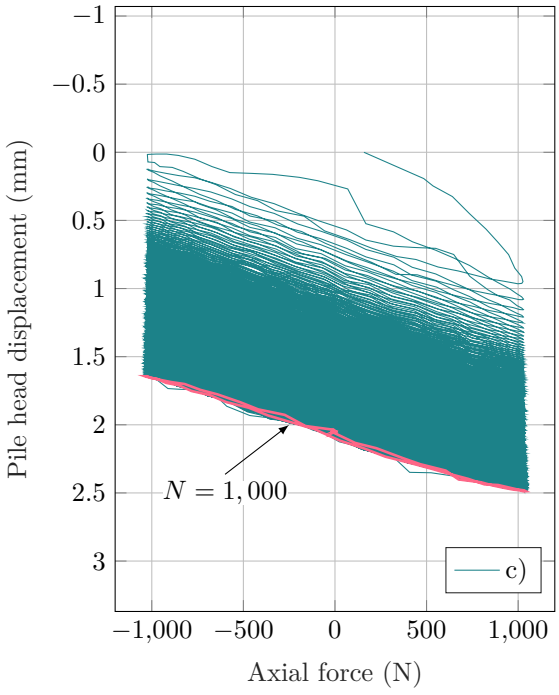

(c) Test CYC-1-C-MS.

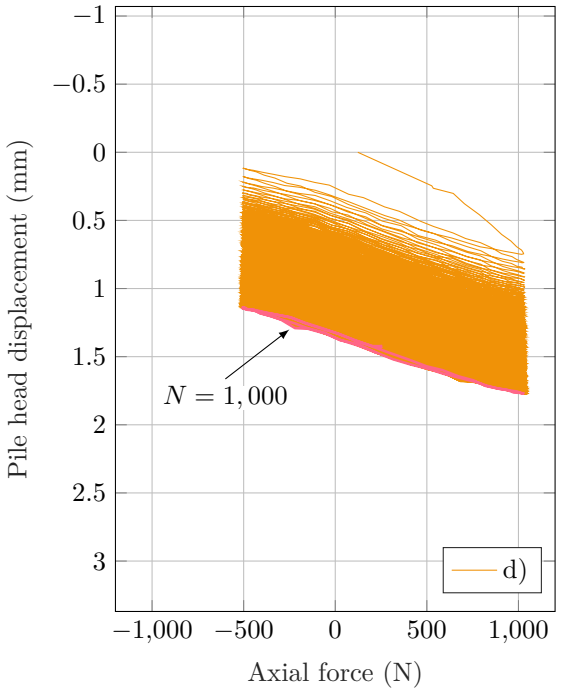

(d) Test CYC-1-D-MS.

Figure 4.8: Comparison of pile-head load-settlement behaviour due to cyclic loading scenarios a), b), c) and d) in medium dense sand.

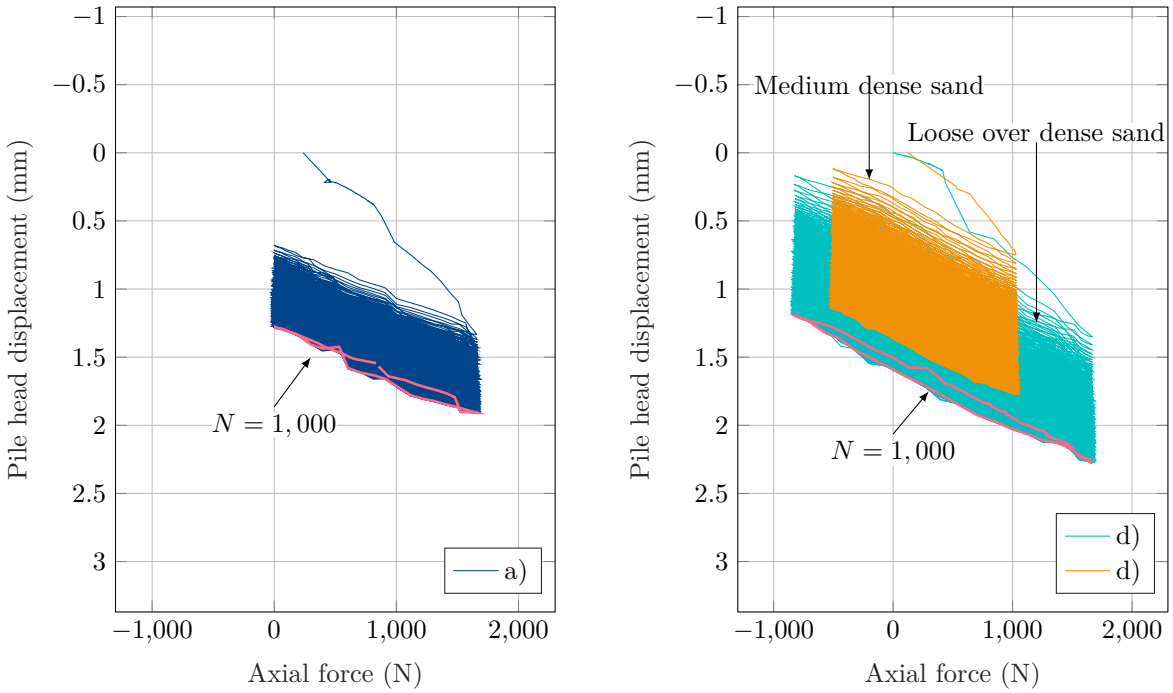

(a) Test CYC-2-A-LoDS.

(b) Tests CYC-1-D-MS and CYC-2-D-LoDS.

Figure 4.9: Comparison of pile-head load-settlement behaviour due to cyclic load scenarios a) and d) in loose over dense sand and load scenario d) in medium dense sand.

higher pile-head displacements are accumulated for load scenario d) compared to load scenario a).

A comparison of the recorded response for load scenario d) in the medium dense and the loose over dense sample is provided in figure 4.9b. In the layered sample, larger ratcheting occurs, showing a softer response compared to the medium dense sample. Please note that from the monotonic response in the loose over dense sample, a higher ultimate capacity was derived compared to the medium dense sample (ref. figure 4.6). Hence, the cyclic loads being estimated on that basis – when the cyclic load ratio remains constant – involve higher values and a larger cyclic amplitude, respectively. Although a stiffer monotonic response was observed in the monotonic loose over dense test, the cyclic test results indicate a softer behaviour and a reduced soil stiffness in the same sample when the pile is subjected to repetitive loading. The decrease in soil stiffness is likely caused by a stress relief and degradation of shaft resistance due to large-amplitude cyclic loading.

However, upon investigating the cyclic axial pile-bearing behaviour, it became evident that the ratcheting evolution plays a key role. This important phenomenon is further explored below.

Ratcheting evolution

Figure 4.10 presents the ratcheting response of the pile for the tests CYC-3-A-MS, CYC-1-B-MS, CYC-1-C-MS and CYC-1-D-MS in a medium dense and for the tests CYC-2-A-LoDS and CYC-2-D-LoDS in a loose over dense sand sample. The figure shows the accumulated vertical strain over the number of load cycles.

A decreasing ratcheting rate is observed in all six tests. Further, the influence of the load scenario on the ratcheting response is evident. A higher displacement accumulation is observed with increasing load amplitude – as seen in both the pile-head load-settlement plots and the ratcheting evolution plots. In test CYC-1-B-MS, the pile is subjected to cyclic loading in tension. As mentioned before, this tensional load results in an initial uplift of the pile, with subsequent ratcheting recorded for the following load cycles. The uplift during initial loading into tension may activate the skin friction along the pile shaft. The subsequent accumulation of pile settlement indicates that the component of skin friction acting along the pile, pulling it further into the soil, is greater than the upward-acting load components of the cyclic load.

Comparing test results in figure 4.10a and b provides insight into the impact of the influence of the relative density of the soil. The shape of the evolution of accumulated strain differs slightly, when comparing load scenarios a) and d) in the medium dense and the loose over dense sand samples. In the layered sample, an accelerated ratcheting behaviour is observed at the first 100 load cycles when $\zeta_c = 0$ compared to $\zeta_c = -0.5$. The magnitude of permanent accumulated strain developing in the layered sample is higher since higher values of the average load and amplitude are estimated when maintaining the cyclic load ratio. However, the ratcheting behaviour is qualitatively similar at both densities.

Conclusively, the test results highlight the importance of load asymmetry in the axial cyclic pile response. An increasing cyclic amplitude, with increasingly negative ζ_c, leads to

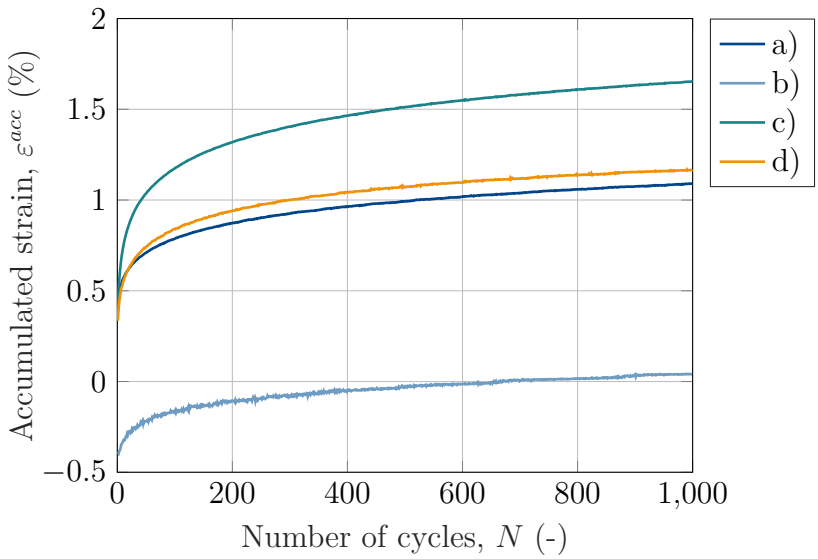

(a)

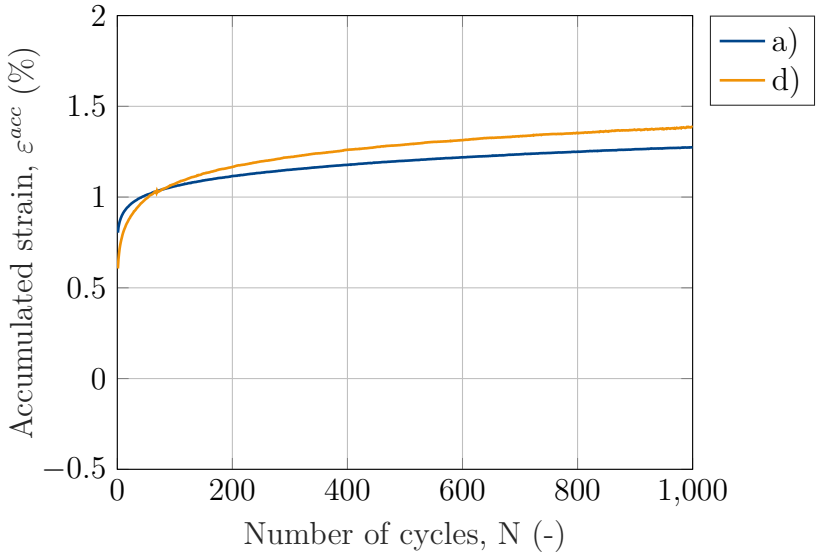

(b)

Figure 4.10: Comparison of cyclic strain accumulation during (a) load scenarios a), b), c) and d) in medium dense sand and (b) load scenarios a) and d) in loose over dense sand.

higher vertical pile displacements and rapidly reduces the soil stiffness. Contrasting this, a decreasing mean load with increasing negative ζ_c does not necessarily reduce the axial strain accumulation. It may be understood from the test results that larger amplitude two-way cyclic loading activates stiffness degradation mechanisms and, therefore, can lead to immense vertical pile settlements. This effect can benefit practical applications such as e.g. vibratory pile driving.

4.6.3 Reloading response

In order to investigate the post-cyclic pile capacity a quasi-static monotonic test was conducted following a cyclic load test. A comparison of the reloading response in compression and tension in medium dense sand is given in figure 4.11. Please note that the cyclic loading phase was omitted in the figure for clarity.

The figure visualises the pile-head load-settlement behaviour in the tests CYC-3-A-MS, CYC-1-B-MS, CYC-1-C-MS and CYC-1-D-MS. The penetration depth is normalised by the outer pile diameter.

The following conclusions are derived from the test results shown in figure 4.11:

- The results in figure 4.11a show an increasing axial force in the post-cyclic monotonic stage compared to the axial monotonic response, discussed earlier in section 4.6.1, indicating beneficial densification effects during cyclic loading. Since the reloading curve crosses the monotonic curve, it is evident that the cyclic loading causes a higher post-cyclic soil stiffness and increases the overall capacity of the pile.
- A significant variation in the magnitude of shaft resistance is observed in all cases, cf. figure 4.11b. The tests with load scenario a) and b) have the same amplitude but a different loading direction, which results in the same post-cyclic capacity in tension. Although load scenario c) involves the largest amplitude, followed by the largest ratcheting (refer to figure 4.10b), a more significant increase in the post-cyclic capacity in tension is found. The increase in post-cyclic capacity is likely to be caused by stress redistributions and rearrangement of particles in the pile-soil interface.

Thus, the results confirm an increased post-cyclic capacity in compression and either a maintained or increased post-cyclic capacity in tension, providing potentially additional capacity for an optimised design.

4.6.4 Fibre optic sensing

The centrifuge experiments were conducted using fibre optic strain gauges to provide insight into the pile response to axial cyclic loading. This section aims at proving the feasibility of using fibre optic sensing to investigate the cyclic axial pile-bearing behaviour and pile-soil interaction. Figure 4.12 shows the axial strain for load scenarios a) and b) in the medium dense sample, estimated from the fibre optic strain gauges. The respective results for load scenario a) in the loose over dense sample can be seen in figure 4.13. For clarity, only the first 100 s of each test are shown. Both figures visualize the strain profiles in four different depths during a cyclic axial load test.

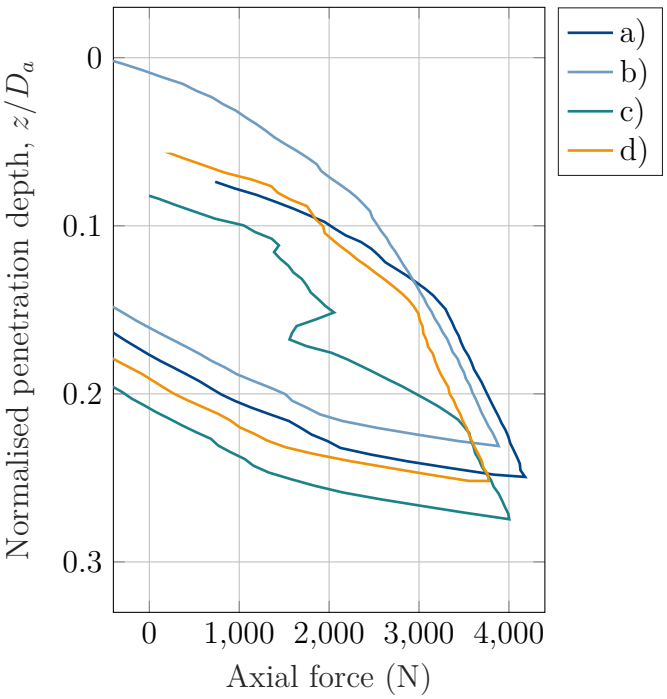

(a)

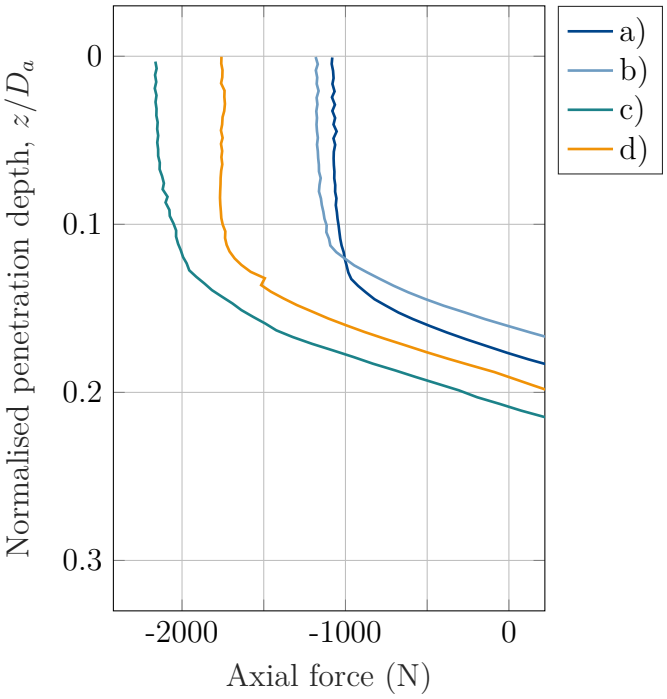

(b)

Figure 4.11: Comparison of post-cyclic capacity in (a) compression and (b) tension for load scenarios a), b), c) and d) in medium dense sand.

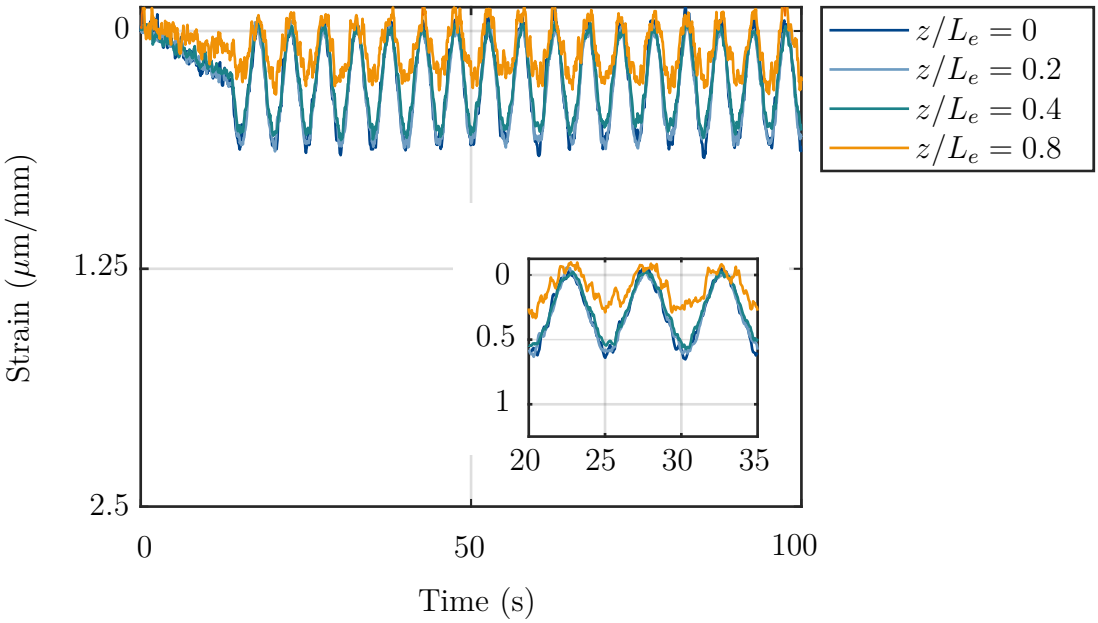

(a) Test CYC-3-A-MS.

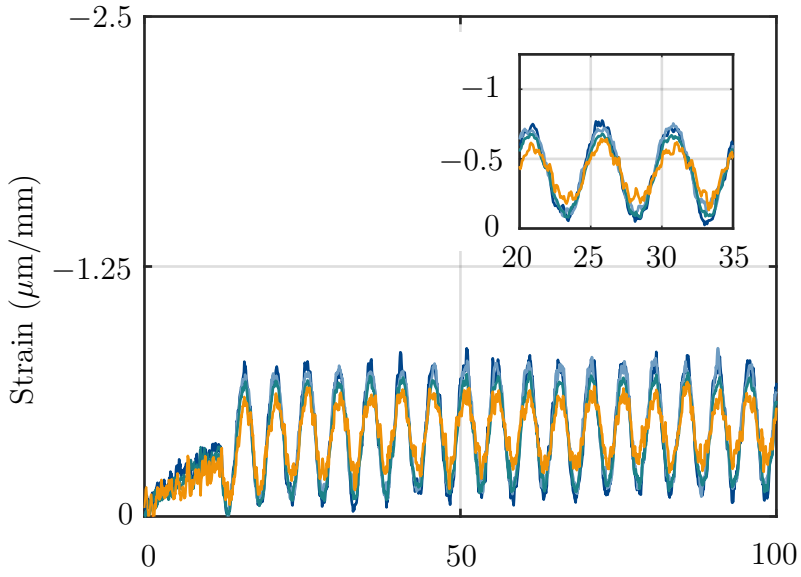

(b) Test CYC-3-B-MS.

Figure 4.12: Fibre optic strain profiles at four different depths for load scenario a) and b) in medium dense sand.

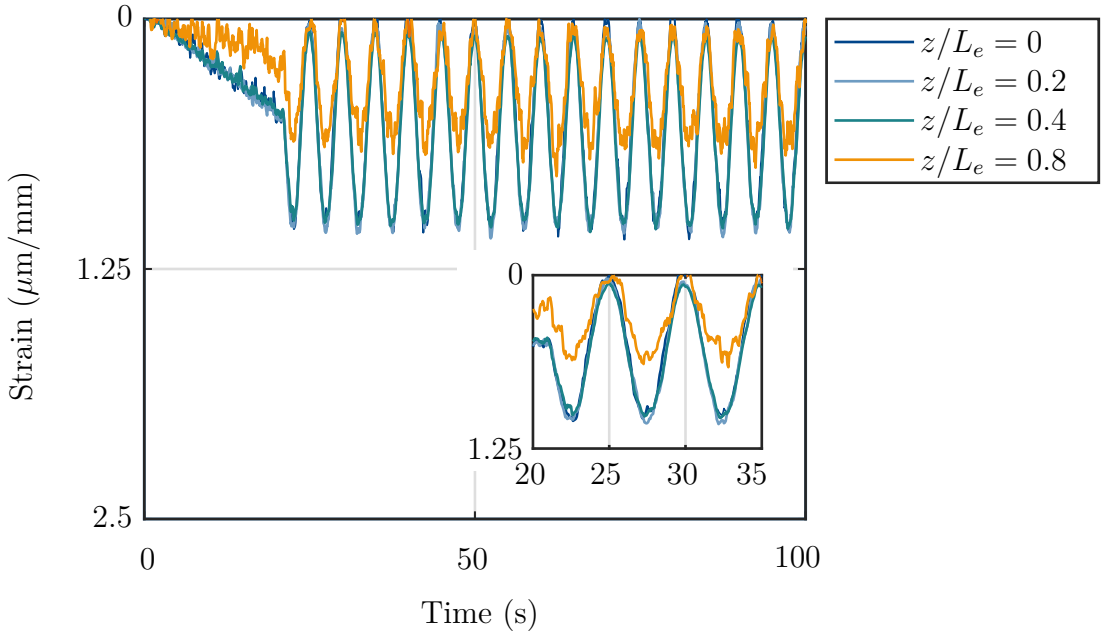

(a) Test CYC-2-A-LoDS.

Figure 4.13: Fibre optic strain profiles at four different depths for load scenario a) in loose over dense sand.

The results in figure 4.12 and 4.13 show that the fibre optic is successfully able to detect the cyclic axial pile response. The same general shape is exhibited at all four depths, indicating the initial loading of the pile to the intended mean load and the subsequent load cycles. Both tests with load scenarios a) (figure 4.12a and 4.13) show positive deformations (compression) while load scenario b) denotes negative pile deformations (tension).

In figure 4.12a the vertical strain decreases slightly up to a normalized depth of $z/L_e = 0.4$, indicating the same magnitude of skin friction along the pile. Closer to the pile tip (i.e. $z/L_e = 0.8$), the axial strain decreases, suggesting a load transfer towards the lower part of the pile and mobilization of the pile tip resistance. A similar pile response is observed in the test with load scenario a) conducted in the loose over dense sample, compare figure 4.13. However, higher strains were recorded from the larger cycles in the loose over dense sample. Up to a depth of $z/L_e = 0.4$ the strain along the pile remains almost constant with only marginal differences being visible. This strongly suggests a minor contribution of the skin friction along the pile and thus a degradation of shaft resistance.

Contrasting this, a narrow band of the strain profiles for all four depth is recorded from load scenario b), cf. figure 4.12b. Negative strains occur with a remaining distance from the neutral axis – that is, clearly related to the uplift of the pile. The strain amplitude decreases slightly with increasing depth. Hence, the results suggest a minor contribution of the pile tip resistance to the overall pile response and confirm observations from figure 4.10a, indicative of a predominant effect of the mobilized shaft resistance.

The key outcome of this study is that fibre optic sensing provides valuable insights into the mechanisms of axial cyclic pile-bearing behaviour. The results prove that the fibre optic

data clearly displays the cyclic pile response in medium dense and loose over dense sand. A similar pile response is found for both relative densities. However, large-amplitude two-way cyclic loading was found to lead to a degradation of shaft resistance, resulting in a higher strain magnitude. Some differences from the one-way cyclic loading into compression and tension were highlighted. However, combining fibre optic sensing together with the overall recorded pile response is essential and thus exhibits superior potential to be used in the investigation of cyclic axial pile-bearing behaviour and pile-soil interaction.

4.7 Summary

This section summarises the results of a series of centrifuge experiments investigating the pile response due to cyclic axial loading. The test series features cyclic loading in compression and tension with the purpose to improve the understanding of pile response to axial cyclic loading. Investigating the effect of different cyclic loading scenarios and different relative densities was also targeted through the experiments. Conclusively, the cyclic loading test results enable for the following key findings:

- The ratcheting evolution in medium dense and loose over dense sand is qualitatively similar, indicating that partial two-way cyclic loading leads to larger ratcheting than one-way cyclic loading to the same maximum load.
- Targeting the role of cyclic loading into tension, the mobilized skin friction acts beneficial to the stability of the structure. Failure is only expected if the tensile load overcomes the frictional pile capacity.
- Pile capacity is increased in compression and either maintained or increased in tension following cyclic loading in water-saturated sand, showing a significantly stiffer post-cyclic response and potentially enhancing the trust in the bearing capacity of cyclic axially loaded piles, since no strength degradation due to cyclic loading was found.
- It is feasible to use fibre optic sensing to detect the cyclic pile response due to axial cyclic loading. The data adds to existing knowledge from the recorded load-displacement response and, thus, sheds light on the mechanisms involved in the pile response to axial cyclic loading. The method exhibits great potential and can contribute to a comprehensive description of the cyclic axial pile-bearing behaviour and pile-soil interaction.

5 Cyclic soil behaviour in direct simple shear testing

Due to wind and wave conditions, offshore structures experience variable and highly cyclic loads from varying directions. The design process simplifies these complex irregular loading scenarios using classification methods and applies cycle packages with constant parameters (i.e., frequency, mean load and amplitude). This procedure assumes that the ordering of cycle packages does not affect the total accumulated strain in the soil, i.e. the validity of Miner's rule (compare section 2.2.3). This chapter presents an experimental study on the validity of Miner's rule in non-cohesive soils based on high cyclic direct simple shear tests. The experiments aim to investigate the effect of the ordering of cycle packages on the cyclic deformation accumulation and address the research question of whether it is acceptable to simplify nonlinear waveform load signals by means of classification methods. In addition, the influence of continuous polarisation changes is investigated.

Please note that the author has already published parts of the results included in this chapter in Stark, Breidenstein, et al. (2022).

5.1 Concept of direct simple shear testing

This section explains the concept of direct simple shear tests. The experimental method is defined by the American Society for Testing and Materials (ASTM) in the standard ASTM D 6528-07. Please note that slightly different methods exist to conduct the experiment, for instance, evaluated in Le et al. (2022). Definitions of stresses and strains in a direct simple shear test are illustrated in Figure 5.1.

In a direct simple shear test, a cylindrical soil sample is placed in a shear box which consists of stacked Teflon-coated aluminium rings surrounded by a latex membrane. A Teflon coating

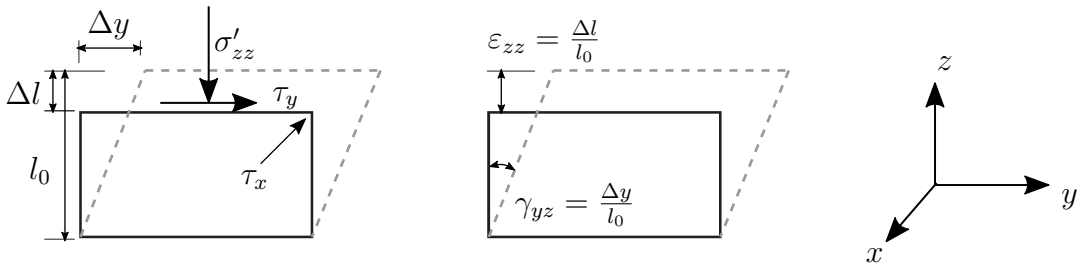

Figure 5.1: Definition of stresses and strains in direct simple shear tests.

is applied to the rings to minimize friction on the contact surfaces. A confining stress σ'_{zz} is applied vertically to the specimen, which results in a one-dimensional consolidation of the specimen. The specimen is subjected to either a horizontal stress in a stress-controlled test or to a shear strain in a strain-controlled test. Stresses and strains are measured during testing. For stress-controlled tests, the horizontal shear stress τ is prescribed in one-dimensional shearing or in two-dimensional shearing, τ_x and τ_y, respectively. In a strain-controlled test, the specimen is sheared by displacing the top and bottom plates towards each other, i.e. a shear strain γ_{yz} is prescribed while measuring the resulting shear force. Due to the aluminium rings at the sample edge, the cross-sectional area remains constant throughout the test, and no horizontal strain occurs. Consequently, the axial strain ε_{zz} equals the volumetric strain ε_v. The experiment may represent either undrained or drained conditions, corresponding to a constant specimen volume or a constant confining stress during shearing. This thesis employs stress-controlled experiments assuming drained conditions.

It is important to note a significant non-uniformity in stress distribution at the boundaries of the specimen when interpreting the experimental limitations (Wichtmann, 2005; Le, 2015; Glasenapp, 2016). The shear stress is applied only to the top and bottom surfaces of the specimen. As no complimentary shear stresses act on the vertical sample edges, the moment caused by the horizontal shear stresses has to be balanced by non-uniformly distributed shear and normal stresses to maintain equilibrium. However, the experiment provides a good representation of idealized field stress, i.e. plane strain conditions. The principle stresses continuously rotate due to the stress application, resulting in a stress state similar to a soil element in the field subjected to vertically propagating shear waves. Thus, the experiment adequately represents the cyclic and dynamic soil behaviour in the near field of the pile.

5.2 Outline of testing

Validity of Miner's rule

Within the scope of testing, Miner's rule is investigated experimentally in high cyclic direct, simple shear experiments on non-cohesive soils under drained conditions. This includes the effect of ordering of different cycle packages on the resulting accumulated strain with constant and varying mean and cyclic load levels separately. An overview of all investigated load scenarios is given in figure 5.2 and 5.3. The experiments employ a constant mean load and a variable load amplitude (test series no. 1), a constant non-zero mean load and a variable load amplitude (test series no. 2), a variable mean load and load amplitude (test series no. 3), a variable mean load and a constant load amplitude (test series no. 4), a variable axial stress (test series no. 5) and stepwise polarisation changes (test series no. 6).

A total number of 100,000 load cycles is envisaged in each test. Hence, each cycle package has 25,000 load cycles. The magnitude of the cyclic load was selected so that the maximum load does not exceed 60% of the monotonic capacity of the sample. Therefore, a static reference test was conducted. The test result of the monotonic test is included in figure A.3 in appendix A.

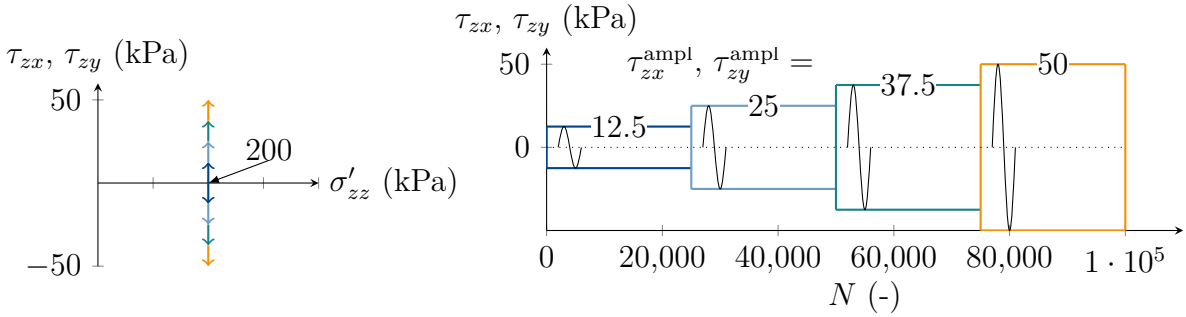

(a) Test series no. 1.

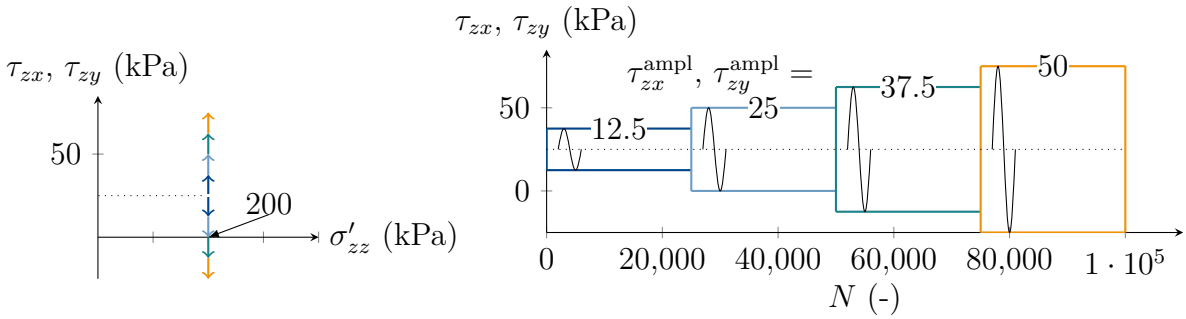

(b) Test series no. 2.

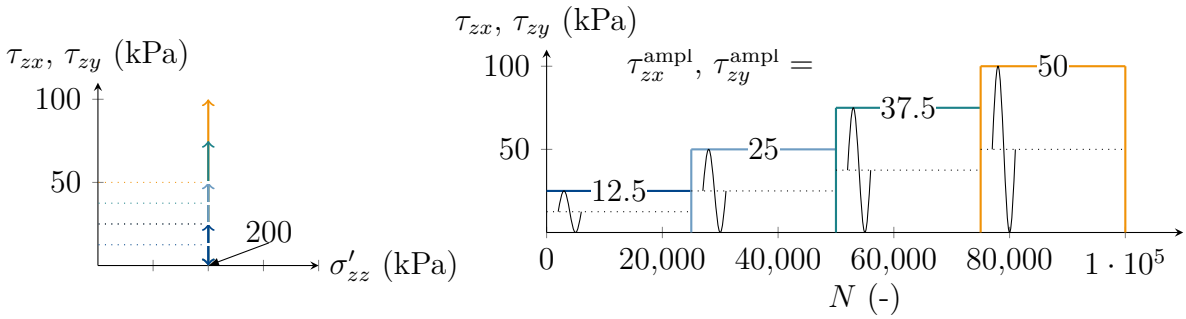

(c) Test series no. 3.

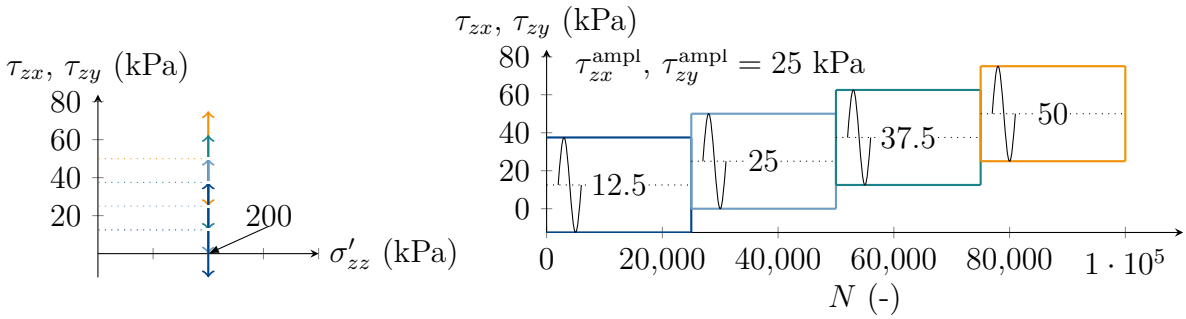

(d) Test series no. 4.

Figure 5.2: Overview of direct simple shear experiments and load scenarios included in the experimental study on the validity of Miner's rule. The experiments involve: (a) a constant zero mean load $\tau^{av} = 0$ kPa and a variable load amplitude $\tau^{\text{ampl}} = 12.5 \rightarrow 25 \rightarrow 37.5 \rightarrow 50$ kPa, (b) a constant non-zero mean load $\tau^{av} = 25$ kPa and a variable load amplitude $\tau^{\text{ampl}} = 12.5 \rightarrow 25 \rightarrow 37.5 \rightarrow 50$ kPa, (c) a variable mean load and load amplitude $\tau^{av} = \tau^{\text{ampl}} = 12.5 \rightarrow 25 \rightarrow 37.5 \rightarrow 50$ kPa and (d) a variable mean load $\tau^{av} = 12.5 \rightarrow 25 \rightarrow 37.5 \rightarrow 50$ kPa and a constant load amplitude $\tau^{\text{ampl}} = 25$ kPa.

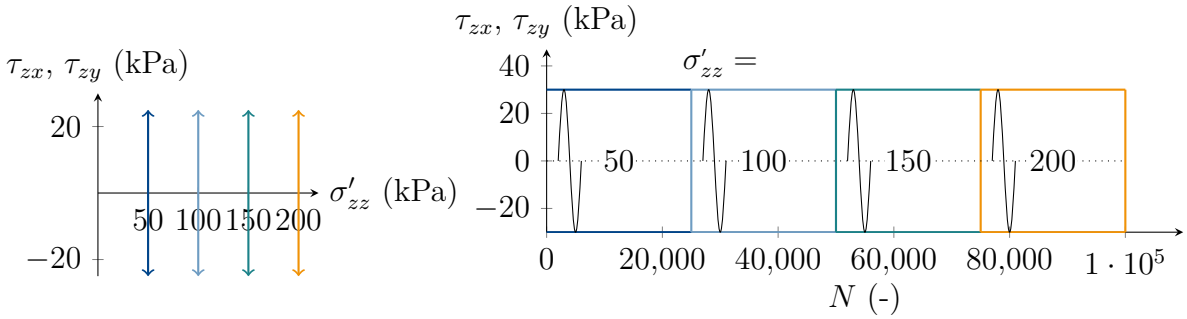

(a) Test series no. 5.

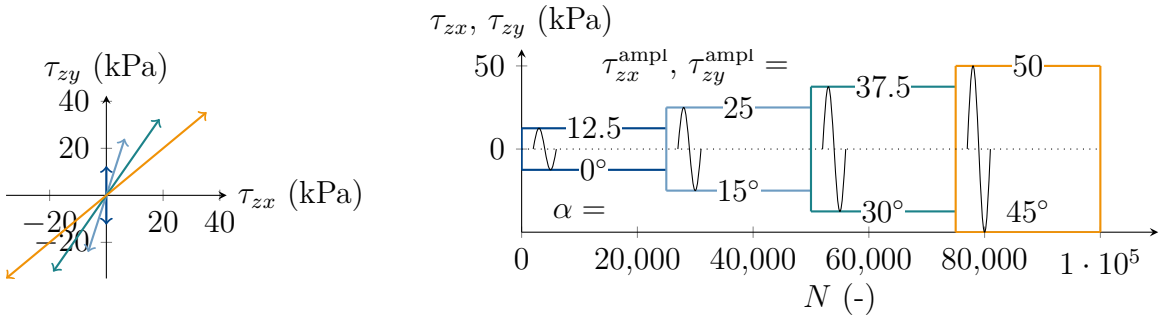

(b) Test series no. 6.

Figure 5.3: Overview of direct simple shear experiments and load scenarios included in the experimental study on the validity of Miner's rule (continued). The experiments involve: (a) a variable axial stress $\sigma'_{zz} = 50 \rightarrow 100 \rightarrow 150 \rightarrow 200$ kPa and (b) stepwise polarisation changes $\alpha = 0 \rightarrow 15 \rightarrow 30 \rightarrow 45°$.

Each test series includes six representative combinations of cycle packages chosen according to Wichtmann (2005). Figure 5.4 illustrates the combinations of cycle packages included in the study.

The cyclic loads are applied at a loading frequency of $f = 1$ Hz. The chosen load frequency is slightly higher than natural wave conditions offshore with a frequency of 0.1 Hz. However, existing research reports no significant impact of the load frequency on the ratcheting response for sand at frequencies below 1 Hz (compare section 2.2). A preliminary study on the effect of load frequency on the ratcheting response in direct simple shear experiments with fine silica sand confirmed this hypothesis (refer to figure 2.4d). In addition, comparability among the direct simple shear experiments is given; therefore, the slightly higher frequency is acceptable.

Waveform streaming

An additional test series with irregular waveform streaming is conducted to investigate whether it is acceptable to simplify nonlinear waveform load signals through classification methods. These tests aim at improving the understanding of:

- What happened on the way to 100 000 cycles? How did we get there?
- Are the loading scenarios comparable?

Within this test series the load scenarios vary constantly while maintaining the energy spectrum in frequency domain. This approach enables natural offshore conditions to be captured during testing and allows for comparing individual loading scenarios by defining the distribution of wave amplitudes through the wave spectrum in the frequency domain. Consequently, these investigations aim to assess the applicability of classification methods in offshore pile design by considering the assumptions made when Miner's rule and classification methods are applied.

Each test has a signal length of 10 minutes. The irregular load sequences were created following the steps listed below:

1. Generate water level elevation time series from wave energy spectrum.
2. Determine waveloads on monopile using Morison's equation.
3. Normalize load sequence by the maximum wave load during a time series.
4. Apply load series with $\tau^{av} = \tau^{\mathrm{ampl}} = 0.3X$, reaching a maximum load of 60% of the ultimate soil resistance.

Please note that steps no. 1 and 2 will be explained in detail in section 6.1.5.

To achieve the aim of investigating the validity of Miner's rule, a series of direct, simple shear experiments is performed. Examination of test results involves the soil damage being quantified in terms of the accumulated volumetric strain.

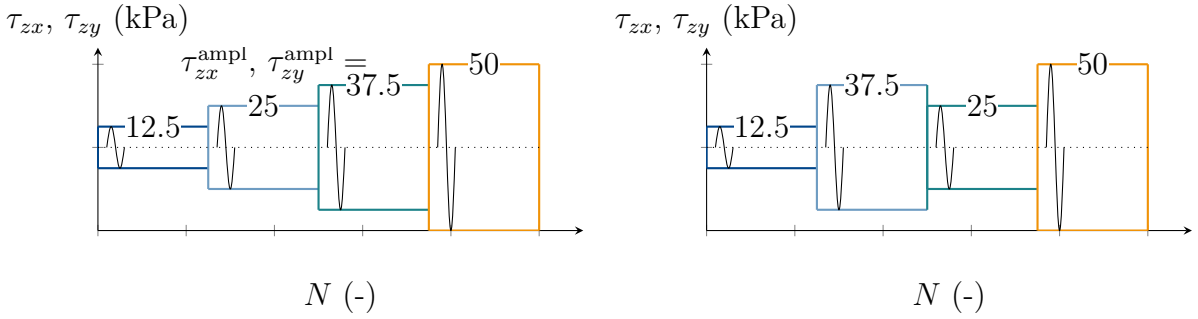

(a) Combination 1.

(b) Combination 2.

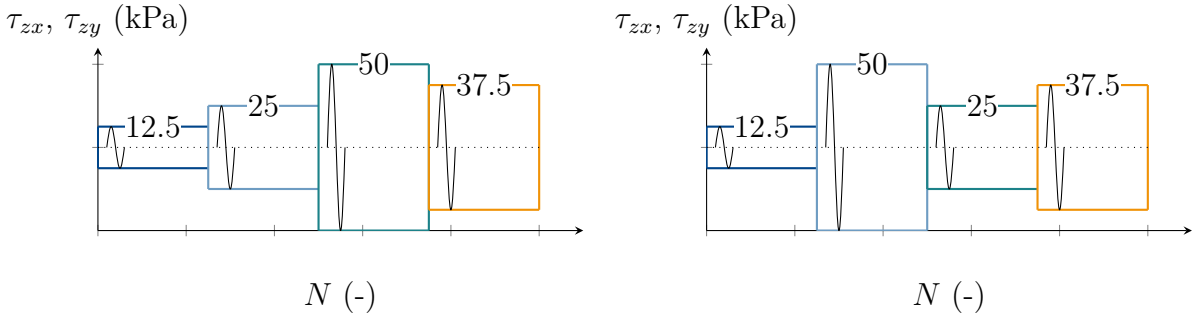

(c) Combination 3.

(d) Combination 4.

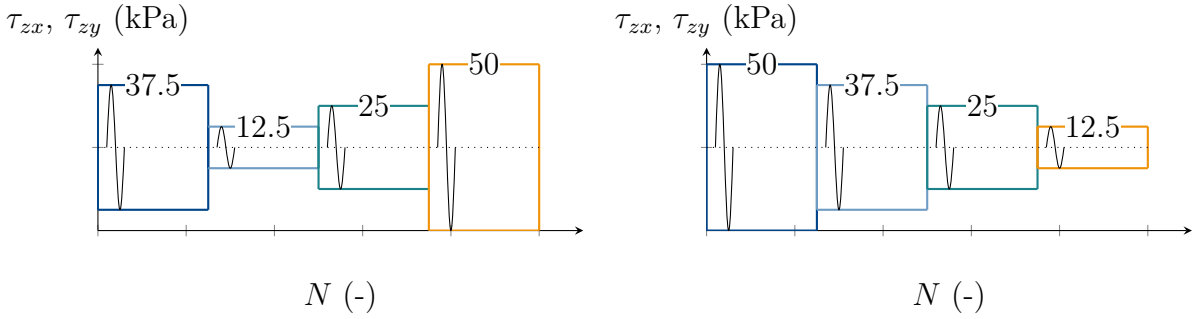

(e) Combination 5.

(f) Combination 6.

Figure 5.4: Combinations of cycle packages included in the study on the validity of Miner's rule. The shown load sequences exemplify test series no. 1 involving a constant zero mean and a variable load amplitude.

5.3 Experimental set up and testing procedure

The experiments were carried out using a GDS Variable Direction Direct Cyclic Simple Shear (VDDCSS) device. The VDDCSS enables a direct, simple shear test to be performed in two directions, i.e., shearing the sample in both horizontal axes. This is achieved by a secondary shear actuator acting at 90° to the primary actuator. The secondary shear axis can be used either independently or together with the primary shear axis and therefore, allows direct simple shear with variable and from any horizontal direction. Figure 5.5 illustrates the bi-directional simple test device, with its main components being highlighted.

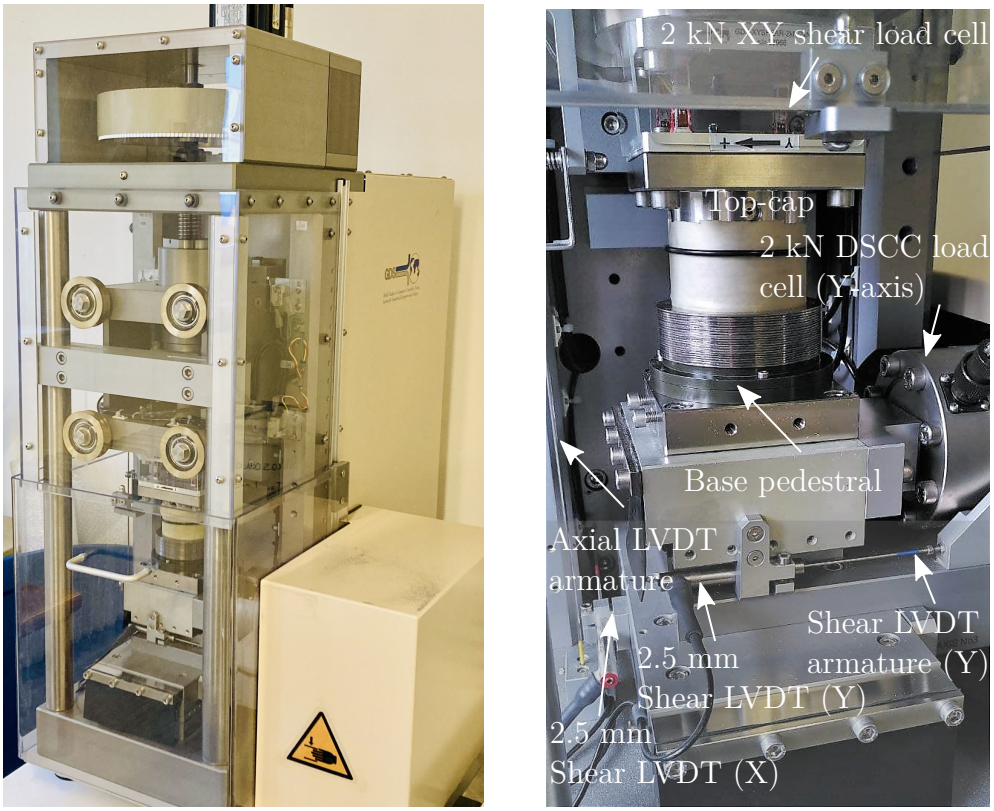

(a) Variable Direction Direct Cyclic Simple Shear (VDDCSS).

(b) Hardware definitions.

Figure 5.5: Bi-directional simple shear test device and its main components.

The device has three AC servo motors working at the three axes with a local closed-loop synchronised control and acquisition unit. This allows for active load and displacement control during cyclic and dynamic shear load application. Cyclic shear loading with different frequencies, mean load, amplitude and phase offset, such as waveform streaming, is available. Small strain measurements can be recorded from LVDTs at all three axes.

The sample preparation steps are visible in figure 5.6. First, a latex membrane is placed over the foot stamp (figure 5.6a) and secured with a rubber ring, which can be seen in

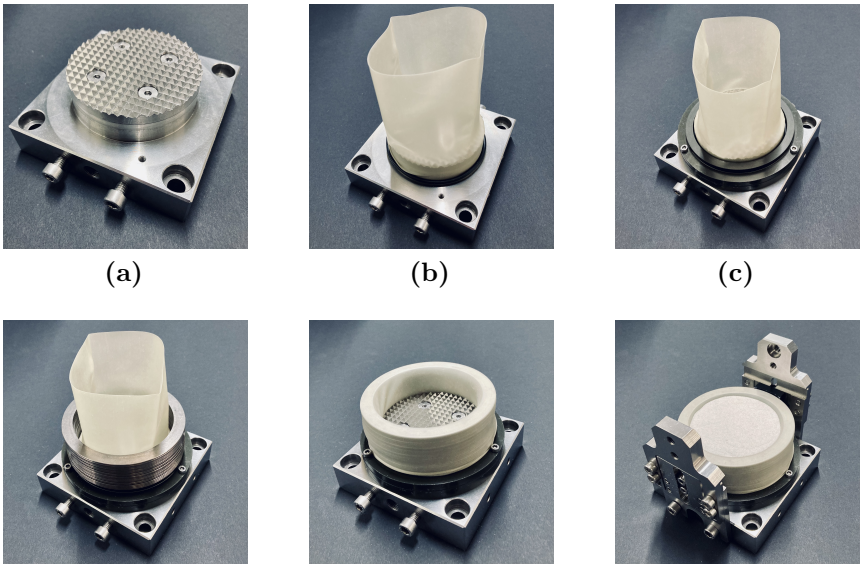

Figure 5.6: Sample preparation steps for direct simple shear tests.

figure 5.6b. Then, two sealing rings are attached to the foot stamp, with a rubber ring in between them and screwed together (figure 5.6c). The sealing rings maintain the position of the latex membrane during sample preparation and testing. In the next step, figure 5.6d, plain teflon-coated aluminium rings are placed over the latex membrane. Afterwards, the latex membrane is tightened around the rings with great care given to avoid gaps between the membrane and the rings (figure 5.6e). Finally, the sand samples are prepared manually and carefully using dry air pluviation.

For the simple shear experiments, the samples are created from very fine silica sand, which was previously characterised in section 4.3. A medium dense sample with a relative density of $I_D = 0.6$ is targeted. The tests are performed with a sample diameter of 70 mm and a height of 20 mm. A constant vertical stress of $\sigma'_{zz} = 200$ kPa is envisaged in many tests assuming drained conditions.

Subsequently, the sample is placed carefully into the direct simple shear test device and attached to the base pedestral with four screws. The lowest possible confining pressure of approximately 10 kPa is envisaged for the sample docking.

After sample preparation, a vertical confining pressure of $\sigma'_{zz} = 200$ kPa is applied to the sample in the consolidation stage. Thereby, the vertical stress is increased linearly over a time period of 5 minutes and maintained constant until no further settlements occur. After sample consolidation, either a cyclic or a dynamic load test is executed.

5.4 Study on the validity of Miner's rule

This chapter features investigations on the validity of Miner's rule. The experiments target ordering effects on the accumulated volumetric strain in high cyclic direct simple shear experiments. The results from the multi-amplitude cyclic load tests are provided in figure 5.7 and 5.8.

Figure 5.7a shows the results for test series no. 1 that involved a constant zero mean load $\tau^{av} = 0$ kPa and a variable load amplitude $\tau^{\text{ampl}} = 12.5 \rightarrow 25 \rightarrow 37.5 \rightarrow 50$ kPa. In tests 1.1 to 1.4, the soil sample was subjected to 25,000 cycles of symmetric two-way cyclic loading with an amplitude of 12.5 kPa. After the first cycle package, the accumulated volumetric strain varies slightly ±4.9%, proving reproducibility in these tests. The load amplitude was varied in the following cycle packages, including an increasing (test no. 1.1) and decreasing order (test no. 1.6), such as combinations of increasing and decreasing amplitude. In all tests from test series no. 1, two-way symmetric cyclic loading was maintained. For increasing amplitudes, an accelerated ratcheting behaviour is observed. The ratcheting rate decreases slightly within the following approximately 100 cycles. A decreasing amplitude causes no further ratcheting. This effect from the order of the cyclic loading is visible in the data from many test series. The largest value of the accumulated volumetric strain from test series no. 1 was recorded for tests 1.5 and 1.6, in which values of $\tau^{\text{ampl}} = 37.5$ and 50 kPa were applied in the first cycle package. A total deviation of ±17.2% was found from the test results.

Figure 5.7b shows the results for test series no. 2 that involved a constant non-zero mean load $\tau^{av} = 25$ kPa and a variable load amplitude $\tau^{\text{ampl}} = 12.5 \rightarrow 25 \rightarrow 37.5 \rightarrow 50$ kPa. As observed in test series no. 1, the rate of accumulated volumetric strain increases significantly with increasing amplitude and slows down while the load amplitude decreases. The higher average load leads to a more considerable accumulated strain than in test series no. 1 with a zero mean load. This results in a total deviation of 8.9%. It has to be noted that test 2.2 failed in the last cycle package. For this reason, this test is not considered in the total deviation of test series no. 2.

Figure 5.7c displays the results for test series no. 3 that involved a variable mean load and a variable load amplitude $\tau^{av} = \tau^{\text{ampl}} = 12.5 \rightarrow 25 \rightarrow 37.5 \rightarrow 50$ kPa. The effect of the load is history is evident from the comparison given in figure 5.7c. Again, ratcheting increases with increasing load, and a shakedown is observed when the cyclic load magnitude decreases. This phenomenon is less pronounced in test series no. 4, figure 5.8a. In the figure, the results for a variable mean load $\tau^{av} = 12.5 \rightarrow 25 \rightarrow 37.5 \rightarrow 50$ kPa and a constant load amplitude $\tau^{\text{ampl}} = 25$ kPa are presented. The lowest level of accumulated strain was measured in these tests. This highlights the effect of load amplitude on the cyclic strain accumulation since the higher-amplitude sequences accumulated higher strains in the respective tests, i.e. figure 5.7.

Figure 5.8b displays the results for test series no. 5 that involved a variable axial stress $\sigma'_{zz} = 50 \rightarrow 100 \rightarrow 150 \rightarrow 200$ kPa and a constant mean load $\tau^{av} = 0$ kPa and amplitude $\tau^{\text{ampl}} = 25$ kPa. A higher strain accumulation is observed at lower axial stress amplitudes. The recorded accumulated volumetric strain differs by ±9.6%.

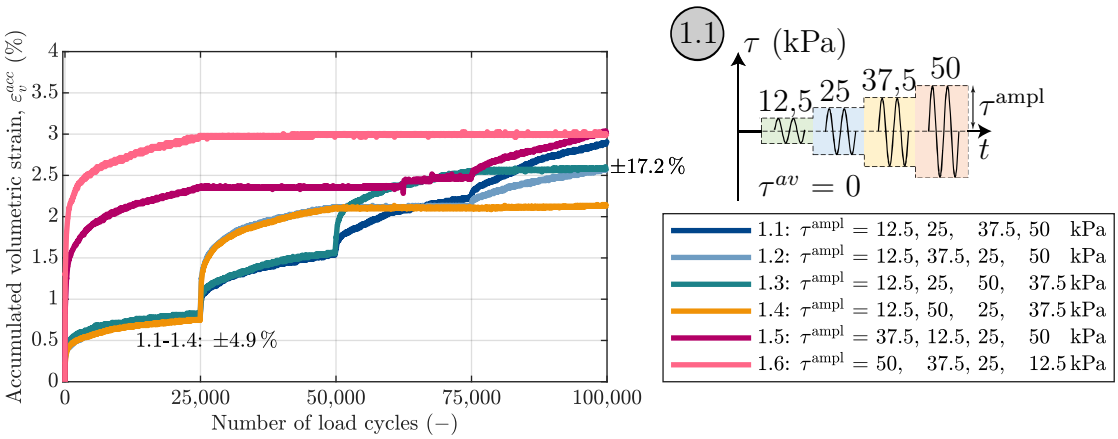

(a) Test series no. 1.

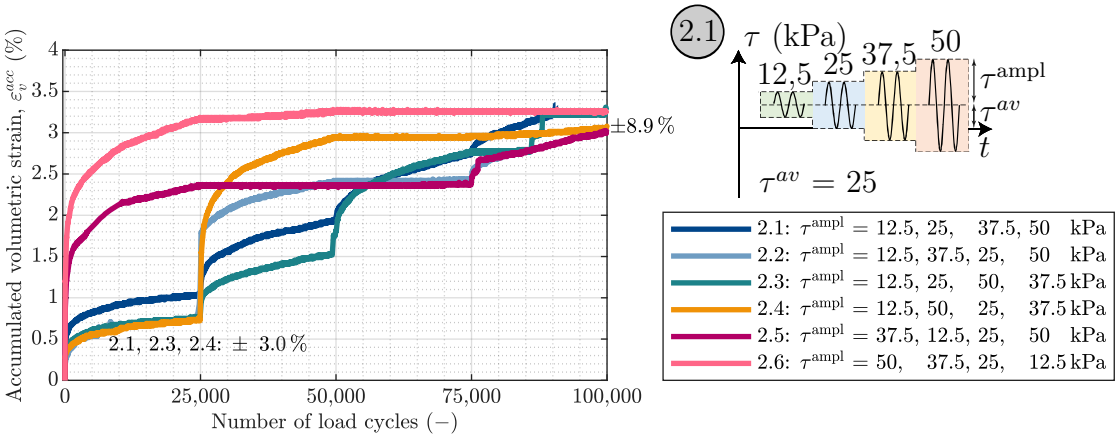

(b) Test series no. 2.

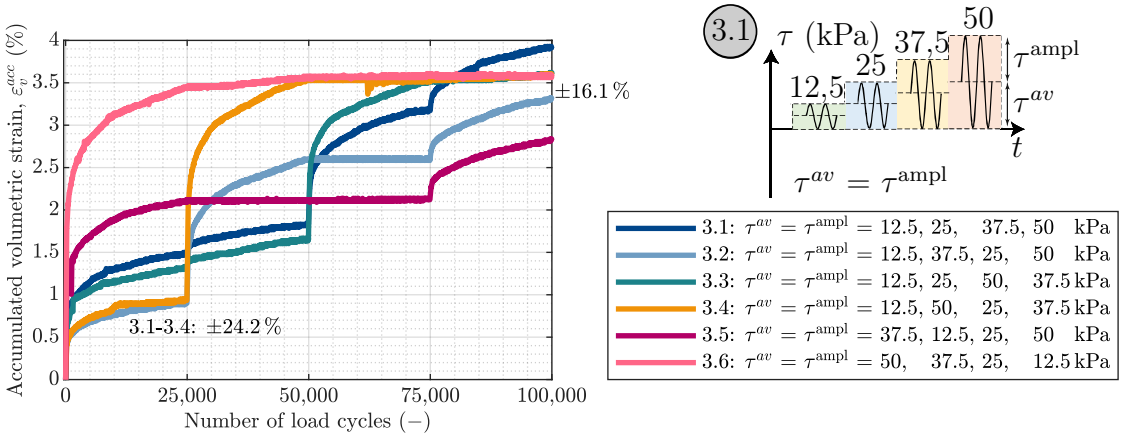

(c) Test series no. 3.

Figure 5.7: Multi-amplitude cyclic test results included in the experimental study on the validity of Miner's rule. The experiments involve: (a) a constant zero mean load $\tau^{av} = 0$ kPa and a variable load amplitude $\tau^{\text{ampl}} = 12.5 \rightarrow 25 \rightarrow 37.5 \rightarrow 50$ kPa, (b) a constant non-zero mean load $\tau^{av} = 25$ kPa and a variable load amplitude $\tau^{\text{ampl}} = 12.5 \rightarrow 25 \rightarrow 37.5 \rightarrow 50$ kPa and (c) a variable mean load and load amplitude $\tau^{av} = \tau^{\text{ampl}} = 12.5 \rightarrow 25 \rightarrow 37.5 \rightarrow 50$ kPa.

Figure 5.8c summarises the results for test series no. 6 which involved a constant mean load $\tau^{av} = 0$ kPa and a variable amplitude $\tau^{\text{ampl}} = 12.5 \rightarrow 25 \rightarrow 37.5 \rightarrow 50$ kPa but with an additional variation of the angle of load application $\alpha = 0 \rightarrow 15 \rightarrow 30 \rightarrow 45°$. The test results reveal an increased ratcheting behaviour compared to test series no. 1 (figure 5.7a), which involved the same load magnitude but uni-directional cyclic loads. This accelerated ratcheting behaviour is also visible in data from multidirectional ng-model tests on monopiles (Rudolph, 2015). However, despite the accumulated strain magnitude, the ratcheting response in both test series shown in figure 5.7a and figure 5.8c is very similar. The variation of the accumulated volumetric strain after 100,000 cycles for test series no. 6 is approximately ±15.9%.

Conclusively, the multi-amplitude cyclic load tests, which involved both a constant and a varying mean load, reveal significant deviations of the accumulated volumetric strain for a large number of load cycles considered in these tests and, thus, provide experimental evidence that the ordering of the cyclic loads matters.

5.5 Waveform streaming

The data obtained from the direct simple shear experiments with waveform streaming are evaluated and analysed in terms of the volumetric strain ε_v. An example of such an irregular cyclic loading test result is shown in Figure 5.9. The horizontal shear stress course over time is visible in figure 5.9 (bottom). This signal has an irregular amplitude and frequency and involves one-way irregular cyclic loading. The graph shows three global peaks, indicated by arrows and labelled as (A), (B), and (C) in the figure. The evolution of the volumetric strain recorded during the test is included in figure 5.9 (top).

Initially, the volumetric strain increases steadily, and a distinct settlement of the sample is measured. At the first load peak (A) at which a double amplitude of $2\tau^{\text{ampl}} \approx 30$ kPa occurs, the volumetric strain increases rapidly, followed by a significant decrease in the deformation rate. After the first global peak, the evolution of the volumetric strain flattens until peak (B) from the wave load signal, with a double amplitude of similar magnitude, occurs. Peak (B) causes a slight discontinuity in the course of the volumetric strain, such as peak (C), the last peak within the load sequence.

Hence, the most significant effect from the irregular cyclic loading is the rapid increase caused by the first peak load in a load sequence, as considered in more detail in the following sections. The repeatability and comparability of the test results of the direct simple shear tests with irregular cyclic loading are explained below.

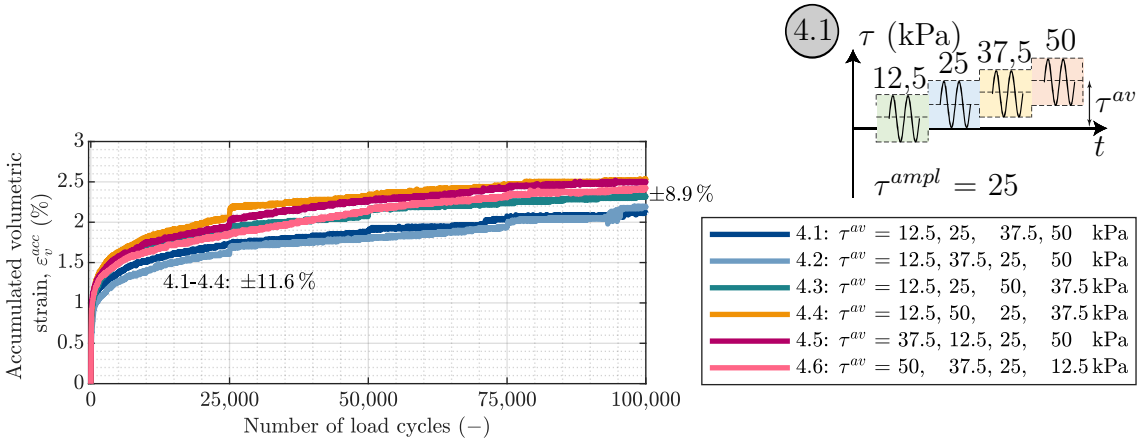

(a) Test series no. 4.

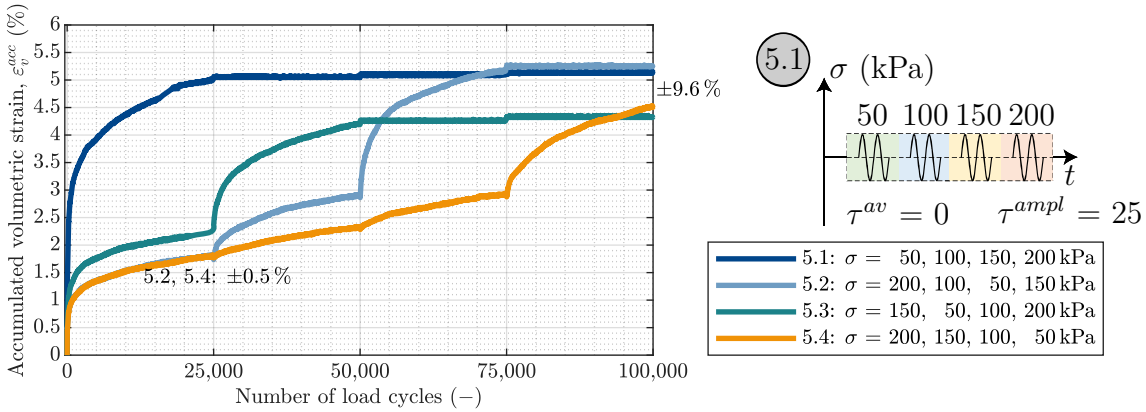

(b) Test series no. 5.

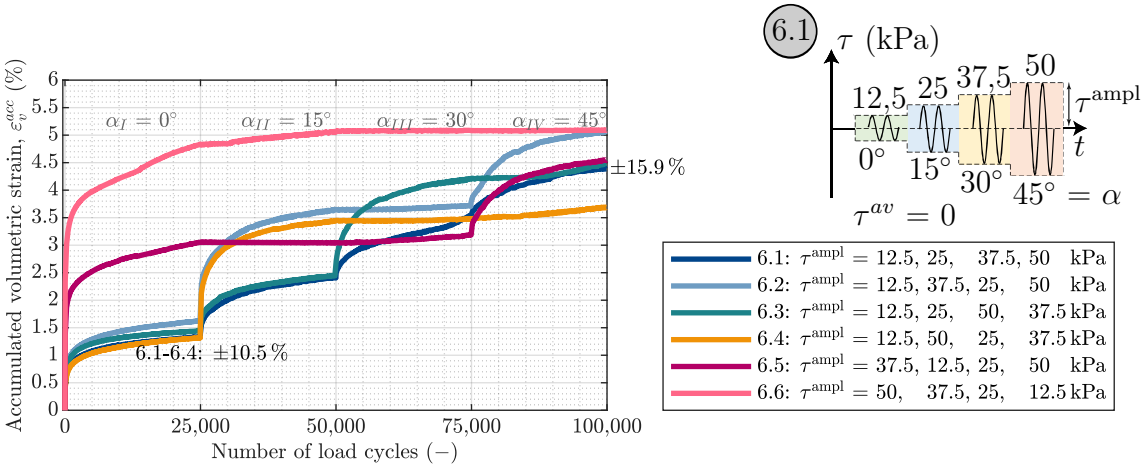

(c) Test series no. 6.

Figure 5.8: Multi-amplitude cyclic test results included in the experimental study on the validity of Miner's rule (continued). The experiments involve: (a) a variable mean load $\tau^{av} = 12.5 \rightarrow 25 \rightarrow 37.5 \rightarrow 50$ kPa and a constant load amplitude $\tau^{\text{ampl}} = 25$ kPa, (b) a variable axial stress $\sigma'_{zz} = 50 \rightarrow 100 \rightarrow 150 \rightarrow 200$ kPa and (c) stepwise polarisation changes $\alpha = 0 \rightarrow 15 \rightarrow 30 \rightarrow 45°$.

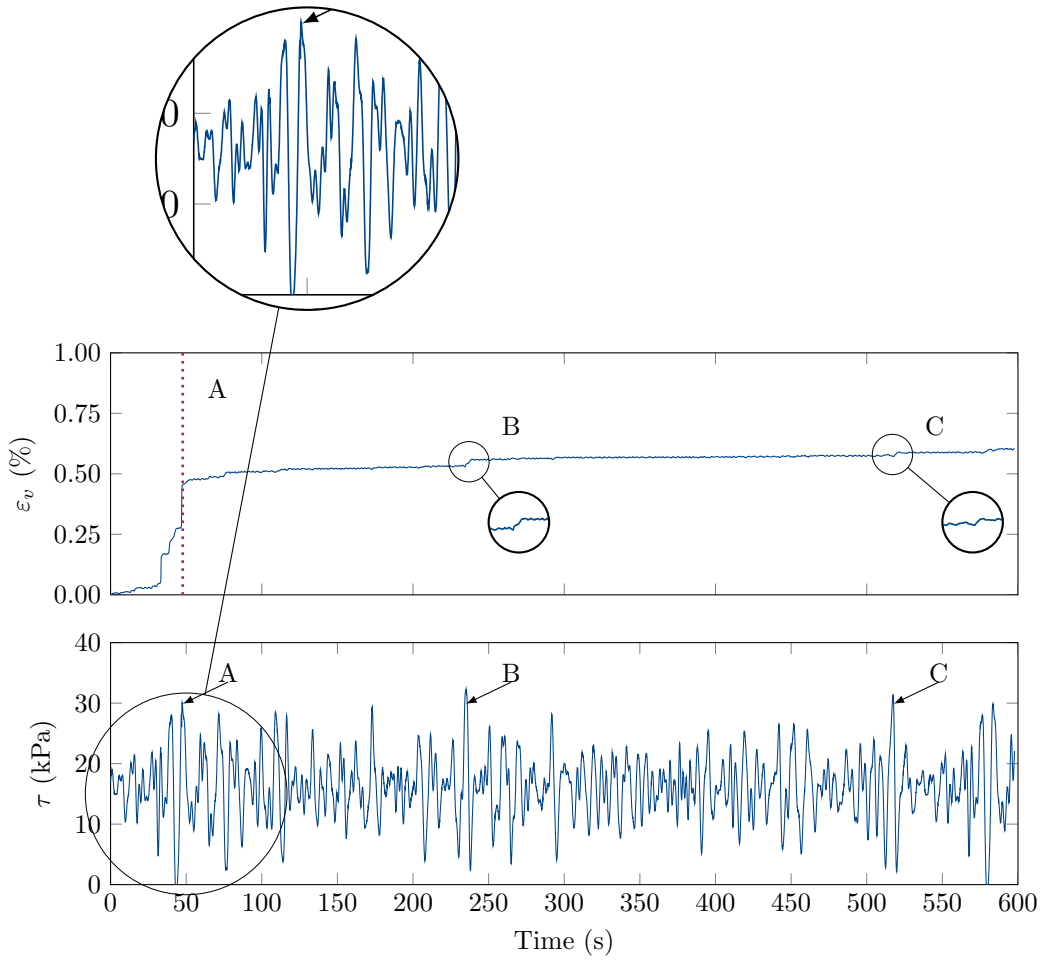

Figure 5.9: Example of direct simple shear test results with irregular cyclic loading: (top) measured volumetric strain ε_v and (bottom) shear stress τ over time.

Repeatability of the irregular cyclic loading tests

For the purpose of comparing the results of direct simple shear tests with different wave load scenarios, the results have to be comparable and repeatable. Figure 5.10 shows the results of this study. The repeatability of the irregular cyclic load test results is shown by comparing the volumetric strain of different tests on the same soil conditions in different samples and tested at the same load scenario. The results of the irregular cyclic load tests of four tests are shown in figure 5.10. The figure depicts the volumetric strain ε_v, figure 5.10 (top), and the horizontal shear stress τ over time, figure 5.10 (bottom). The differences in the results are small. The peak load, indicated in the figure by an orange circle, causes a sudden increase in the volumetric strain in all four tests. Thus, comparability and repeatability of the irregular cyclic load test results are proven.

Influence of load scenario on irregular cyclic loading test results

The figures 5.11, 5.12 and 5.13 show the course of the volumetric strain measured in six irregular cyclic load tests. Each test involved a different wave load sequence. Obviously, there is a significant effect of the peak loads of the irregular cyclic loading. For instance, in figure 5.11a, the volumetric strain approximately doubled at the peak load, indicated by the vertical red dotted line. Only marginal permanent strains develop after this peak load, which is considered to be due to densification effects and grain redistributions. Thus, the effect of the stress history is evident from the test results. While the load maxima cause inevitable damage in the soil, smaller cycles are considered to have beneficial densification effects. It follows that the magnitude of the permanent strain recorded in an irregular cyclic test depends on the total maximum load in a loading series and the pre-load that the soil has experienced. Thus, when a second peak of higher amplitude follows a first peak, it rapidly reaccelerates the evolution of the volumetric strain, compare wave loads no. 3, 4 and 6 (cf. figure 5.12 and figure 5.13b).

Conclusively, the figures 5.11, 5.12 and 5.13 support the following observations:

- The magnitude of the permanent strain recorded in an irregular cyclic test depends on the total maximum load in a load series relative to its pre-loading history.
- Subsequent smaller loads may act beneficial and do not necessarily accumulate further permanent strains.
- Thus, the stress history impacts the dynamic soil behaviour: at the same time, low-amplitude cyclic loads may act beneficially and enhance the overall soil stiffness, while peak loads cause obvious damage to the soil.
- The realistic irregular cyclic load tests show a significant deviation in the total volumetric stain of approximately $\pm 44.2\,\%$. This indicates a wide range of variability and suggests that simplifying irregular cyclic loads may be necessary to make them applicable in the design process.

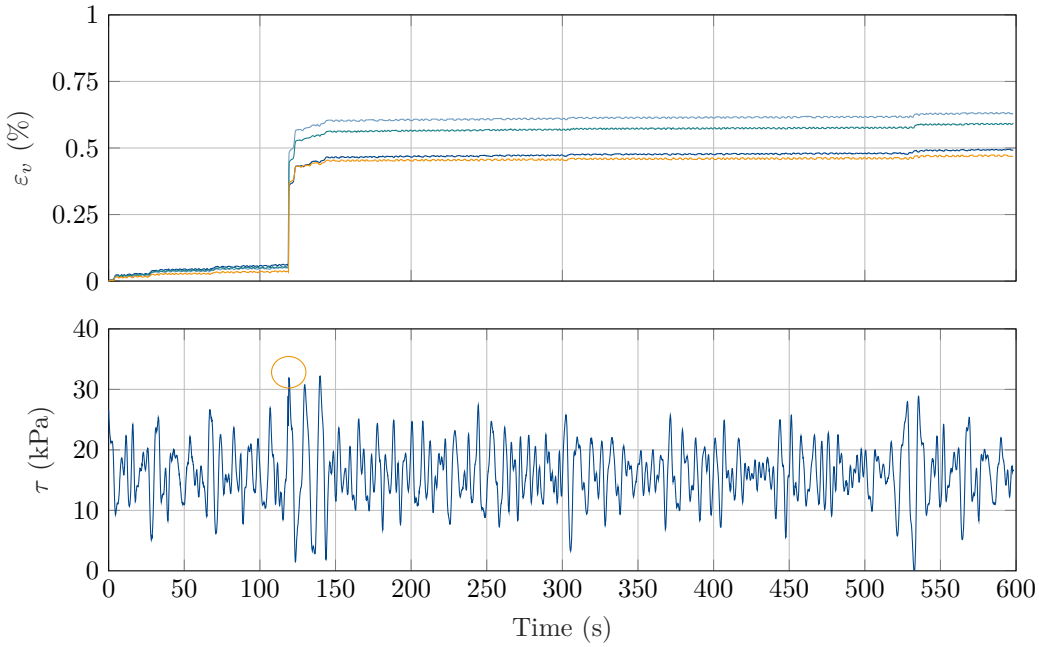

Figure 5.10: Repeatability of direct simple shear tests with waveform streaming.

5.6 Influence of stepwise polarisation changes

In order to investigate the effect of stepwise polarisation changes, a supplementary series of high cyclic direct simple shear experiments was performed. The tests involved a constant mean load and load amplitude, $\tau^{ampl} = \tau^{av} = 25$ kPa and a varying polarisation angle between cycle packages. Please note that the polarisation refers to the initial loading direction and is kept constant during a cycle package. To illustrate the influence of a varying angle at which an applied load affects the ratcheting behaviour, the accumulated shear strain is evaluated in terms of γ_{xz}^{acc} and γ_{yz}^{acc}. Perspectivewise, this corresponds to a top view of the sample in the direct simple shear device. The results are shown in figure 5.14, 5.15 and 5.16 and involve different polarisation angles $\alpha = 0° \rightarrow 15° \rightarrow 30° \rightarrow 45°$, $\alpha = 0° \rightarrow 30° \rightarrow 60° \rightarrow 90°$ and $\alpha = 0° \rightarrow 45° \rightarrow 90° \rightarrow 135°$. The ordering of the angle of load application varies threefold. A total number of 100,000 load cycles was envisaged in each test.

Figure 5.14a shows the results of stepwise polarisation changes of $\alpha = 0° \rightarrow 15° \rightarrow 30° \rightarrow 45°$ (test series no. 7.1). The test series is obtained for a polarisation angle, which is increased by $+15°$ in each load package. The first load package shows an evident accumulation of shear strain in the x-direction, with a slight drift in the y-direction. Since the load was applied to the x-direction, the deviating shear in the y-direction could be explained by inhomogeneous stress conditions within the sample and/or at the sample edges. Only a minor accumulation of shear strain in the x-direction is observed during the following

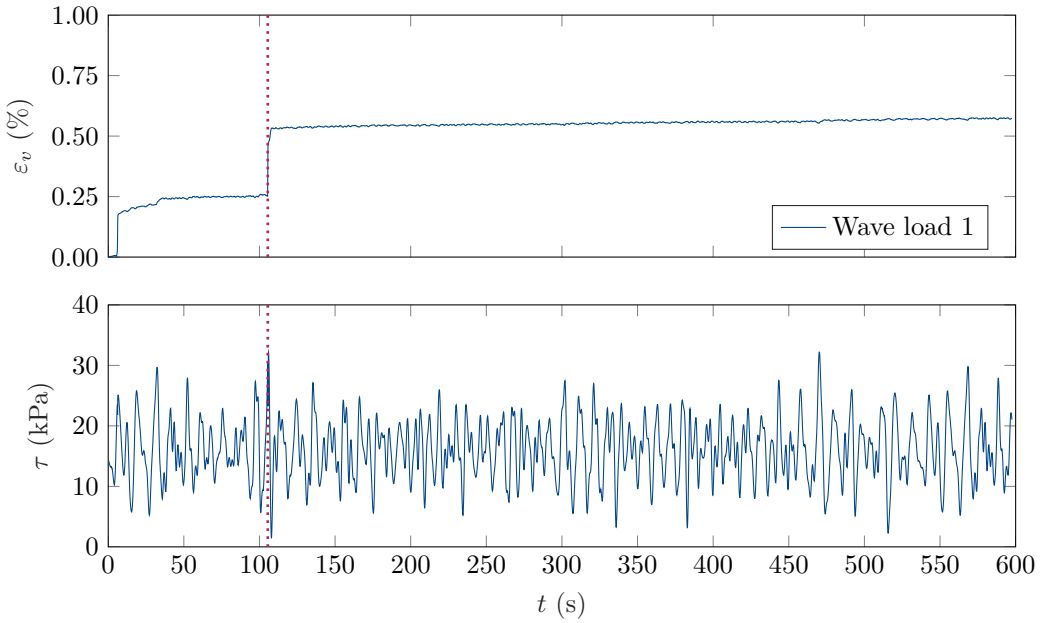

(a) Wave load no. 1.

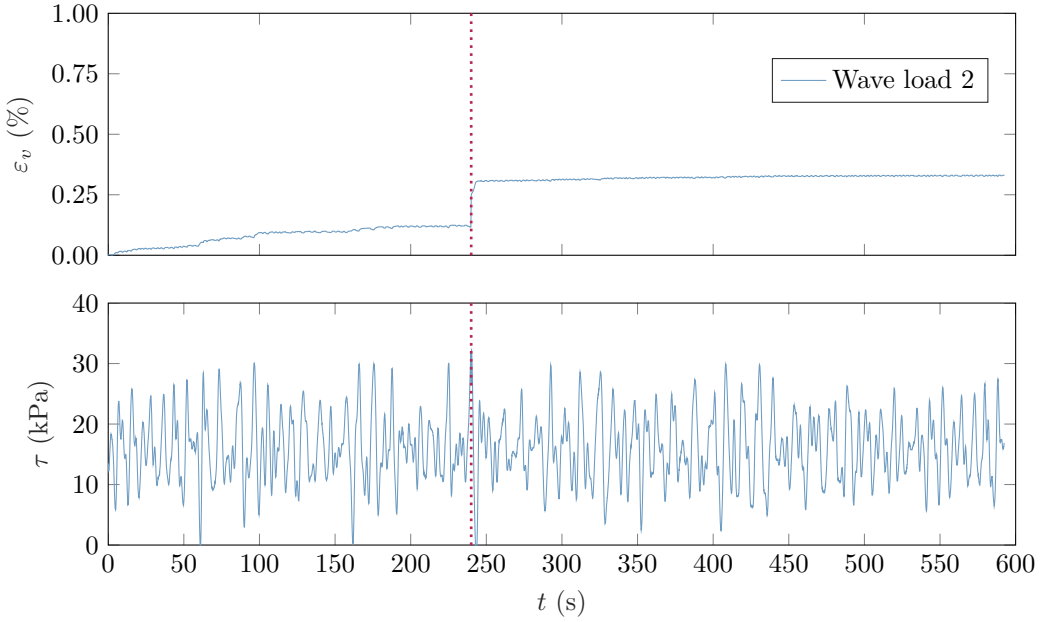

(b) Wave load no. 2.

Figure 5.11: Irregular cyclic load test results for very fine silica sand on a medium dense sample with $\sigma'_{zz} = 100$ kPa: measured volumetric strain during the irregular cyclic load test (top) and shear stress τ over time (bottom).

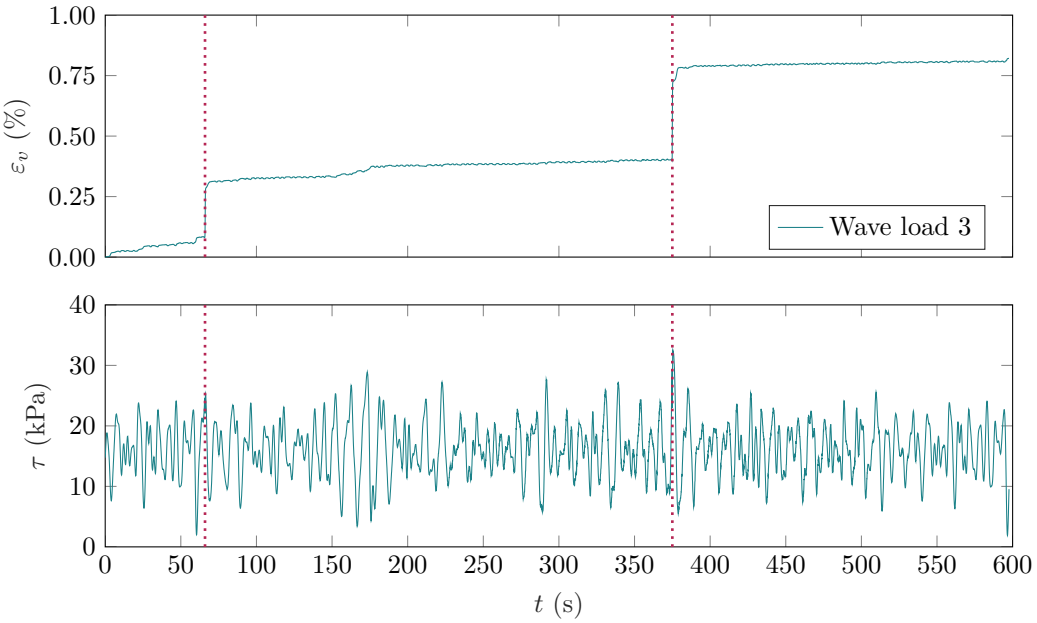

(a) Wave load no. 3.

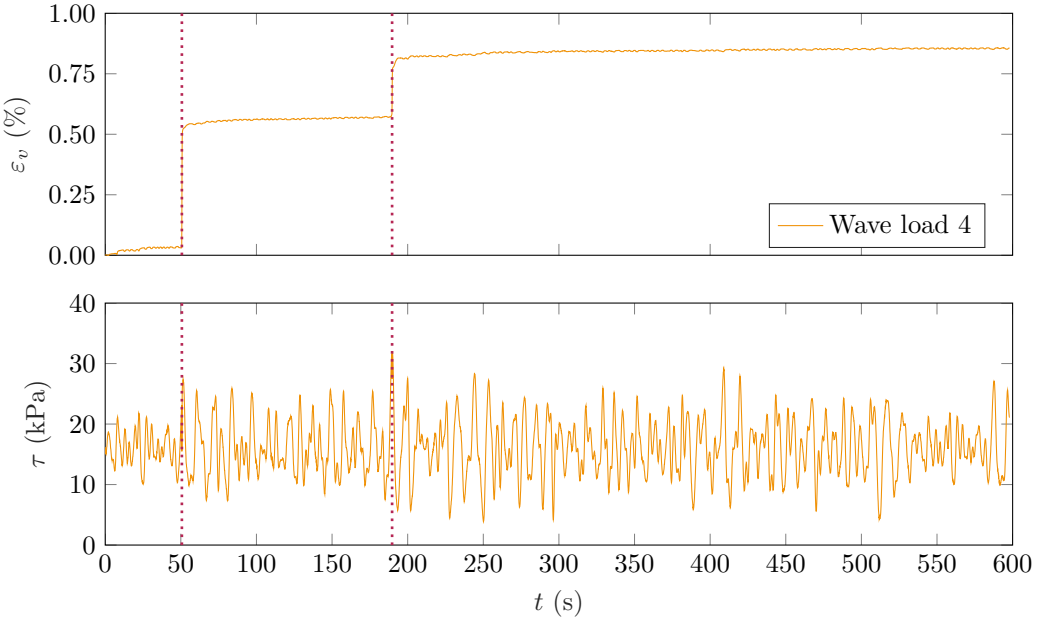

(b) Wave load no. 4.

Figure 5.12: Irregular cyclic load test results for very fine silica sand on a medium dense sample with $\sigma'_{zz} = 100$ kPa (continued): measured volumetric strain during the irregular cyclic load test (top) and shear stress τ over time (bottom).

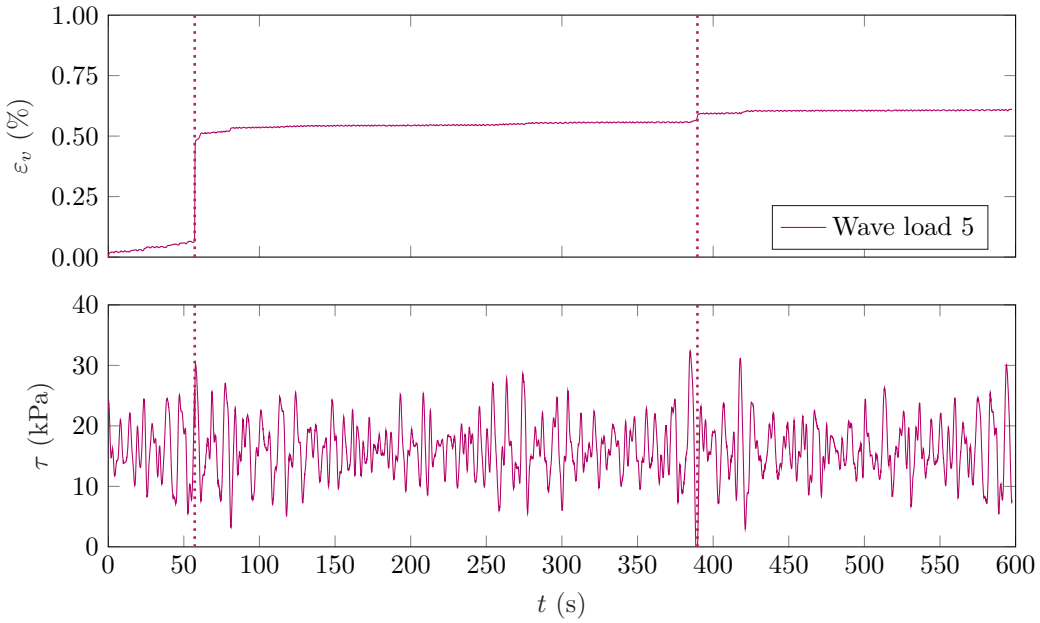

(a) Wave load no. 5.

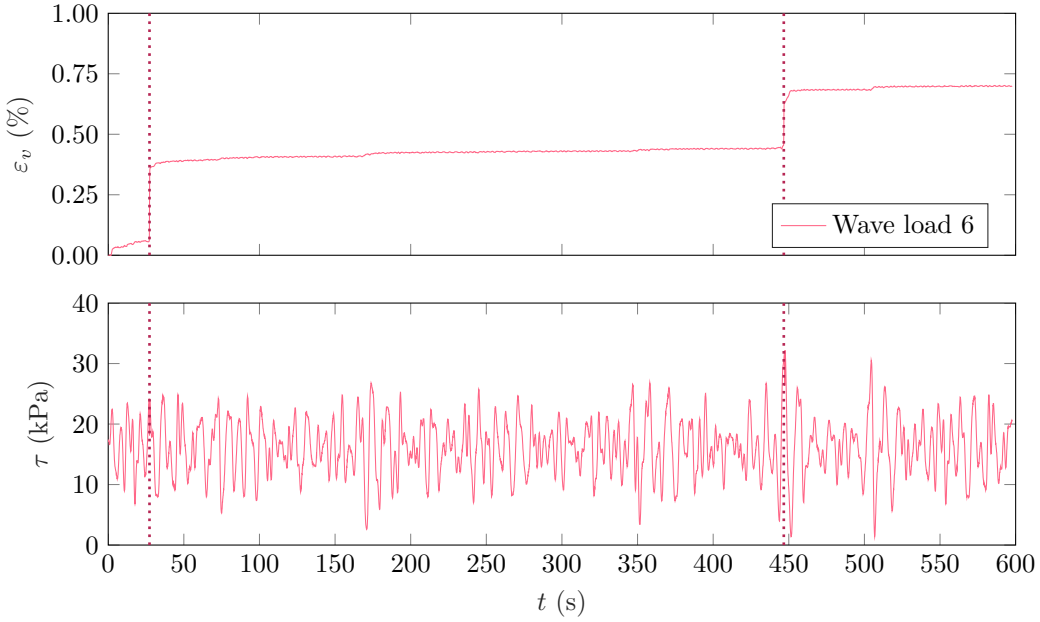

(b) Wave load no. 6.

Figure 5.13: Irregular cyclic load test results for very fine silica sand on a medium dense sample with $\sigma'_{zz} = 100$ kPa (continued): measured volumetric strain during the irregular cyclic load test (top) and shear stress τ over time (bottom).

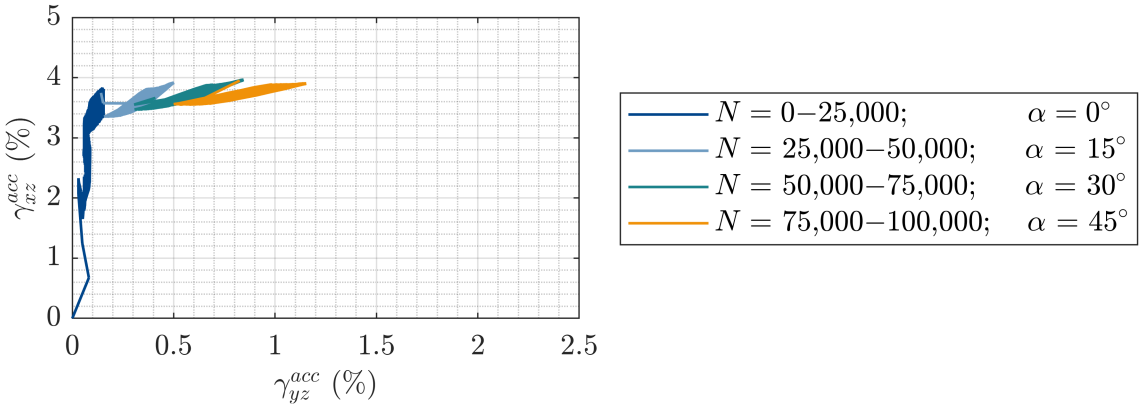

(a) Test series no. 7.1.

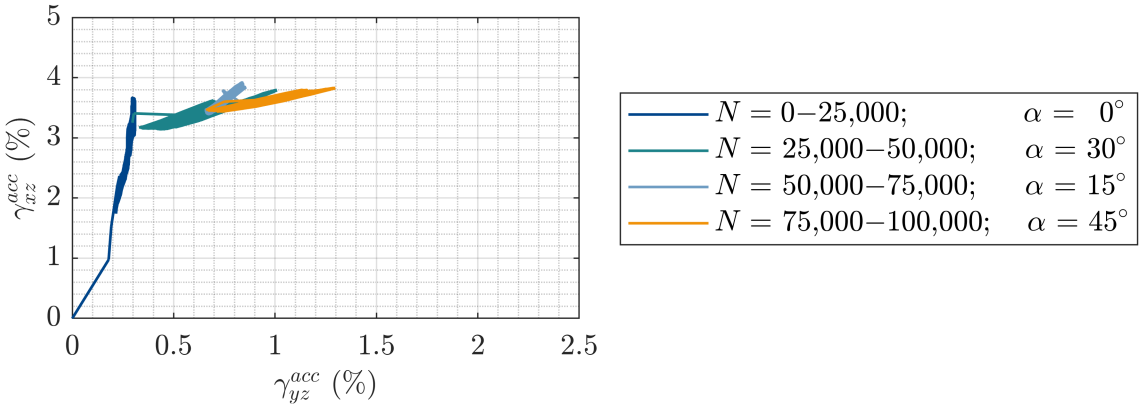

(b) Test series no. 7.2.

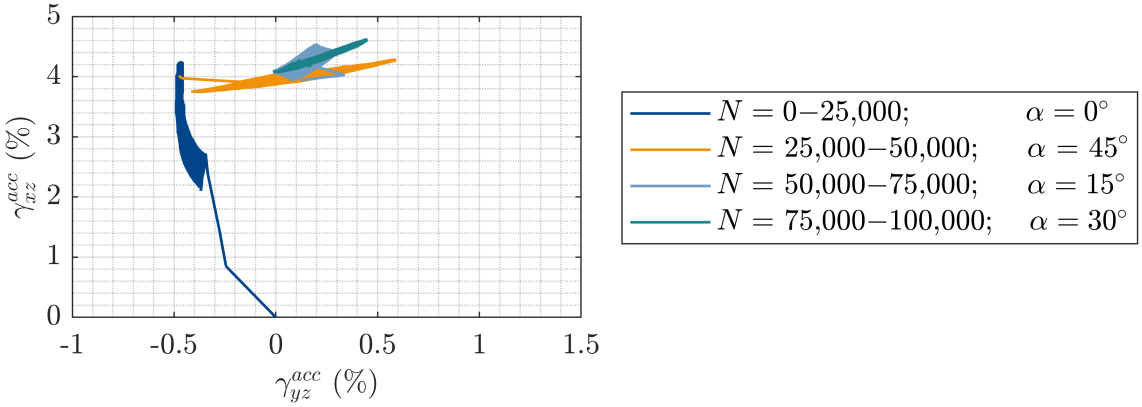

(c) Test series no. 7.3.

Figure 5.14: Comparison of cyclic shear strain accumulation due to stepwise polarisation changes. The experiments involve a constant mean load and load amplitude of $\tau^{\text{ampl}} = \tau^{av} = 25$ kPa and a variable polarisation angle (a) $\alpha = 0° \rightarrow 15° \rightarrow 30° \rightarrow 45°$, (b) $\alpha = 0° \rightarrow 30° \rightarrow 15° \rightarrow 45°$ and (c) $\alpha = 0° \rightarrow 45° \rightarrow 15° \rightarrow 30°$.

load packages. However, it is evident that the shear strain accumulation in the y-direction increases with each of the following cycle packages, and the orientation of the strain loops rotates in line with the load application angle.

Figure 5.14b depicts the test results of test series no. 7.2 for polarisation angles of $\alpha = 0° \rightarrow 30° \rightarrow 15° \rightarrow 45°$. An increasing ratcheting behaviour is observed in the second cycle package due to the higher polarisation angle of 30° compared to test no. 7.1, where the polarisation was 15°. As the polarisation angle increases, the strain amplitude becomes larger, significantly altering the shape of the strain loops. Unlike in test series no. 7.1, an ascending and descending polarisation angle of $\alpha = 0° \rightarrow 30° \rightarrow 15° \rightarrow 45°$ is considered in test series no. 7.2. After reducing the polarisation angle to 15° in the third load package, increased ratcheting in the x-direction is observed. Similarities between the strain loops of the last load package and those of the previous experiment are evident.

The test results of test series no. 7.3 are shown in Figure 5.14c. This test series involves polarisation angles of $\alpha = 0° \rightarrow 45° \rightarrow 15° \rightarrow 30°$. The load sequence is characterised by an increasing, then decreasing and again increasing polarisation angle. A higher shear strain accumulates in the x-direction when compared to test series no. 7.1 and 7.2.

These experiments with α ranging from 0° to 45° allow for two main observations. First, it was found that the ratcheting develops in the direction of load application. Second, a significant effect of the pre-strain is observed since the ratcheting following a polarisation change develops in the direction of the previously undisturbed sample. The response in tests with higher polarisation angles of $\alpha = 0° \rightarrow 30° \rightarrow 60° \rightarrow 90°$ (figure 5.15) and $\alpha = 0° \rightarrow 45° \rightarrow 90° \rightarrow 135°$ (figure 5.16) is consistent with these obersations. In addition, these high-angle polarisations show how the shape of the strain loops become more altered for larger polarisation changes. This is clearly visible in figure 5.16b and 5.16c which include polarisation changes of $\alpha = +90°$ and $\alpha = +135°$.

Further, it is observed that the strain loops in many tests presented in figures 5.14 to 5.16 have in common small overlap areas. This suggests that the sample is deformed in a new way every time there is a change in the angle of load application. This highlights the importance of the loading history and cyclic pre-loads, indicating a rearrangement of particles during repetitive loading.

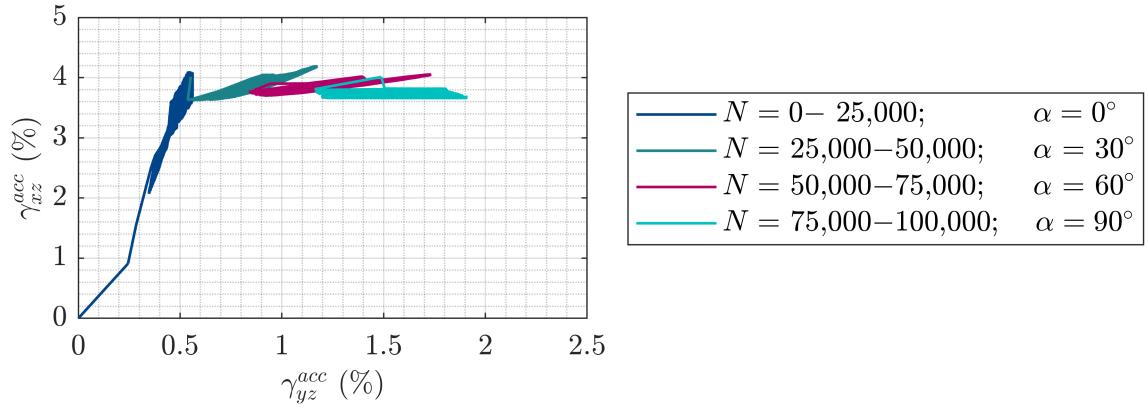

(a) Test series no. 7.4.

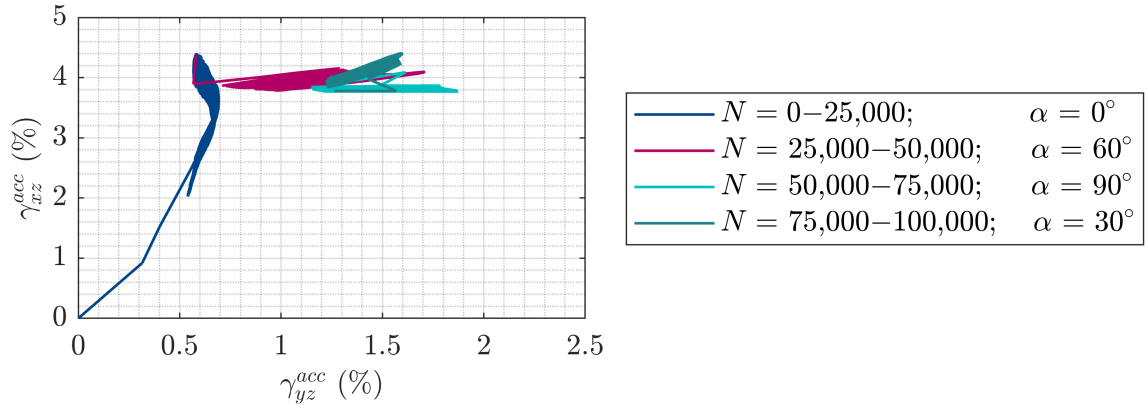

(b) Test series no. 7.5.

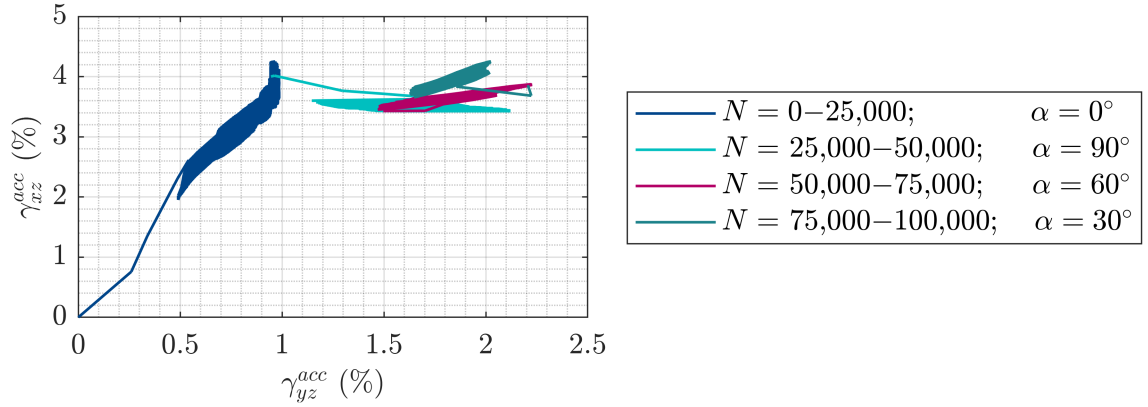

(c) Test series no. 7.6.

Figure 5.15: Comparison of cyclic shear strain accumulation due to stepwise polarisation changes. The experiments involve a constant mean load and load amplitude of $\tau^{\text{ampl}} = \tau^{av} = 25$ kPa and a variable polarisation angle (a) $\alpha = 0° \rightarrow 30° \rightarrow 60° \rightarrow 90°$, (b) $\alpha = 0° \rightarrow 60° \rightarrow 90° \rightarrow 30°$ and (c) $\alpha = 0° \rightarrow 90° \rightarrow 60° \rightarrow 30°$.

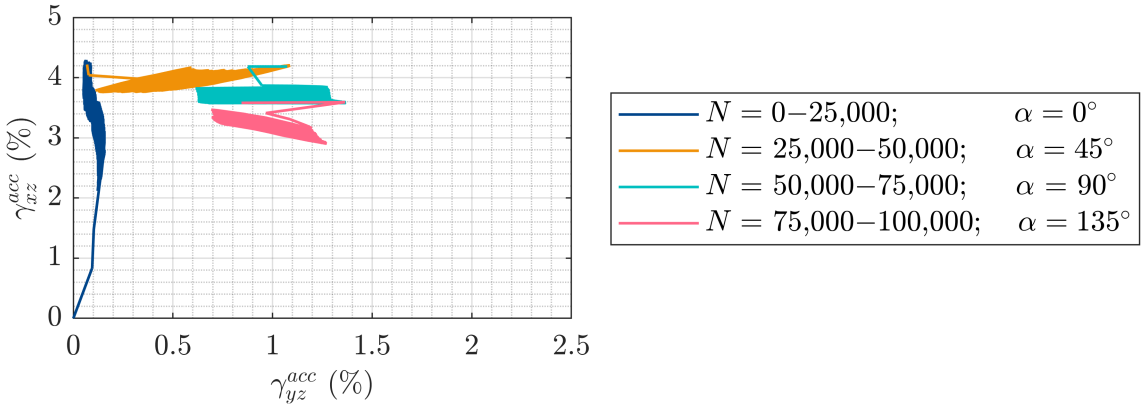

(a) Test series no. 7.7.

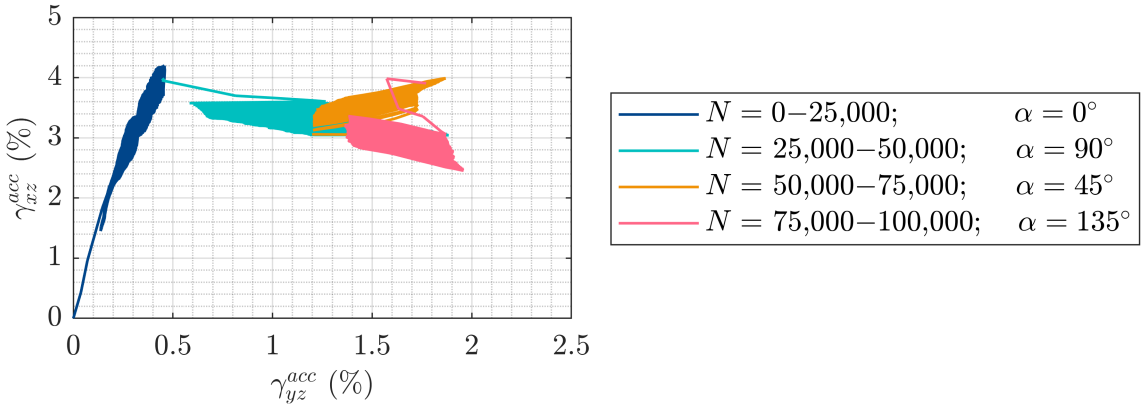

(b) Test series no. 7.8.

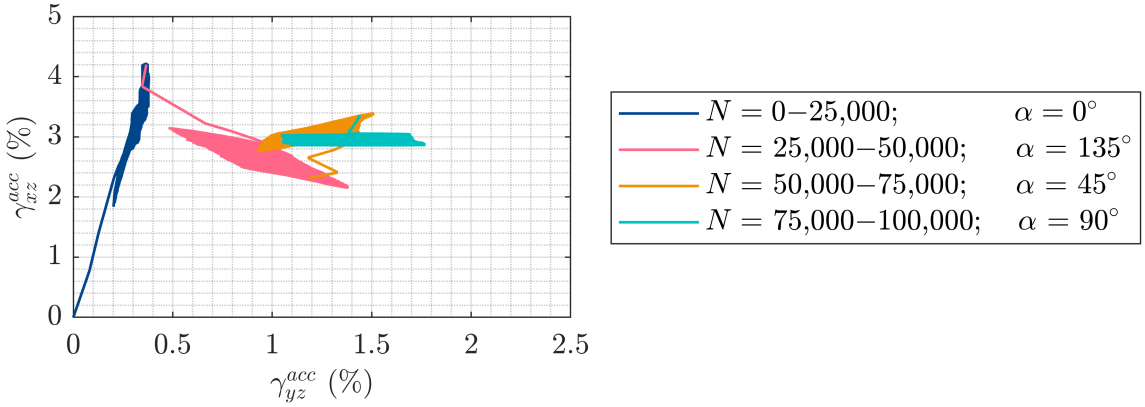

(c) Test series no. 7.9.

Figure 5.16: Comparison of cyclic shear strain accumulation due to stepwise polarisation changes. The experiments involve a constant mean load and load amplitude of $\tau^{\text{ampl}} = \tau^{av} = 25$ kPa and a variable polarisation angle (a) $\alpha = 0° \rightarrow 45° \rightarrow 90° \rightarrow 135°$, (b) $\alpha = 0° \rightarrow 90° \rightarrow 45° \rightarrow 135°$ and (c) $\alpha = 0° \rightarrow 135° \rightarrow 45° \rightarrow 90°$.

5.7 Hydrodynamic loading vs. design load cases

Concluding the investigations on the validity of Miner's rule, this section sheds light on the research question of whether it is appropriate to simplify nonlinear load signals using classification methods. The discussion involves the experimental studies presented in section 5.4 and 5.5 and contrasts the investigations on the response of pile and soil to hydrodynamic loading and design load cases.

The effect of the ordering of different cycle packages was investigated in high cyclic direct simple shear experiments on non-cohesive soil under drained conditions. Different load scenarios of one-way and two-way symmetric and unsymmetric cyclic loading were investigated, including a constant and a varying mean load. Further, the effect of a varying axial confining pressure and of stepwise polarisation changes was within the scope of testing.

Figure 5.17 summarizes the results of the multi-amplitude cyclic load test results in a boxplot and displays the deviation of the accumulated volumetric strain after 100,000 load cycles for each test series discussed in section 5.4 separately. The red dots represent

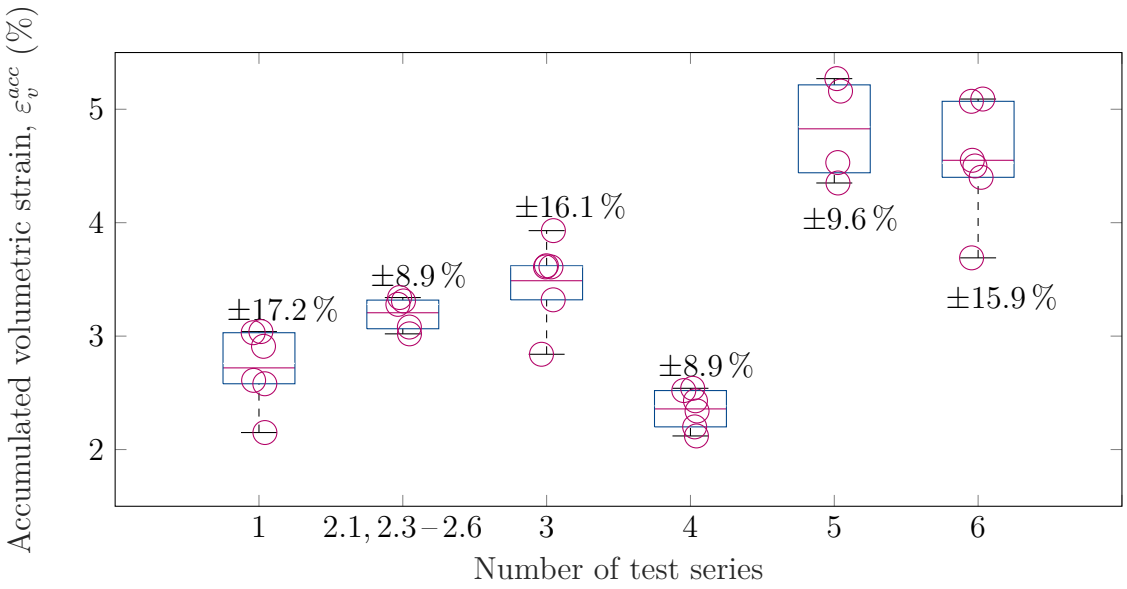

Figure 5.17: Overview of the deviation of the volumetric strain after 100,000 load cycles in the multi-amplitude cyclic load tests.

the resulting volumetric strains in each test. The red line represents the average value of this data, and the blue box covers 50 % of the test data. A maximum value 17.2 % deviation of the accumulated volumetric strain is found from the test results. Evidently, the multi-amplitude cyclic load tests reveal a significant effect of the ordering of the cyclic loads in terms of the accumulated volumetric strain.

In addition, the test results indicated that the magnitude of ratcheting developing in a cycle package depends on the total maximum load applied to the soil in relation to the previous loading history. This brings into play the load differences compared to a previously experienced maximum load. Hence, an ascending order of cycle packages leads

to an accelerated ratcheting behaviour at the beginning of each cycle package. In contrast, a descending order of cycle packages does not necessarily accumulate further strains after the initial load parcel.

In order to understand what happened on the way to 100,000 cycles and to further investigate whether the loading scenarios are comparable, an additional test series involving irregular wave load signals was conducted, compare section 5.5. The results of all irregular cyclic load tests are shown in figure 5.18. The final volumetric strain differs by ±44.2 %. Contrasting previous investigations, the load scenarios varied constantly while the underlying energy spectrum remained constant. The experiments confirmed that an increased accumulation of volumetric strain naturally accompanies the load maxima of a load sequence. The magnitude of permanent strain developing during such a peak load is found to be highly dependent on the previous loading history, i.e. the pre-load involved in each particular load sequence.

Conclusively, the presented findings underpin, that the ordering of cycle packages does influence the cyclic deformation accumulation. Significant deviations of the accumulated volumetric strain were found for different combinations of cycle packages. However, simplifying nonlinear waveform load signals through classification methods is necessary to make highly irregular loads useful for the designer. Attention should be given when idealising regular cycle packages with constant cyclic properties. However, in view of the soil's spatial variability, this procedure is considered acceptable when providing an overall reliable and conservative design.

5.8 Summary

This chapter discussed a series of direct simple shear experiments on granular soil. The experiments were employed to assess the effect of ordering of cycle packages on the ratcheting evolution and investigated the soil behaviour under irregular loading and from variable directions. The presented experimental investigations support the following findings:

- The multi-amplitude cyclic tests, which involved 100,000 load cycles at both a constant and varying mean load, reveal a significant effect of the ordering of cycle packages on the accumulated volumetric strain, suggesting that the damage of the soil depends on the load sequence.
- Targeting the effect of irregular load sequences, peak loads play a significant role, indicating that the magnitude of permanent strain that develops due to such a peak load is highly dependent on the pre-load involved in each particular load sequence and the previous loading history. Relating to the design process, this observation can justify the frequent use of monotonic design loads (Richards et al., 2020).
- The ratcheting occurs in the direction of load application. Additional pre-loading effects are demonstrated from the multidirectional cyclic load tests, indicating significant particle rearrangements in each polarisation step.

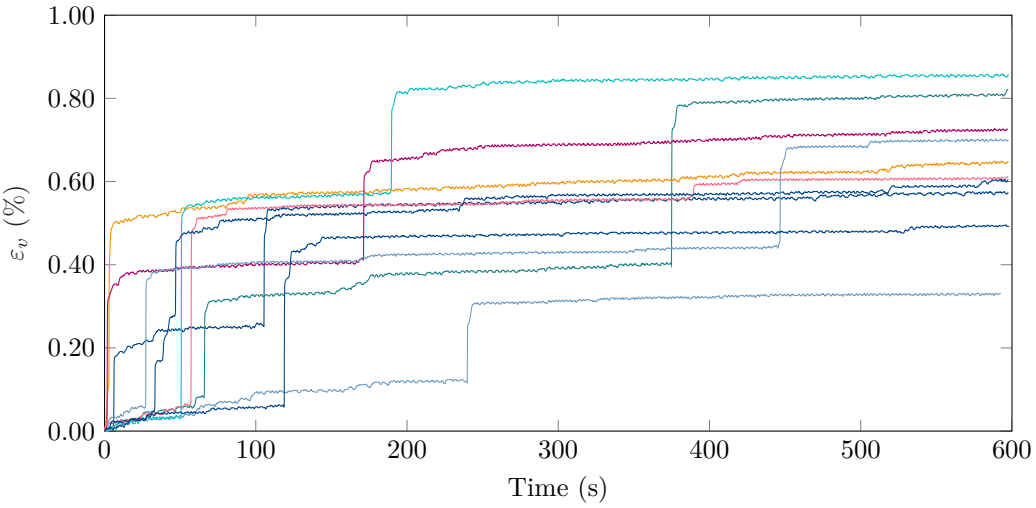

Figure 5.18: Results of irregular cyclic direct simple shear experiments for very fine silica sand on a medium dense sample with an axial stress of $\sigma'_{zz} = 100$ kPa. A total deviation of $\pm 44.2\,\%$ is found from the test results.

6 A p-y model for sand

Offshore wind turbine structures experience many load cycles during their lifetime. Numerical modelling of those high cyclic boundary value problems is challenging. On the one hand, there is a need for advanced numerical models that can describe cyclic deformation accumulation precisely and depict stiffness degradation mechanisms. On the other hand, those numerical simulations are highly time-consuming and computationally complex. P-y models can significantly reduce the computation demand compared to finite element simulations, particularly in practical offshore pile design where time efficiency is critical.

The concept of p-y models is based on a beam on an elastic foundation, originally proposed by Winkler (1867). In subgrade reaction modelling, the elastic foundation in Winkler's initial model is replaced with nonlinear load-deflection curves, known as p-y curves. The p-y curves represent the response of the surrounding soil and depict the nonlinear soil-structure interaction. A subgrade reaction model may comprise either a single rheological element or a combination of rheological elements, such as springs or viscous dampers, that describe specific soil reaction components.

This thesis investigates whether it is possible to describe the cyclic and dynamic pile-bearing behaviour using a p-y model. Figure 6.1 illustrates the different steps in the model development process. Following the objectives of this thesis formulated earlier in chapter 3, the main idea of the model is to represent relevant aspects and mechanisms of cyclic and dynamic pile-bearing behaviour. Thus, those are identified in the first phase of model development. Second, boundary conditions, acting forces and relevant mechanical properties are described for an infinite soil volume in the nearfield of the pile. Based on this mechanical approach a 1D mathematical description of the expected stress-strain response will be derived. Finally, the model components, i.e. the p-y element, and the global model behaviour, are verified and validated.

This chapter presents a p-y model that combines cyclic and dynamic pile-bearing behaviour of monopile foundations subjected to lateral loading in sand. First, the p-y model formulation is described in detail in section 6.1. Second, the model behaviour and sensitivity to certain parameters are studied in a sensitivity analysis in section 6.2. Following this, the pile response to lateral loading is verified for exemplary load cases (ref. section 6.3). Section 6.4 concludes the chapter with a discussion on model limitations that must be considered in further applications of the p-y model in chapter 7.

The contents of chapter 6 and 7 were partly published in Hagemann and Grabe (2019), Stark and Grabe (2021), Stark and Grabe (2022), and Stark and Grabe (2023).

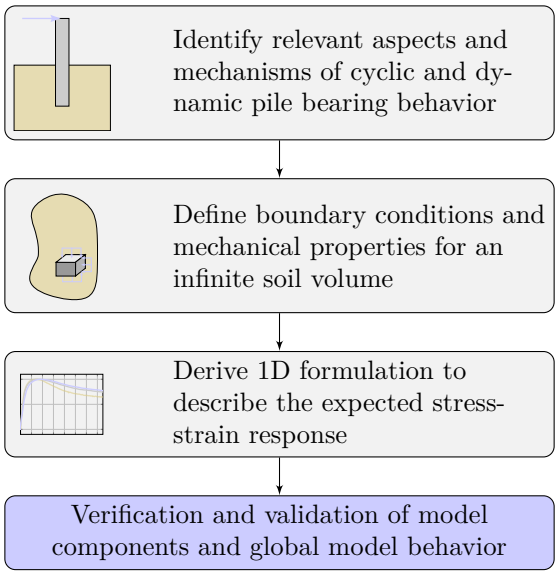

Figure 6.1: Process steps in p-y model development.

6.1 Model formulation

Existing approaches for numerical modelling of the cyclic load-deflection behaviour of piles mainly rely on neglecting inertia forces in the low-frequency range and therefore represent purely cyclic behaviour (ref. section 2.4). Time-dependent impacts resulting from wind and wave loading can include high-frequency load components followed by a mobilisation of inertia forces due to the mass distribution of the structure. As the model presented herein is intended to account for high cyclic as well as dynamic loading scenarios an all-embracing formulation of the equations of motions is chosen, including inertia forces.

Figure 6.2 illustrates the main components of the p-y model. The horizontal load H applied at the pile head is transferred to the soil via the lateral bedding of the pile in the soil. The pile is modelled using a finite element model consisting of an Euler-Bernoulli beam embedded on a series of nonlinear spring elements and parallel viscous dampers. The pile is discretised with structure elements of a constant height Δz. Each element has two translational and one rotational degree of freedom. Accordingly, normal and transverse forces and bending moments can be transmitted. The pile is modelled with a linear-elastic material behaviour expecting only small pile deflections and stresses below the yield strength and no plastic deformations during loading. The material parameters are chosen with a Young's modulus of $E = 210 \cdot 10^6$ kN/m^2 and a density of $\rho = 7.85$ kN/m^3 according to steel. System characteristics like axial and bending stiffness are derived from the material parameters and pile dimensions.

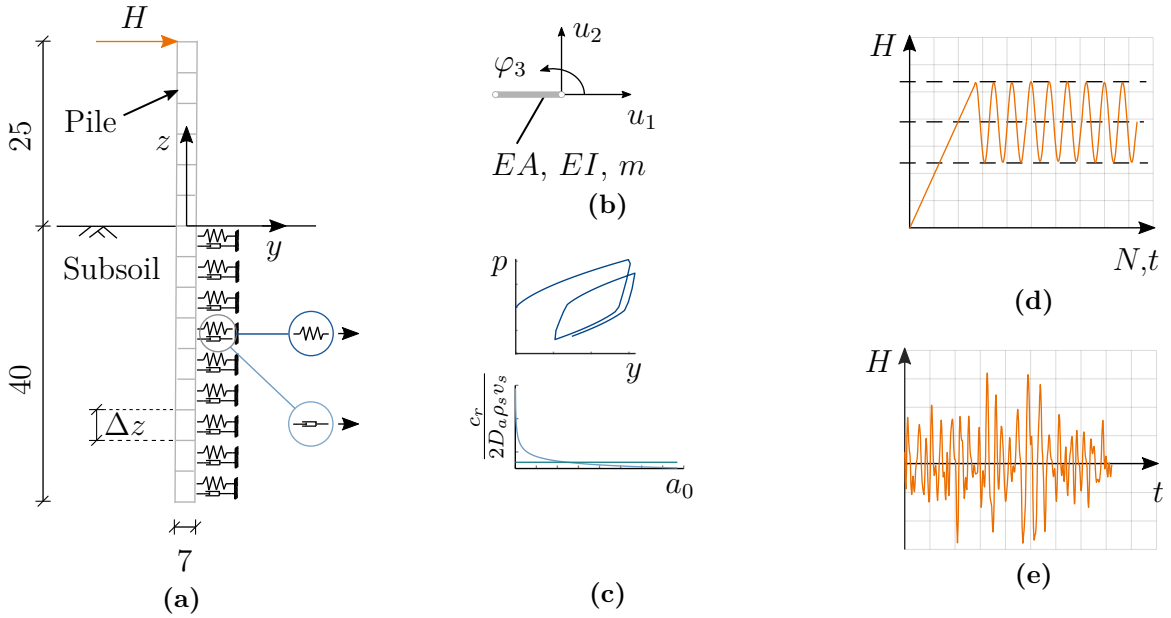

Figure 6.2: Illustration of the main components of the p-y model: (a) pile dimensions, discretization and spring-dashpot arrangement, (b) two-dimensional beam element: degrees of freedom and material properties, (c) nonlinear p-y spring element and frequency-dependent damping coefficient, (d) time series of horizontal cyclic loading and (e) a wave loading scenario. (All values are given in m unless stated otherwise.)

6.1.1 Numerical integration of the nonlinear dynamic equation of motion

The motion behaviour of the system can be described using the nonlinear dynamic equation of motion:

$$\mathbf{M}\ddot{\mathbf{u}} + \mathbf{C}\dot{\mathbf{u}} + \mathbf{f}_s(\mathbf{u}) = \mathbf{f}(t) \quad . \tag{6.1}$$

Therein, $\mathbf{M}$ and $\mathbf{C}$ describe the system mass and damping matrices and $\dot{\mathbf{u}}$ and $\ddot{\mathbf{u}}$ the first and second derivative of the displacement vector $\mathbf{u}$ by time t. $\mathbf{f}_s$ is the internal force vector depending on current pile displacement. Thus, the nonlinear initial value problem

$$\begin{cases} \mathbf{M}\ddot{\mathbf{u}}_n + \mathbf{C}\dot{\mathbf{u}}_n + \mathbf{f}_s(\mathbf{u}_n) = \mathbf{f}(t_n) \\ \mathbf{u}(t_0) = \mathbf{u}_0, \quad \dot{\mathbf{u}}(t_0) = \dot{\mathbf{u}}_0 \end{cases} \tag{6.2}$$

is to be solved. Assuming a constant time interval $\Delta t_n = t_{n+1} - t_n$ it follows that at t_{n+1}

$$\mathbf{M}\ddot{\mathbf{u}}_{n+1} + \mathbf{C}\dot{\mathbf{u}}_{n+1} + \mathbf{f}_s(\mathbf{u}_{n+1}) = \mathbf{f}(t_{n+1}) \quad . \tag{6.3}$$

Equation (6.3) is solved for the current pile displacement using an implicit method which involves Newmark's method (Newmark, 1959) and the Newton-Raphson iteration. Implicit methods, comparing to explicit methods, have the advantage that the size of the time interval is acceptable considering the required computation steps. In addition, it is beneficial

that the equilibrium of the system is ensured in every time step. The solution scheme for a nonlinear system is summarised in algorithm 1.

$\ddot{\mathbf{u}}_{n+1} \leftarrow 0$
$\mathbf{u}_{n+1} \leftarrow \mathbf{u}_n + \dot{\mathbf{u}}_n \Delta t + \ddot{\mathbf{u}}_n (\frac{1}{2} - \beta)\Delta t^2 + \ddot{\mathbf{u}}_{n+1} \beta \Delta t^2$
$\dot{\mathbf{u}}_{n+1} \leftarrow \dot{\mathbf{u}}_n + \ddot{\mathbf{u}}_n (1 - \gamma)\Delta t + \ddot{\mathbf{u}}_{n+1} \gamma \Delta t$
$\mathbf{r}_{n+1}^{j-1} \leftarrow \mathbf{f}(t_{n+1}) - \mathbf{f}_s(\mathbf{u}_{n+1}, \dot{\mathbf{u}}_{n+1}) - \mathbf{M}\ddot{\mathbf{u}}_{n+1}$
while $err_f >= Tol_f$ **do**
  $\Delta \ddot{\mathbf{u}}_{n+1}^{j} \leftarrow \left(\mathbf{M} + \mathbf{C}\gamma\Delta t + \mathbf{K}\beta\Delta t^2 \right)^{-1} \mathbf{r}_{n+1}^{j-1}$
  $\ddot{\mathbf{u}}_{n+1}^{j} \leftarrow \ddot{\mathbf{u}}_{n+1}^{j-1} + \Delta \ddot{\mathbf{u}}_{n+1}^{j}$
  $\dot{\mathbf{u}}_{n+1}^{j} = \dot{\mathbf{u}}_{n+1}^{j-1} + \Delta \ddot{\mathbf{u}}_{n+1}^{j} \gamma \Delta t$
  $\mathbf{u}_{n+1}^{j} = \mathbf{u}_{n+1}^{j-1} + \Delta \ddot{\mathbf{u}}_{n+1}^{j} \beta \Delta t^2$
  $\mathbf{r}_{n+1}^{j} \leftarrow \mathbf{f}(t_{n+1}) - \mathbf{f}_s(\mathbf{u}_{n+1}^{j}, \dot{\mathbf{u}}_{n+1}^{j}) - \mathbf{M}\ddot{\mathbf{u}}_{n+1}^{j}$
  $err_f = \frac{||\mathbf{r}_{n+1}^{j}||}{||\mathbf{f}(t_{n+1}) - \mathbf{f}(t_n)||}$; $j = j + 1$
end

Algorithm 1: Implicit solution algorithm based on Newton-Raphson iteration and Newmarks method.

It is noted that $\gamma = \frac{1}{2}$ and $\beta = \frac{1}{6}$.

6.1.2 P-y foundation model

With the API p-y curves (API, 2000) the p-y method has proven its suitability for the development of simple and efficient foundation models (cf. section 2.4). P-y approaches can be based on existing soil models and involve a one-dimensional formulation of the constitutive equations (Kelm, 2004). One main task in constitutive model development is to understand the mechanical response and derive a constitutive relation which includes the relevant mechanisms to the actual problem. This also holds for the development of p-y models which require appropriate assumptions being closely related to the boundary value problem and the initial value problem.

Carstensen et al. (2018) proposed a hypoplastic p-y formulation to describe the soil response due to cyclic loading. The hypoplastic spring element captures relevant aspects of cyclic soil behaviour such as barotropy, pycnotropy and a directionality of loading. The approach proved good agreement against finite element simulations and current standards (Carstensen et al., 2018). The flowgraph in figure 6.3 summarises the governing equations of this p-y approach.

The spring element is based on the rate dependent hypoplastic formulation:

$$\dot{p} = k_{s,0} \left(\dot{u} - \left(\frac{p}{p_u} \right)^{\kappa} |\dot{u}| \right) \quad . \tag{6.4}$$

Hence, the change of bedding resistance is defined as a function of the initial soil stiffness $k_{s,0}$ (A), the change of displacement $\dot{u}$, the bedding resistance p, the ultimate bedding

resistance p_u (B) and an exponent κ (C), which describes the curvature of the p-y curve. From this, explicit time integration gives the resulting bedding resistance and the corresponding displacement, i.e. the p-y curve. Thereby, the total bedding resistance of the pile is decomposed of the front resistance caused by normal stresses at the pile front and the friction resistance due to tangential shear stresses (cf. section 2.3). The soil stiffness is derived as the secant stiffness from the p-y curve. Two state variables are defined to account for the previous loading history. Those are the bedding resistance and the element displacement prior to the current load step. The p-y formulation includes a depth-dependent distribution of void ratio (D) according to Bauer (1996). During cyclic loading, the soil around the pile is loaded, unloaded and sheared which results in a change in void ratio in the soil adjacent to the pile. Eventually, this causes also the initial stiffness to be altered. This change in void ratio is described analogously to the volume change in triaxial tests (F) and is related to the change in friction angle (Pucker et al., 2013) (E).

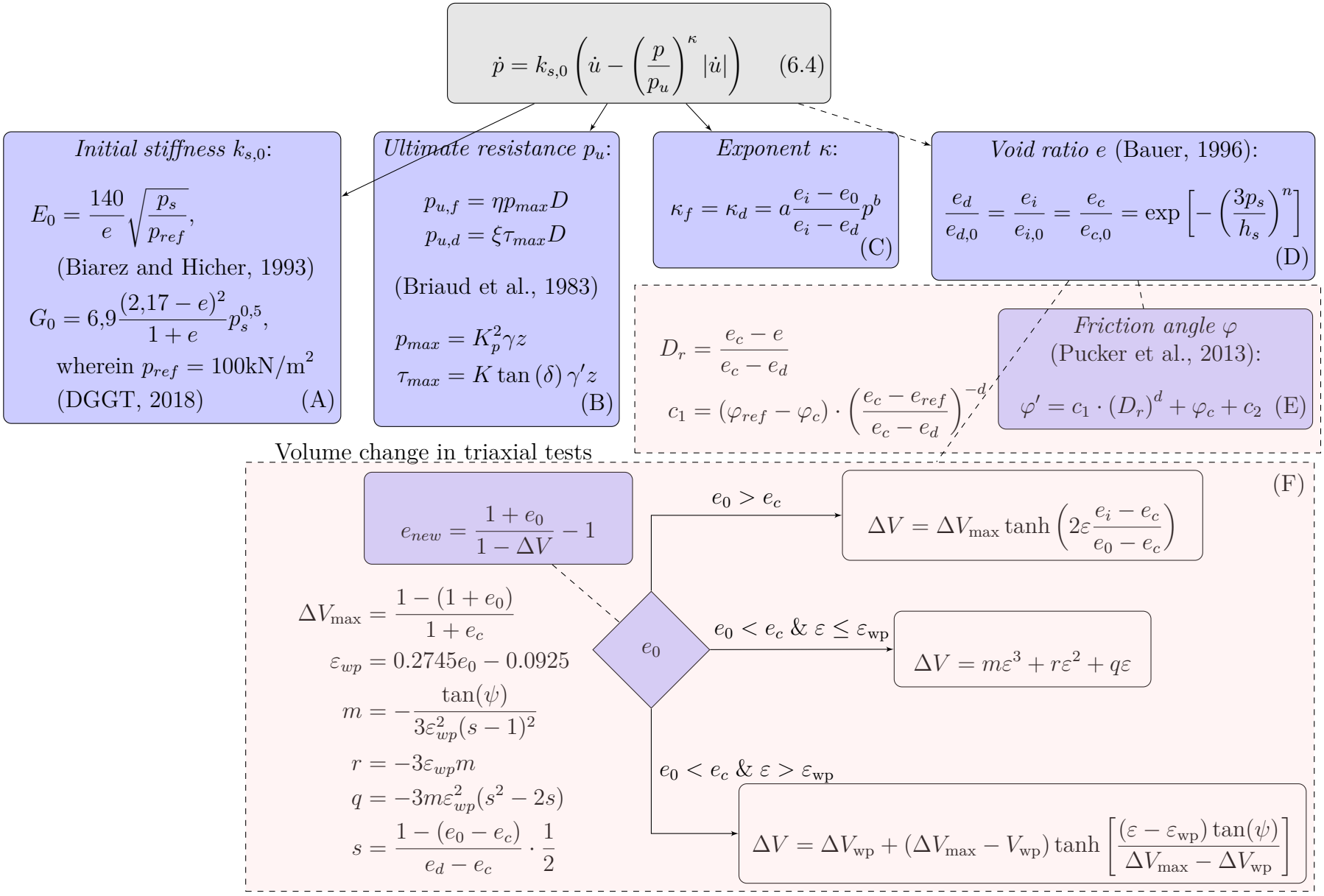

Figure 6.3: Constitutive equations of the hypoplastic spring element according to Carstensen et al. (2018).

6.1.3 Material parameter identification for Wunder sand

For calculations with the hypoplastic p-y model the following parameters are necessary:

- The critical state friction angle φ_c can be determined either from undrained triaxial tests or as the steepest angle of descent relative to the horizontal plane in a bulk cone test.
- The granular hardness h_s and the exponent n describe the decrease of e_i, e_c, e_d and e with increasing pressure p. These constants can be derived from uniaxial compression tests and are estimated by curve fitting of equation (D) to $e(p)$ (Herle, 1997).
- The parameters e_{ref}, φ_{ref}, a, b and d can be estimated from at least six consolidated drained (CD) triaxial tests with different initial relative density and average stresses. The parameters are estimated in that way that the formulation given in equation (C) and (E) meet $\varphi'(e)$ and $p(y)$.
- According to Herle (1997), the maximum void ratio e_{i0}, the critical void ratio e_{c0} and the minimum void ratio e_{d0} can be estimated to be $e_{i0} \approx 1.15 e_{max}$, $e_{c0} \approx e_{max}$ and $e_{d0} \approx e_{min}$.

For further details and alternative methods regarding the parameter calibration, please refer to Herle (1997) and Carstensen et al. (2018).

The used material parameters for the hypoplastic p-y model for Wunder sand are summarized in table B.1 of the appendix. In order to proof that the chosen parameter set is able to describe the stress-strain response suitably, a series of triaxial tests is simulated numerically. Figure 6.4 shows the normalised stress-strain behaviour in triaxial tests for Wunder sand on a loose, medium dense and dense sample and at reference pressures of $p_0 = 100$ kPa, $p_0 = 200$ kPa and $p_0 = 400$ kPa such as the numerical simulated results with the hypoplastic spring element. The strain of the hypoplastic spring element relates to an influence radius of $2.5D$ (Carstensen et al., 2018). The comparison to the laboratory data reveals a good agreement - particularly before reaching the maximum shear stress.

6.1.4 On damping effects

Damping of offshore wind turbine structures is caused by an energy dissipation which can occur in multiple ways (Kementzetzidis, Metrikine, et al., 2021), involving

- aerodynamic damping caused by the interaction between wind and rotating blades,
- hydrodynamic damping due to the structure-water interaction,
- damping associated with the structural materials (steel) and connections and finally,
- soil damping, arising from material dissipation and wave radiation.

The dynamic material properties of a soil can be investigated in a resonant column test. Within this experiment a cylindrical soil specimen is subjected to small strain amplitude torsional vibrations. During testing, the excitation frequency is varied and the natural frequency of the system is determined. From this, the shear wave velocity v_s, the dynamic shear modulus G_{dyn} and the damping ratio D of a soil can be derived (Wichtmann et al.,

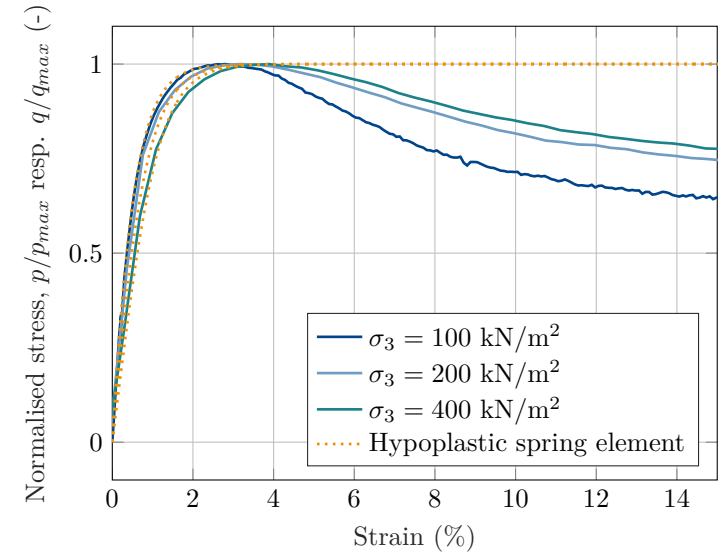

(a)

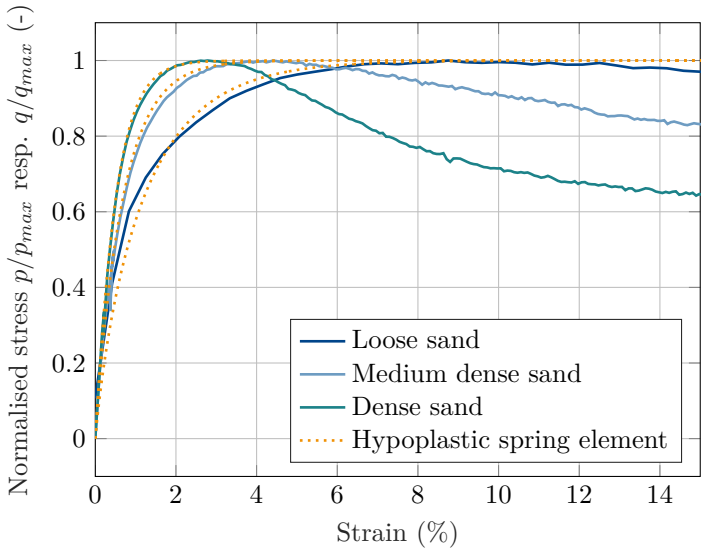

(b)

Figure 6.4: Comparison of the p-y model formulation against element test data: Normalised stress-strain behaviour in triaxial tests for Wunder sand with (a) three different reference pressures and (b) three different relative densities, modified from preliminary work of the Institute of Geotechnical Engineering and Construction Management at Hamburg University of Technology for the publication Carstensen et al. (2018).

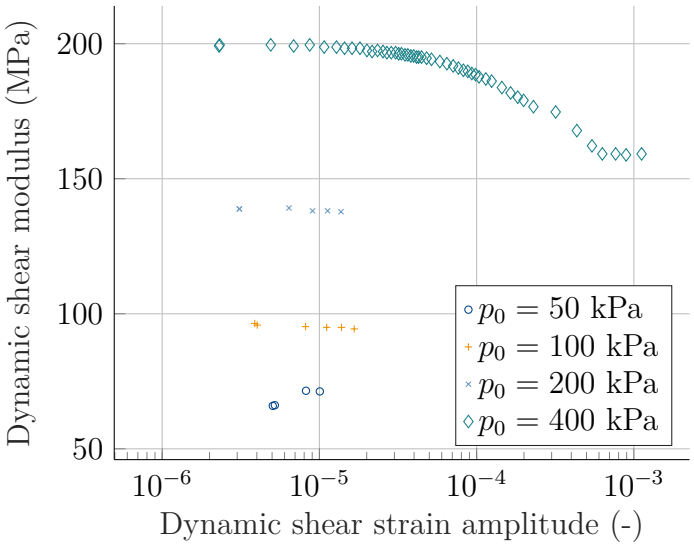

Figure 6.5: Results of resonant column tests with four different reference pressures for very fine silica sand sand on a dense sample.

2001). Figure 6.5 shows the result of a resonant column test with four different reference pressures for very fine silica sand sand on a dense sample. Clearly, the dynamic shear modulus depends on both the static reference pressure and the dynamic shear strain amplitude γ, which confirms early suggestions e.g. by Prange and Huber (1983).

Soil damping during dynamic loading results from material dissipation (material damping) and wave radiation (geometric damping). The hypoplastic p-y formulation, as introduced in section 6.1.2, includes a material dissipation through the change in void ratio. To take into account geometric damping effects the p-y foundation model is extended by parallel radiation damping. A commonly used approach in literature is the radiation damping model proposed by Gazetas and Dobry (1984).

This approach involves the plain strain model visualised in figure 6.6. The model is based on the idea of compression-extension waves propagating in the two quarter-planes in the loading direction while shear waves disseminate in the two quarter-planes perpendicular to the loading direction. Figure 6.6 indicates that the model allows only for horizontal soil deformations within the quarter-planes, i.e. the vertical strain $\varepsilon_z = 0$. Each quarter-plane vibrates independently not being influenced by the others. A circular pile section is replaced by a square section with an equivalent perimeter $2\pi D_a$. The radial damping coefficient is determined as the sum of disseminated energies in the four quarter planes. Thereby, shear waves propagate with a velocity v_s and compression-extension waves propagate with a wave velocity $v_{la} = 3.4v_s/(\pi(1-\nu))$. Assuming a circular cross-section, the following expression is associated for the frequency dependent radiation dashpot coefficient c_r

$$\frac{c_r}{4r_a\rho_s v_s} = \left[1 + \left(\frac{3.4}{\pi(1-\nu)}\right)^{\frac{5}{4}}\right]\left(\frac{\pi}{4}\right)^{\frac{3}{4}} a_0^{-\frac{1}{4}} \quad , \tag{6.5}$$

wherein $a_0 = 2\pi f r_a/v_s$ is the frequency factor, ref. Gazetas and Dobry (1984), and $\nu = 0.33$

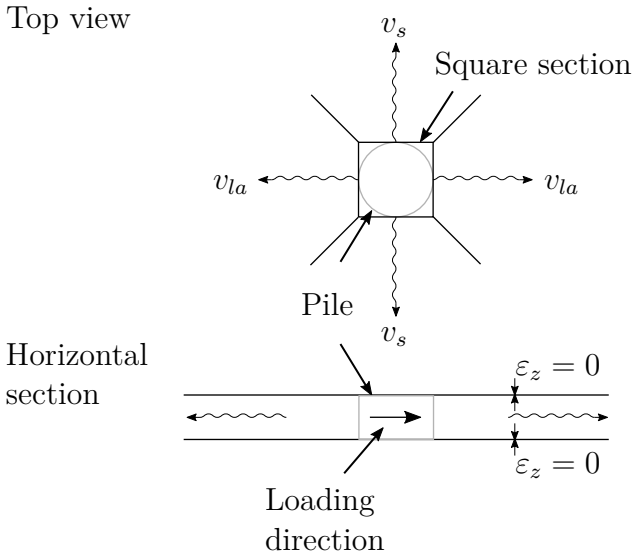

Figure 6.6: Visualisation of the radiation damping model according to Gazetas and Dobry (1984).

the Poisson's ratio for sand. r_a is the radius of the pile and ρ_s the density of the soil particles.

In shallow depths equation (6.5) overestimates the radiation dashpot coefficient. Hence, v_s delivers a better approximation for the wave propagation velocity of surface waves. Considering this, for depths $z_r \leq z = 2.5D_a$ equation (6.5) is replaced by

$$\frac{c_r}{4D_a\rho_s v_s} \approx 2\left(\frac{\pi}{4}\right)^{\frac{3}{4}} a_0^{-\frac{1}{4}} \quad \text{if} \quad z_r \leq z = 2.5D_a \quad . \tag{6.6}$$

The radiation dashpot coefficient is incorporated in the element damping matrix as proposed by Gazetas (1991). Within the model framework a constant mean damping coefficient is applied, which is indicated in figure 6.2c. Thus, geometric damping effects are underestimated in low frequency range which is acceptable considering offshore conditions.

Aerodynamic, hydrodynamic damping such as structural material damping of the pile are not within the scope of this thesis and by now, are not included in the model formulation.

6.1.5 Modeling of natural sea state

The wind induced sea state is modelled based on linear wave theory as a superposition of single sinusodial waves with constant period and wave amplitude. Thus, the irregular wave motion, cf. figure 6.7b, can be approximated by a Fourier series:

$$\zeta(t) = \sum_{n=1}^{N} \zeta_{an} \cos(k_n x - \omega_n t + \epsilon_n) \quad . \tag{6.7}$$

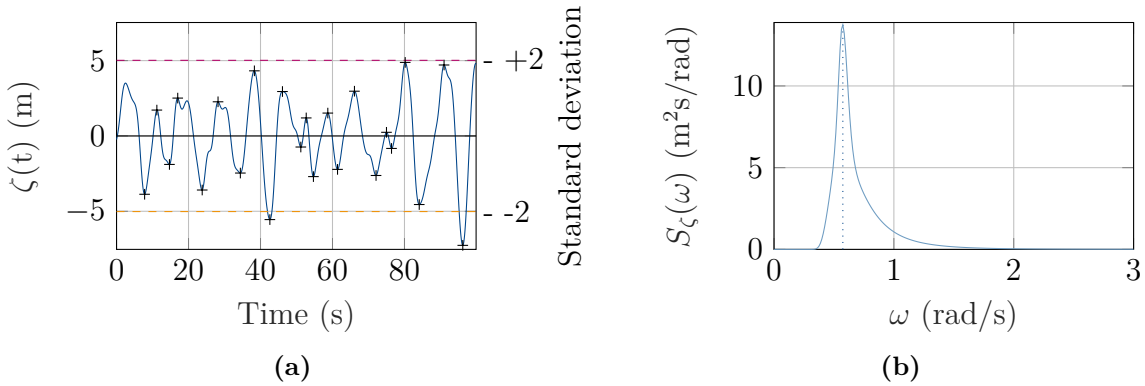

Figure 6.7: Modeling of natural sea state: (a) Exemplary time series of wave motion at a distinct location x, (b) JONSWAP-spectrum for a significant wave height of $H_{m0} = 7$ m and a peak period of $T_p = 11$ s.

Thereby, the wave equation $\zeta(t)$ in the time domain is the entirety of an infinite number of harmonic waves in the frequency domain. Consequently, the water level in a distinct location x as a function of time t depends on the wave number k_n, the angular frequency ω_n and the phase shift ϵ_n of the individual waves. As a two-dimensional model is considered directionality of proceeding waves is neglected within this simple wave model formulation.

Various wave spectra exist which characterise the natural sea state in frequency domain $S_\zeta(\omega)$. In the north sea the JONSWAP-spectrum with a significant wave height of $H_{m0} = 7$m and a peak period of $T_p = 11$s, as shown in figure 6.7a, describes conventional conditions and can be applied to derive the wave amplitudes ζ_{an}

$$\zeta_{an} = 2\sqrt{S_\zeta(\omega)\Delta\omega} \quad . \tag{6.8}$$

To evaluate the pile response due to wind and wave conditions offshore, Morison's equation is applied to calculate the resulting loads on a circular pile with a diameter D_a. Equation (6.9) gives a depth and time dependent description of wave loading which is mainly induced by the horizontal flow velocity $v(z,t)$ and acceleration $\dot{v}(z,t)$ of water particles

$$F_{\text{wave}}(z,t) = \frac{\pi}{4}\rho_w C_M D_a^2 \dot{v}(z,t) + \frac{1}{2}\rho_w C_D(z) D_a v(z,t)|v(z,t)| \quad . \tag{6.9}$$

In this equation, $C_D = 0.8$ and $C_M = 2$ are the current and inertia coefficients chosen based on DNV (2014). ρ_w is the density of water. Numerical integration of equation (6.9) leads to the resulting wave loads on a pile element which are then assigned to the corresponding degrees of freedom of the finite element model.

6.2 Sensitivity analysis

In this section the p-y model, developed in section 6.1, is studied. This includes the model behaviour and its sensitivity to certain parameters. The pile discretisation with finite elements, the discretisation of time in time increments and the tolerance criterion which predefines the condition to terminate the equilibrium iteration in incremental iterative algorithms can have a significant impact on the pile response to cyclic and dynamic loading. Within a sensitivity analysis the influence of those variables on the horizontal pile displacement can be evaluated. Further, these unknown variables are determined to guarantee the stability of the calculation result and to minimize the calculation time.

Therefore, a numerical model with a diameter of $D_a = 7$ m, a wall thickness of $t_w = 0.07$ m and an embedded length of $L_e = 40$ m is created. The horizontal pile displacement is investigated by means of a quasi-static deformation analysis. A parametric study enables to investigate the influence of the relevant variables. Assuming a reference case, one parameter is varied at once. Five cases for each considered parameter are chosen, in order to cover a representative range of higher and lower values. The considered parameters are summarised in Table 6.1.

Influence of pile discretisation

The influence of element height Δz is evaluated in terms of the horizontal pile displacement, the required simulation time and the lateral deflection curve of the pile. The results are shown in figure 6.8. Obviously, the element height has a small influence on the value of horizontal displacement. Whereas, the simulation time increases exponentially with decreasing element height. It is noted that small displacement increments, following a fine discretization of the pile, can lead to a locally increasing soil stiffness which can affect the stability of the solution algorithm of the p-y model. This limit is indicated by the dashed vertical line in figure 6.8a. Considering this, an element height of $\Delta z = 0.5$ m is found to be acceptable.

Table 6.1: Parameters for the sensitivity study of the influence of numerical parameters on the pile response to cyclic and dynamic loading.

parameter	variation 1	variation 2	variation 3	variation 4	variation 5
element height, Δz (m)	$\Delta z = 0.1$	$\Delta z = 0.25$	$\Delta z = 0.5$	$\Delta z = 1$	$\Delta z = 2.5$
time increment, Δt (s)	$\Delta t = 10^{-1}$	$\Delta t = 10^{-2}$	$\Delta t = 10^{-3}$	$\Delta t = 10^{-4}$	$\Delta t = 10^{-5}$
tolerance, ε (-)	$\varepsilon = 10^{-2}$	$\varepsilon = 10^{-3}$	$\varepsilon = 10^{-4}$	$\varepsilon = 10^{-5}$	$\varepsilon = 10^{-6}$

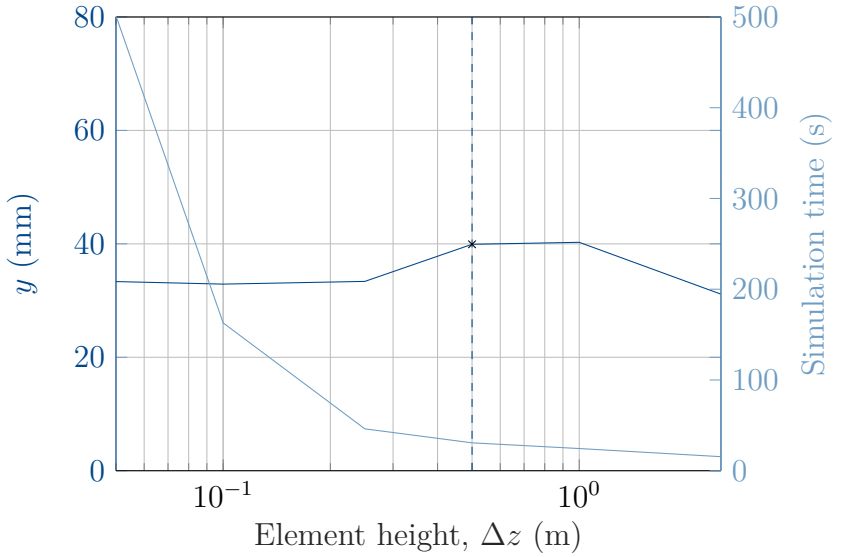

(a)

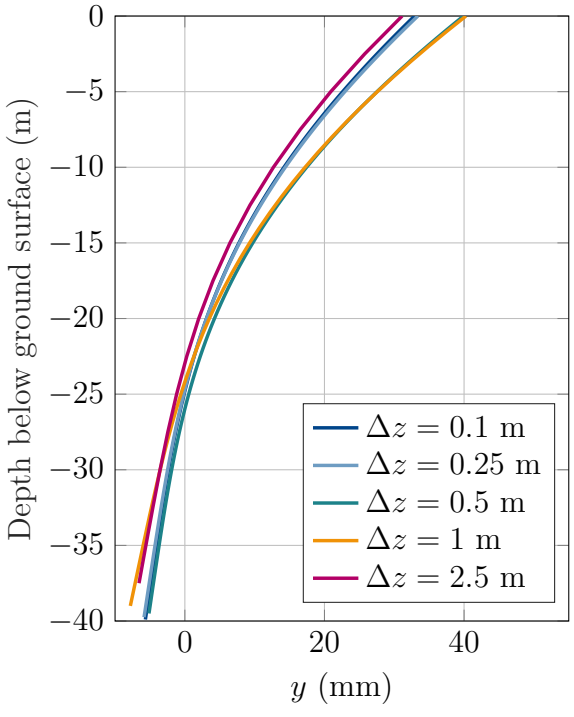

(b)

Figure 6.8: Influence of element height Δz (a) on the horizontal pile displacement and the simulation time and (b) on the lateral pile deflection curve.

Influence of time increment

With the aim to investigate the influence of the increment on the horizontal displacement and the simulation time, the time increment is varied for a fixed element height and tolerance. Figure 6.9a shows the influence of the time increment on the horizontal displacement and the simulation time. The value of horizontal displacement remains almost constant while the simulation time increases with decreasing time increments. A minor influence of the time increment on the pile deflection curve in figure 6.9b is observed. Since the chosen time increment impacts the load increment and therefore the magnitude of displacement change in a calculation step, again the stability of the stiffness iteration needs to be considered when deriving the time increment. Thus, a time increment of $\Delta t = 2 \cdot 10^{-2}$ is chosen. This time step is slightly larger than the recommended time step for Newmark's method which is 10^{-3}. However, Newmark's method is an implicit solution algorithm, which delivers a stable solution independently of the dimension of the chosen time step.

Influence of tolerance criterion

To minimize the influence of abort errors during stiffness iteration within the solution of the nonlinear equation of motion, the tolerance criterion is varied for a fixed pile discretisation and time increment. The influence of the tolerance criterion on the horizontal pile displacement and the simulation time is shown in figure 6.10a. The lateral pile deflection curves are visualised in figure 6.10b. The solution for the horizontal pile head displacement converges for a break-off tolerance of one per cent. Below this value, the calculated solution remains constant. This holds for the pile head displacement as well as for the lateral pile deflection curve. Hence, in order to define a tolerance criterion the simulation time is crucial. To minimize the calculation time a tolerance criterion of $\varepsilon = 0.01$ is chosen.

6.3 Verification of pile response to lateral loading

In order to verify the pile response to lateral monotonic loading the influence of pile diameter, wall thickness and embedded length is investigated. Additionally, the lateral deflection of the p-y model is compared against the current industry design standard.

Influence of pile geometry

Figures 6.11, 6.12 and 6.13 show the lateral deflection curves with varying pile diameter, wall thickness and embedded length for a monotonic horizontal load of magnitude $H = 5000$ kN which is applied to the pile head. A monopile with a diameter of $D_a = 7$ m, a wall thickness of $t_w = 0.07$ m and an embedded length of $L_e = 40$ m is chosen as the base case.

Figure 6.11 shows the lateral deflections curves of a monopile with diameter $D_a = 5$ m, $D_a = 7$ m and $D_a = 9$ m. The embedded length and the wall thickness are the same as for the reference case. The pile with a diameter of $D_a = 5$ m shows the largest value of horizontal deformation. With increasing pile diameter the horizontal pile displacement

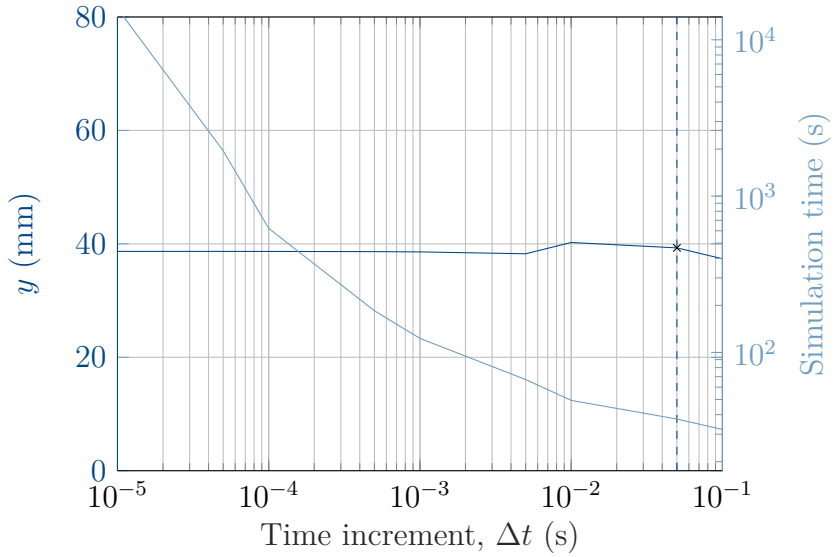

(a)

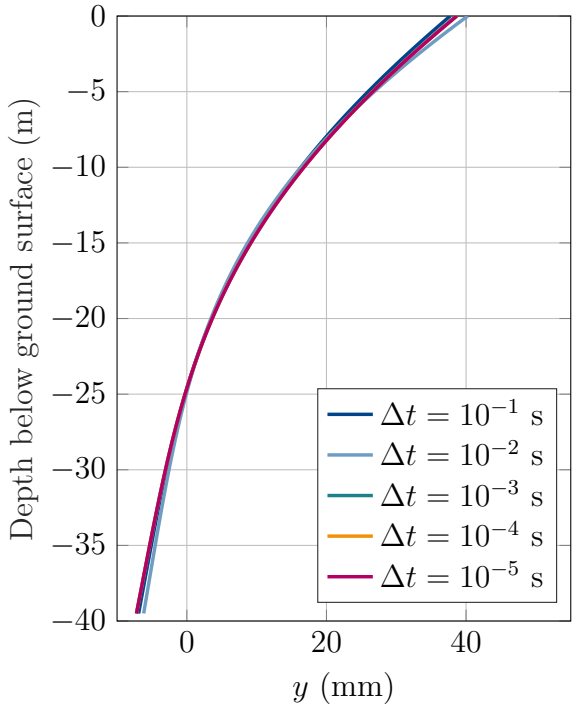

(b)

Figure 6.9: Influence of time increment Δt (a) on the horizontal pile head displacement and the simulation time and (b) on the lateral pile deflection curve.

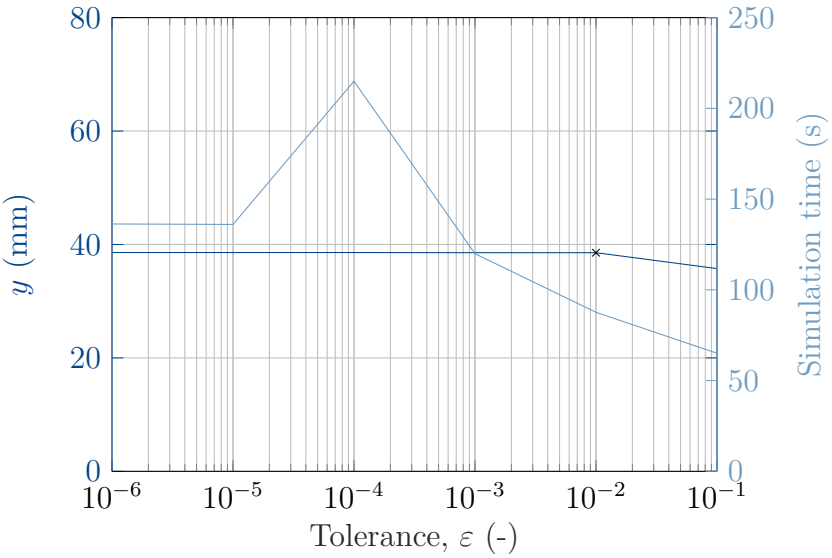

(a)

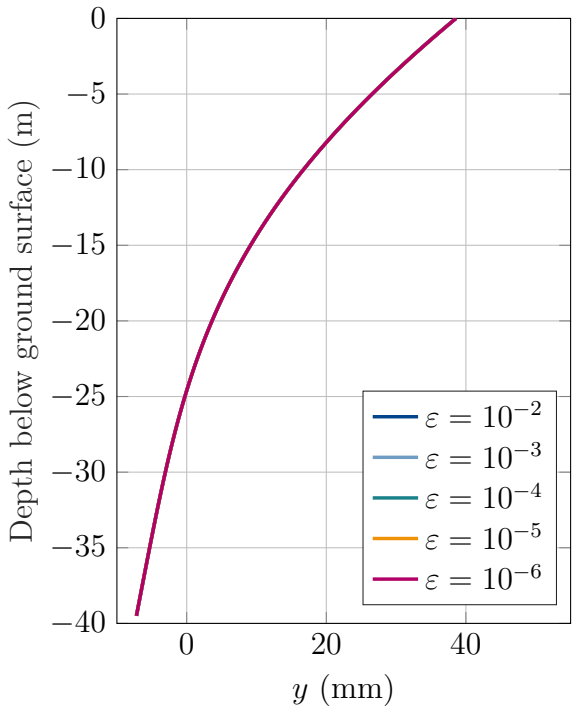

(b)

Figure 6.10: Influence of tolerance criterion ε (a) on the horizontal pile head displacement and the calculation time and (b) on the lateral pile deflection curve.

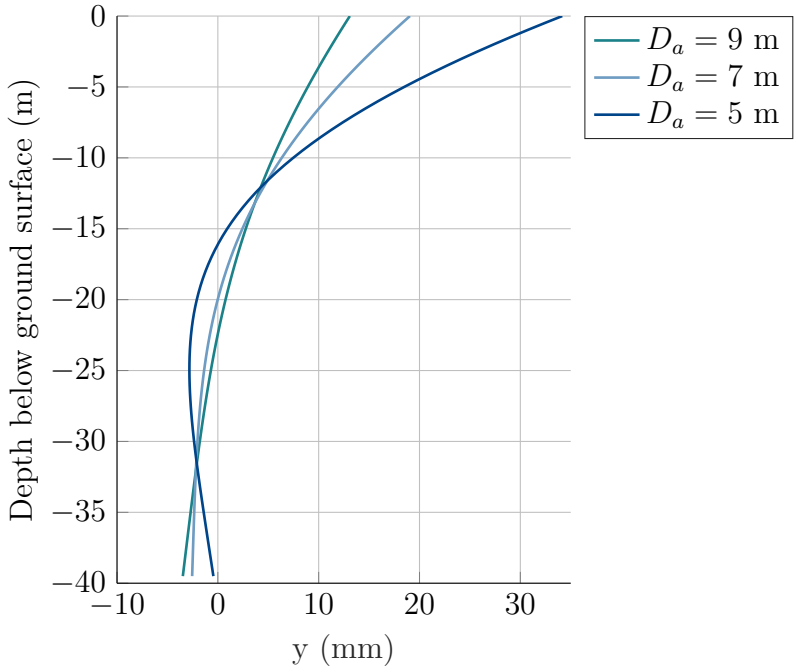

Figure 6.11: Comparison of lateral deflection curves of monopiles with different diameters for monotonic lateral loading with a load of $H = 5{,}000$ kN applied to the pile head. The reference case is a pile with a diameter $D_a = 7$ m, a wall thickness of $t_w = 0.07$ m and an embedded length of $L_e = 40$ m.

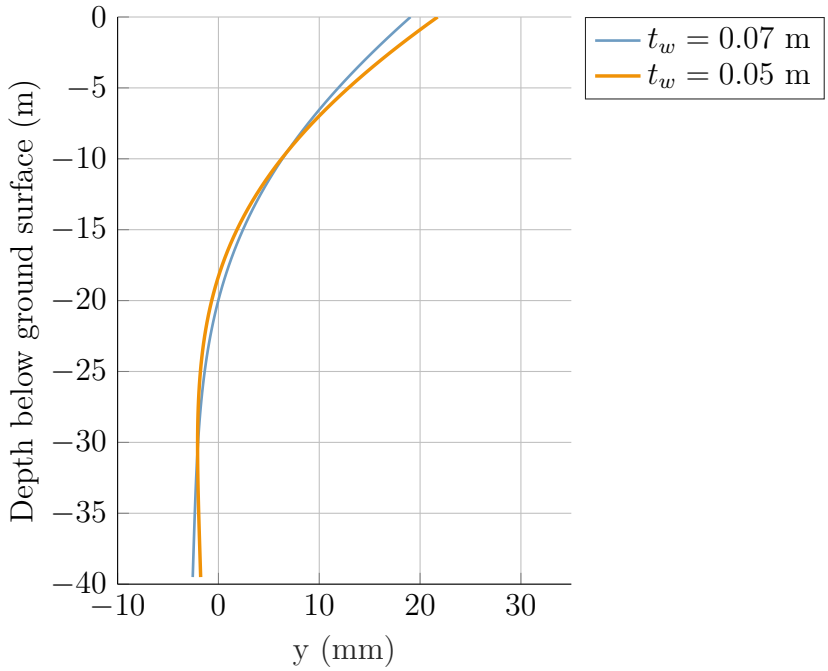

Figure 6.12: Comparison of lateral deflection curves of monopiles with different wall thicknesses for monotonic lateral loading with a load of $H = 5{,}000$ kN applied to the pile head. The reference case is a pile with a diameter $D_a = 7$ m, a wall thickness of $t_w = 0.07$ m and an embedded length of $L_e = 40$ m.

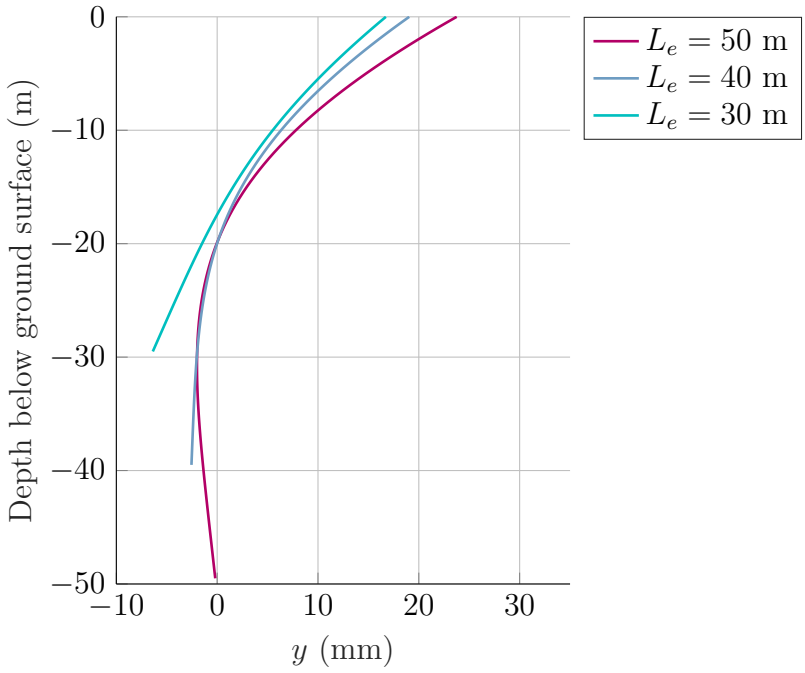

Figure 6.13: Comparison of lateral deflection curves of monopiles with different embedded lengths for monotonic lateral loading with a load of $H = 5{,}000$ kN applied to the pile head. The reference case is a pile with a diameter $D_a = 7$ m, a wall thickness of $t_w = 0.07$ m and an embedded length of $L_e = 40$ m.

decreases. Expectedly, the pile diameter influences the lateral capacity of the pile and simultaneously the stiffness pile-soil system which causes the horizontal displacement to decrease for larger diameter values.

The influence of the wall thickness is investigated in figure 6.12. A small increase in pile deformation with a wall thickness of $t_w = 0.05$ m can be observed compared to the pile with a wall thickness of $t_w = 0.07$ m.

The influence of the embedded length is investigated in figure 6.13. Note that for this investigation the horizontal load was scaled linearly with increasing pile length. Similar to the results with varying diameters, the pile response is closely related to the stiffness of the pile-soil system. The pile with a length of $L_e = 30$ m shows the lowest value of horizontal displacement compared to the other two piles. The pile deforms almost rigid, i.e. the pile tilts around a centre of rotation with almost no bending. The pile with a length of $L_e = 50$ m shows the largest value of horizontal displacement. Especially in the upper part of the pile significant bending occurs. However, for the longer pile, a higher lateral resistance is mobilised around the pile tip which is indicated by the small pile tip displacement.

Comparison against the API p-y curves

In order to verify the magnitude of lateral deflection a comparison of the pile displacement to monotonic lateral loading of the p-y model against the API p-y curves is included in figure 6.14. For this purpose, the API p-y approach according to API (2000) was incorporated in the model formulation. The chosen pile geometry corresponds to the previously defined base case. Obviously, the API p-y formulation leads to a higher value of horizontal displacement when compared to the p-y model. This holds for the pile head displacement as well as for the horizontal deflection of the pile tip. Since the API p-y approach was reported to overestimate the pile displacement and therefore, to lead to a conservative design by several authors (ref. section 2.4) the model response and the order of magnitude of horizontal displacement are considered acceptable.

6.4 Summary and discussion on model limitations

Summarising this chapter, a p-y model for lateral loading in sand, which combines relevant aspects of cyclic and dynamic soil-pile interaction, was developed. The model is based on a finite element formulation of a beam on nonlinear spring elements. The spring elements are established on a hypoplastic formulation to represent the nonlinear soil behaviour accurately. This way, relevant stress and density-dependent soil properties are captured, directly impacting the stress-strain behaviour due to cyclic loading. The formulation of the soil model includes material damping as well as geometric damping effects. The main idea during the development process was to create a simple model for cyclic and dynamic loading analysis. Therefore, the equilibrium of the system is described by the nonlinear dynamic equation of motion, considering inertia forces.

The foundation model was calibrated carefully based on triaxial test results. A comparison of the p-y spring element against element test data has shown a good agreement for different initial relative densities and average stresses. However, it is noted that for the final validation of the entire model, the calculation results should be compared with the time series of cyclic and dynamic field tests at the prototype scale. Unfortunately, no field test data was available during the model development. Hence, this is to be done in the future. The model sensitivity to certain numerical parameter changes was evaluated in a sensitivity analysis, and the unknown variables were derived to guarantee stability of the calculation result and to minimize numerical errors. The pile response to monotonic lateral loading was verified and compared against current standards. However, as the model enables combining the analysis of cyclic deformation accumulation and dynamic structural analysis of monopile-supporting OWTs, it provides a promising and efficient approach to assessing the cyclic and dynamic pile-bearing behaviour. Thus, the model has several applications within the offshore design practice, highlighted and explained in detail in the following chapter.

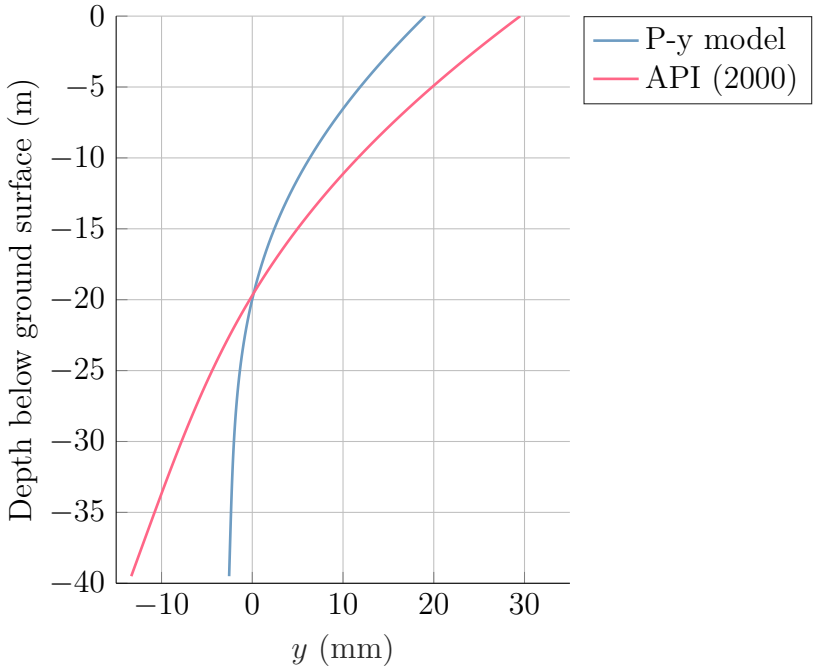

Figure 6.14: Comparison of pile response to monotonic lateral loading of the p-y model against the API p-y curves.

7 Applications in OWT design practice

This chapter investigates the lateral pile response in sand due to cyclic and dynamic loading using the p-y model introduced in chapter 6 and explains different model applications related to the current design practice. First, section 7.1 briefly reviews the current design practice for offshore monopiles. Second, section 7.2 studies the pile response to cyclic lateral loading. Section 7.3 focuses on aspects of dynamic structural analysis of a monopile supporting OWT. Section 7.4 concludes the chapter.

7.1 Review of current design practice

Offshore wind turbine foundations are designed, among others, according to the Standard DNV-ST-0126. This standard defines regulations and safety concepts for the design, construction, operation and maintenance of offshore wind turbine structures. In addition, the standard sets minimum requirements for geotechnical investigation and laboratory testing (to determine cyclic and dynamic soil parameters) and provides recommendations for numerical simulations.

Offshore wind turbine structures are subjected to significant permanent and variable loads, which must be considered in the design process to ensure a safe and reliable operation. These include self-weight, inherent vibration from turbine operation, horizontal loads from ship impacts during installation and maintenance activities, and wind, wave and current loads with varying amplitude and frequency from different directions. Additional relevant factors throughout the operating time are steel corrosion, biological growth, scouring at ground level and earthquake loads in regions prone to seismic activity.

In the design process, various limit states are considered. In the Ultimate Limit State (ULS), the axial and lateral capacity of the structure is assessed, considering the cyclic degradation of soil properties. In the Serviceability Limit State (SLS), requirements are imposed on the inclination of the structure due to installation and cyclic horizontal loading since even slight inclinations can affect the functionality of the turbine. Tolerances for permanent rotation typically range from 0.25° to 0.50°. In the Fatigue Limit State (FLS), the operational strength is demonstrated for the intended operating time, between 20 to 30 years, respectively. This includes an accurate characterization of the vibration and damping behaviour. Additionally, the Accidental Limit State (ALS) considers extraordinary loading scenarios, such as ship impacts during installation and maintenance activities.

Since the design parameters highly depend on the location, the pile diameter, wall thickness and embedded length are determined in an iterative procedure. Various analytical and numerical approaches are employed in the design process to optimize the design. Numerical

methods can contribute to an efficient design, e.g. by allowing for modelling complex geometries and considering the nonlinear soil behaviour and soil-structure interaction. However, time-saving procedures are often preferred over a more detailed numerical analysis for economic reasons. Hence, numerical methods are primarily used to calibrate key parameters for p-y models and to investigate selected queries. In this way, the benefits of numerical methods are combined with the p-y method's computational efficiency, leveraging the advantages of both approaches.

This chapter will reveal whether it is possible to describe the behaviour of piles and soil due to cyclic and dynamic loading using a p-y model.

7.2 Numerical modeling of pile response to cyclic lateral loading

First, the aspect to study is the behaviour of piles and soil due to cyclic lateral loading. The cyclic strain accumulation and the ordering of cycle packages are analyzed. This is done based on numerical investigations using the p-y model as introduced in chapter 6. A pile with a diameter of $D_a = 7$ m, a wall thickness of $t_w = 0.07$ m and an embedment length of $L_e = 40$ m was used. The simulations were performed with an initial relative density of a medium dense sand with $I_D = 0.6$. The lateral loading of the pile is applied at a height of $e = 20$ m above the ground surface.

7.2.1 Investigation of cyclic strain accumulation

The p-y model is employed to investigate the cyclic strain accumulation of a laterally loaded pile in sand. Therefore, a cyclic load with a mean load and amplitude of $H_{av} = H_{cyc} = 2{,}500$ kN is applied to the pile head. Figure 7.1 shows the lateral pile deflection curve and the corresponding p-y curves at 0.25, 10 and 40 m depth after 10,000 load cycles. Due to the applied cyclic load, permanent displacements accumulate, accompanied by a softening of the soil. With increasing load cycles, the accumulation rate decreases until no further strain accumulation occurs. The p-y curve is an open hysteresis loop near the ground surface with a high degree of permanent displacements developing. The soil stiffness significantly increases during unloading. At 10 m depth, the shape of the hysteresis loop is less expanded and ratcheting decreases. At 40 m depth, an almost linear soil response is observed. This may be related to the higher stress level and the increased capacity of the soil in greater depth. Hence, small pile deflections occur at the pile tip, with some ratcheting.

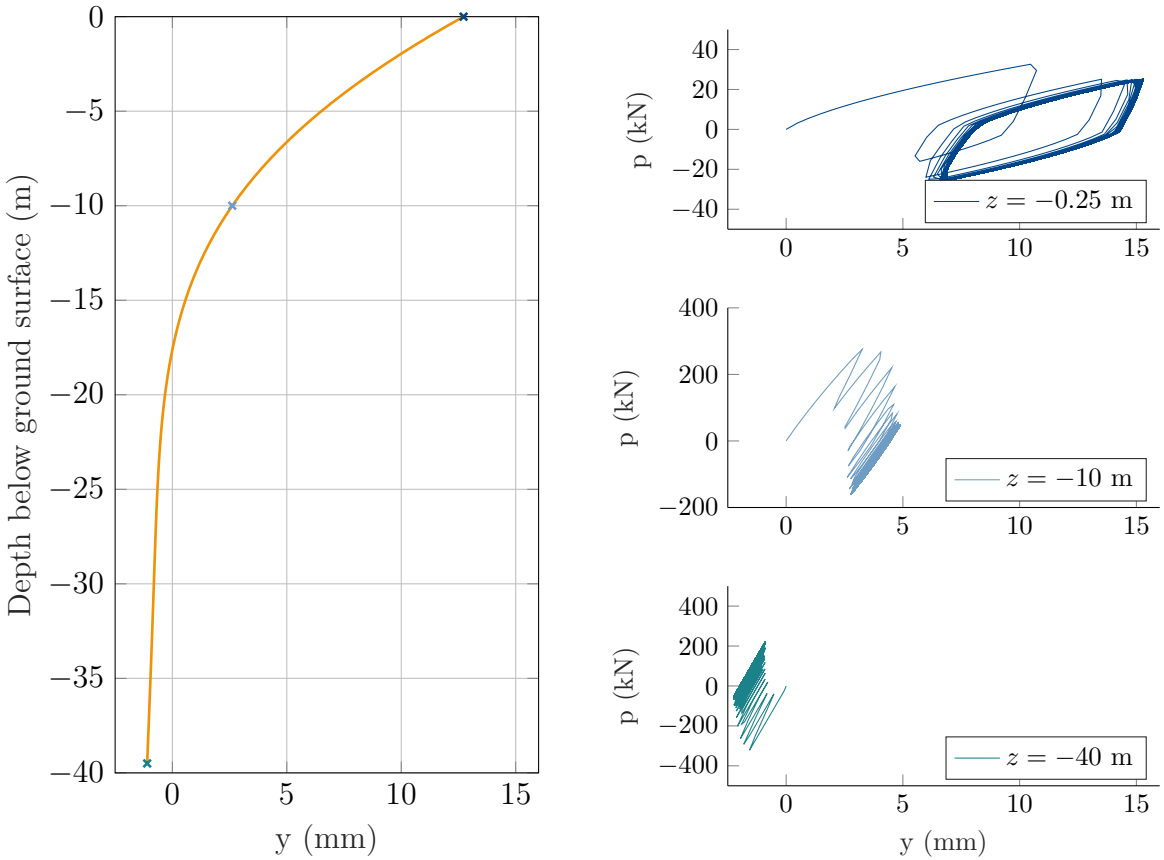

Figure 7.1: Investigation of strain accumulation due to cyclic lateral loading: (a) lateral pile deflection curve after 10,000 load cycles with an average load and amplitude of $H_{av} = H_{cyc} = 2{,}500$ kN and (b) p-y curves in 0.25, 10 and 40 m depth, respectively, highlighting the different shapes of the p-y curves and a decreasing accumulation rate for many cycles (Stark and Grabe, 2021).

7.2.2 Influence of ordering of cycle packages

This study will evaluate the influence of ordering of cycle packages using the p-y model and aims to investigate the validity of Miner's rule further. The chosen load packages are consistent with the direct simple shear tests discussed in Section 5.2. A load scenario with a constant average load of $H_{av} = 1{,}250$ kN and a varying load amplitude is considered to represent offshore conditions appropriately. This load scenario is equivalent to test series no. 2 from the direct simple shear experiments illustrated in figure 5.2. The variable load amplitude contains four levels, i.e. $H_{cyc} = 1{,}250 \rightarrow 2{,}500 \rightarrow 3{,}750 \rightarrow 5{,}000$ kN, with 25,000 load cycles each. Based on previous findings, three representative combinations of cycle packages are investigated, including an ascending, a descending and a descending and then ascending load sequence. The results are shown in Figure 7.2 and indicate the following observations:

- An ascending order of cyclic amplitude leads to an accumulation of permanent displacement in each cycle package. The maximum permanent displacement accumulates in the first load package, while less ratcheting occurs in the following cycle packages, cf. figure 7.2a.
- When the cyclic loads are arranged in descending and then ascending order of cyclic amplitude, a minor accumulation of permanent displacements is found for subsequent sequences with lower amplitude, cf. figure 7.2b. Thus, evident permanent strains develop in the first and the last cycle package. This is consistent with that response observed in the direct simple experiments discussed in section 5.4.
- Arranging the cyclic loads in descending order (figure 7.2c) leads to an accumulation of permanent displacements that was about of the same magnitude of that when the cyclic loads were arranged in ascending order. However, the displacement amplitude in the first cycle package is significantly larger compared to the other load combinations. Ratcheting occurs during the first cycle package, while no further strain accumulation occurs for the following lower amplitude cycles. This observation is consistent with the direct simple test results discussed in section 5.4.
- The shape of the p-y curve is an open hysteresis loop but is less expanded for low-amplitude cyclic loads.

Hence, the effect of cyclic loading on the accumulated displacement is magnitude-dependent and closely related to the ordering of cycle packages.

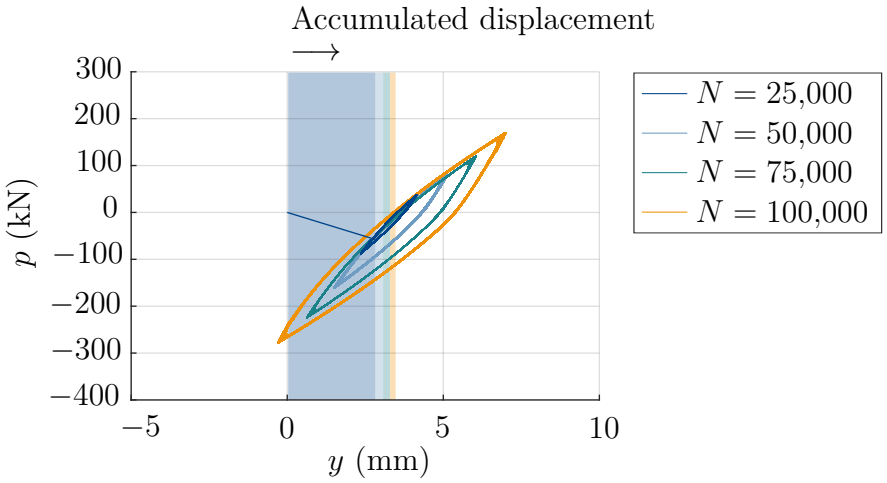

(a) $H_{cyc} = 1{,}250 \rightarrow 2{,}500 \rightarrow 3{,}750 \rightarrow 5{,}000$ kN

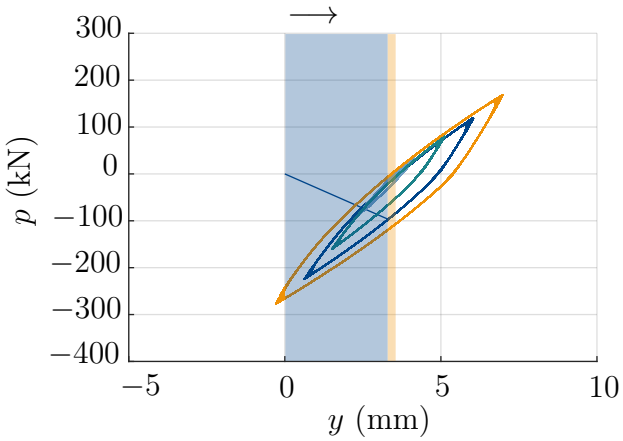

(b) $H_{cyc} = 3{,}750 \rightarrow 1{,}250 \rightarrow 2{,}500 \rightarrow 5{,}000$ kN

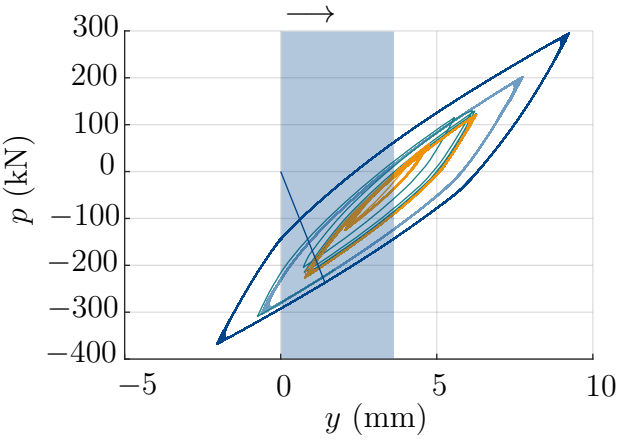

(c) $H_{cyc} = 5{,}000 \rightarrow 3{,}750 \rightarrow 2{,}500 \rightarrow 1{,}250$ kN

Figure 7.2: P-y curves at 5 m depth for different combinations of cycle packages with a constant average load of $H_{av} = 1{,}250$ kN and a variable load amplitude after 25,000, 50,000, 75,000 and 100,000 load cycles. The colour shading indicates the accumulated displacement during a cycle package.

7.3 Dynamic structural analysis of a monopile supporting OWT

Second, the dynamic pile response is investigated. This involves the pile response due to hydrodynamic loading, the damping behaviour, the frequency response and the pile response due to a storm load history. The aspects listed above are investigated numerically using the p-y model, which was introduced in chapter 6. The geometry of the pile is the same as described in section 7.2 ($D_a = 7$ m, $t_w = 0.07$ m, $L_e = 40$ m). In order to depict the dynamic response of a monopile supporting OWT more realistically, the turbine at the pile head is modelled as an additional point mass of 435,000 kg in a height of 100 m above the ground surface.

7.3.1 Pile response due to hydrodynamic loading

To investigate the pile response due to hydrodynamic loading, the natural sea state in the North Sea is modelled as described in section 6.1.5. A water depth of $h = 25$ m is assumed, representing shallow close-coastal regions in the North Sea. Figure 7.3a shows the time series of the resulting wave force on the pile for a time period of 600 s. Please note that this graph shows the integral of the depth-dependent wave force distribution over the water depth, i.e. the resulting wave force on the pile. A depth-dependent load distribution is considered in the p-y model. The resulting lateral pile displacement at different locations along the pile is included in figure 7.3b and c. Figure 7.3b illustrates the lateral pile deflection at a height of $z = 100$ m. The lateral pile displacement at the ground surface ($z = 0$ m) and at the pile tip ($z = -40$ m) is illustrated in figure 7.3c. As highlighted in the spy, referring to figure 7.3a, the wave load sequence is highly dynamic and involves frequent, irregular load changes. In contrast, a slow cyclic deflection of the pile with a frequency of approximately 0.2 Hz is observed, cf. figure 7.3c. This behaviour can be explained by inertia forces counteracting small and frequent load changes. However, the load maxima result in a reversible peak displacement and a temporary tilting of the pile. At ground level, the maximum value of the lateral displacement is 0.02 m. This corresponds to a maximum tilting of the pile of 0.1662° within the acceptable tolerance for rotation, cf. section 7.1. Hence, it can be concluded that no limitations in terms of serviceability of the structure result from the applied loading scenario.

For most of the investigated time intervals, the pile displacement follows the applied load, considering previously discussed observations. However, this does not necessarily hold for the whole time period. In the time interval marked by the vertical red dotted lines, the pile head displacement oscillates periodically with an increased displacement amplitude. This behaviour was unexpected since the wave load amplitude decreased significantly in that sequence. Consequently, this amplified vibration was caused by the peak load occurring at $t = 413$ s, indicating the impact of dynamic effects on the pile response. In conclusion, this highlights the importance of considering nonlinear loading scenarios and dynamic soil-structure interaction in the design of offshore monopiles.

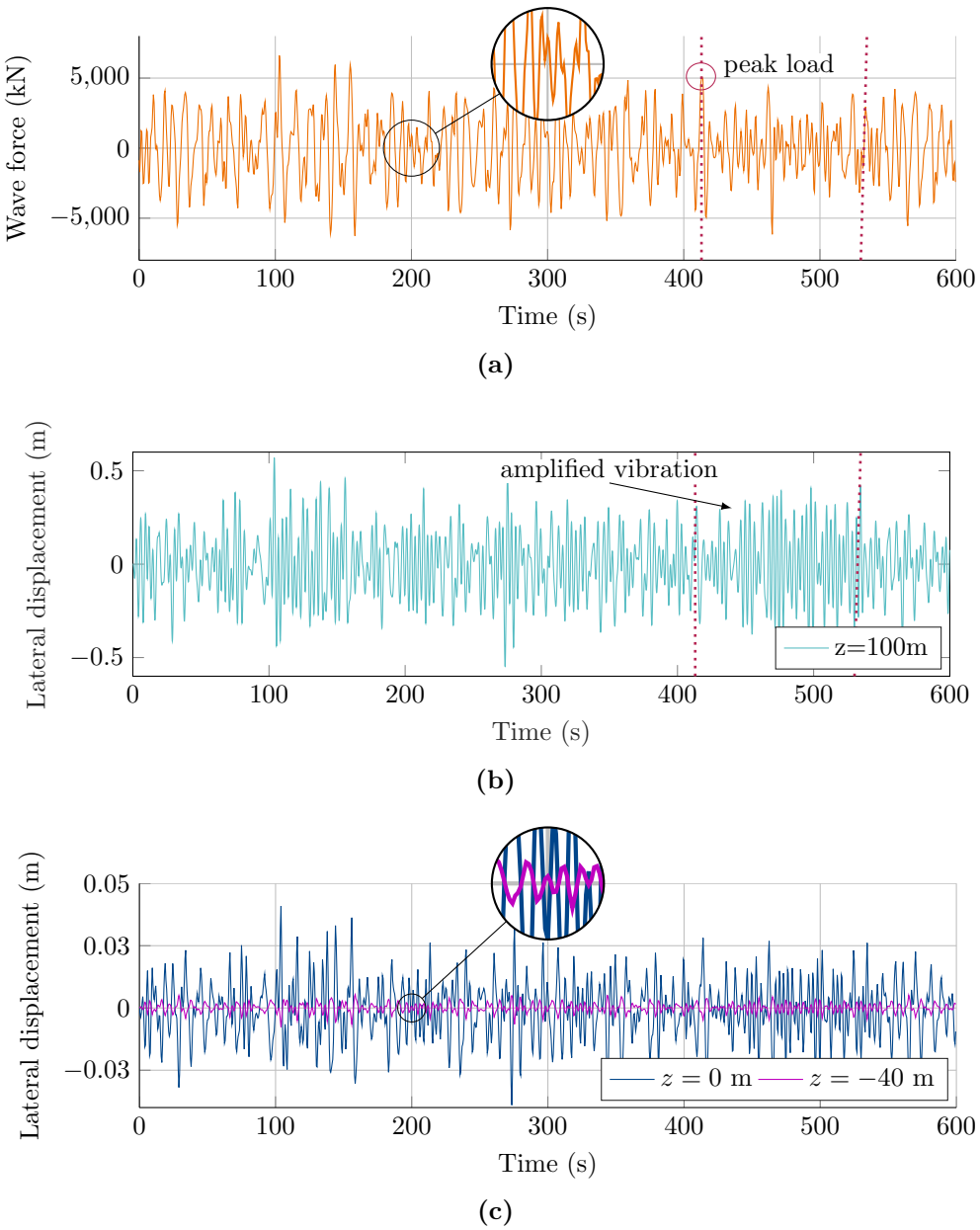

Figure 7.3: Pile response due to hydrodynamic loading: (a) resulting wave force on the pile induced by natural sea state in the North Sea assuming a water depth of $h = 25$ m, (b) lateral pile displacement at pile head and (c) lateral pile displacement at ground level and at the pile tip.

7.3.2 Damping behaviour and frequency response

For the purpose of evaluating the damping behaviour and the frequency response, the pile is subjected to an initial deflection of $0.02D_a$ at ground level. The oscillation behaviour is included in figure 7.4a regarding the lateral pile head displacement over time. It is observed that the pile head oscillates with a decreasing amplitude around its neutral position until the harmonic oscillation has completely decayed after a 30 s period. To evaluate the observed behaviour, the oscillation of a multibody system consisting of two bodies is included in figure 7.4b. Again, the system oscillates from one side to the other until it reaches its neutral position. Thereby, the time required for the oscillation to decay is significantly longer when comparing to the p-y model. This behaviour can be related to damping effects. The cyclic displacement can potentially introduce changes to the soil's density, which results in material damping, especially in the upper part of the pile. Further, energy is disseminated via wave radiation from the system. The p-y formulation captures both effects (cf. section 6.1.4).

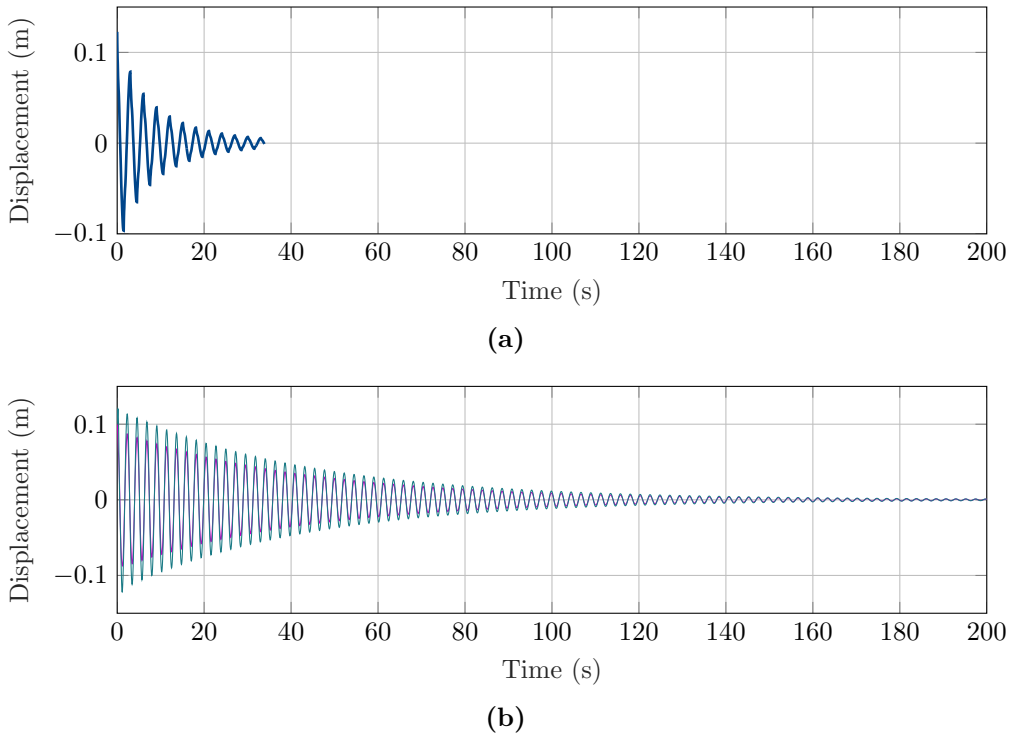

Figure 7.4: Oscillation behaviour (a) of a pile being subjected to an initial deflection of $0.02D_a$ at ground level and (b) of a multibody system consisting of two bodies.

The fundamental frequencies of the model can be interpreted from the frequency spectrum of the time series of the acceleration signal, which is shown in figure 7.5. Coloured circles mark the peak spectral frequencies within the expected frequency range. The first fundamental frequency is at 0.3281 Hz. Alternatively, the fundamental frequencies of the p-y model can be interpreted from a modal analysis. Solving the generalized eigenvalue problem, the first and second fundamental frequency were found at 0.3409 Hz and 2.504 Hz. Thus, both approaches led to very similar results. Comparing to field test data, the results are in good

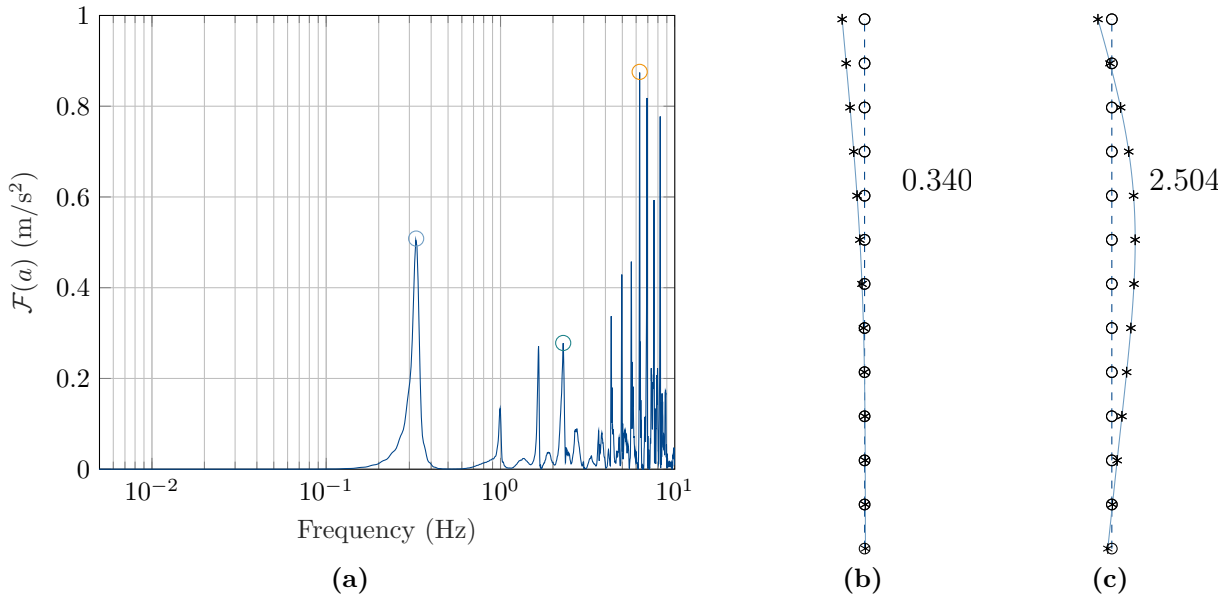

Figure 7.5: Frequency response of the p-y model: (a) natural frequencies derived from the frequency spectrum of the acceleration signal, following an initial deflection of $0.02D_a$ at ground level (Stark and Grabe, 2021), (b) first and (c) second eigenmode and natural frequency determined by a modal analysis.

agreement with the eigenfrequencies measured at the offshore research platform FINO3 (Jeromin et al., 2014) and an offshore wind turbine, at Horn's Reef II Offshore Wind Farm, compare Kallehave, LeBlanc Thilsted, and Troya (2015).

Suppose the fundamental frequencies of a structure are considered as a system-dependent quantity. In that case, it is reasonable to assume that a change in the fundamental frequency is related to a change in the pile-soil stiffness. Extraordinary loads, for instance, in a storm event, can cause a temporary reduction of the fundamental frequency. Possible mechanisms involve pore pressure effects, gapping between pile and seabed, followed by a reduced lateral support of the pile and increased seafloor displacements due to a temporary increase of the wind speed (Kallehave, LeBlanc Thilsted, and Troya, 2015). However, all those mechanisms lead to a (temporary) reduction of the stiffness of the pile-soil system. To further evaluate and understand the dynamic pile response, the pile displacements during a storm event are estimated. The results are presented in the following section.

7.3.3 Storm load history

This section investigates the dynamic pile response due to storm load sequences. For this purpose, a six-hour storm in the North Sea is modelled according to Norwegian Petroleum Directorate (1977). It has to be noted that this approach involves classification methods as discussed in chapter 5. Figure 7.6a includes an exemplary composition of cycle packages. A model storm consists of a random combination of cycle packages which involve a certain number of load cycles and a load amplitude, which is given as a percentage of a maximum storm load. Those are related to the probability of occurrence during a storm event.

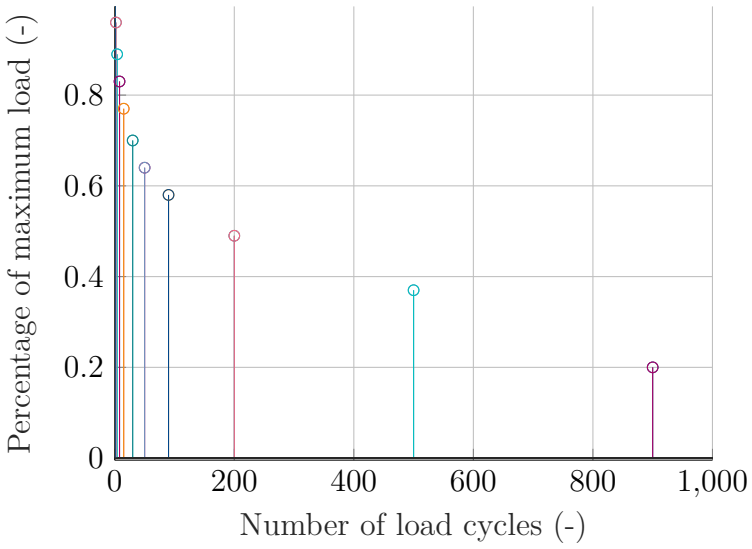

(a)

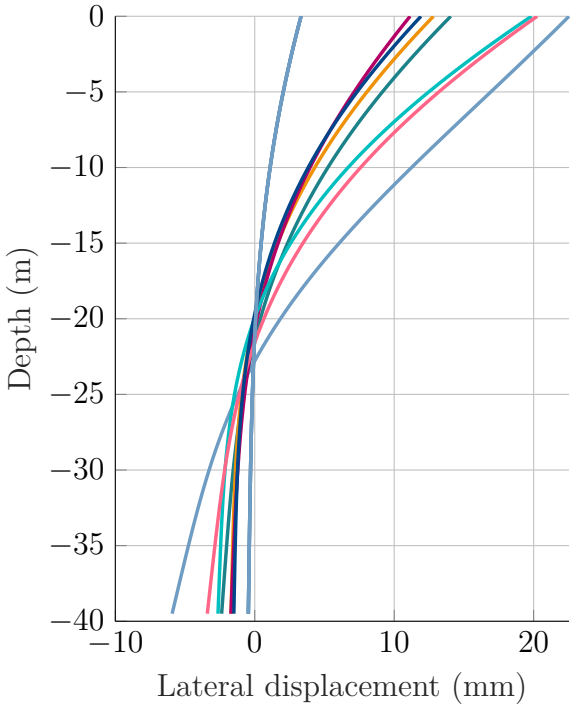

(b)

Figure 7.6: Investigation of pile response due to storm events: (a) exemplary composition of cycle packages of a six-hour model storm in the North Sea according to Norwegian Petroleum Directorate (1977), (b) pile deflection curves after a six-hour model storm for various random combinations of load packages with a maximum load of $H_{max} = 5{,}000$ kN (Stark and Grabe, 2021).

The maximum storm load was chosen as H_{max} = 5,000 kN, which was found to be the approximate maximum wave force on the pile when modelling the natural sea state. Please note that this study does not consider other site-specific influencing factors during storm events, such as wave height, peak period, dynamic turbulences and pile-wave interaction.

The lateral pile deflection curves for various randomly selected combinations of load packages are shown in figure 7.6. Significant deviations are observed regarding the lateral pile displacement at ground level after the model storm. The range extends from a minimum value of 3.32 mm to a maximum of 22.54 mm. Deflections between 0.46 mm and 5.93 mm are observed at the pile tip. At ground level, this results in a deviation of 74.33 %, far beyond the deviations found in the experimental study on the validity of Miner's rule in section 5.4. However, although this observation requires experimental verification, the results indicate that the order of cycle packages matters.

7.4 Summary

Numerical simulations of pile response to hydrodynamic loading highlight the impact of dynamic effects on the load-displacement behaviour of piles and, therefore, emphasise the importance of investigating the behaviour of pile and soil to cyclic and dynamic loading and to consider the dynamic soil-structure interaction within the design practice. Further, numerical simulations of a storm load history show large deviations in the resulting pile displacements, indicating that the order of cycle packages matters.

8 Conclusion

Due to the increased interest in renewable energy, the offshore wind industry grows continuously. Offshore wind turbines are subjected to large, multicomponent and cyclic loads due to wind and sea conditions. Thus, designing offshore piles is a challenging task which requires on the one hand a comprehensive understanding of the soil-structure interaction and the system response and on the other hand careful consideration of the surrounding environment. The present thesis studied the bearing-behaviour of piles under cyclic and dynamic loading in sand. A consistent model for predicting long-term deformations of pile foundations under various cyclic loading scenarios was developed. The following conclusions are drawn from the conducted research:

- Since the ratcheting evolution plays a key role when investigating the pile-bearing behaviour during cyclic and dynamic loading, the ratcheting response of piles subjected to cyclic axial loading was studied experimentally in centrifuge experiments. High cyclic direct simple shear tests supplemented this research to gain further insights on the cyclic soil behaviour in the near field of the pile.
- The successful application of fibre optic strain gauges in cyclic axial centrifuge experiments at 200g on typical offshore piles into water-saturated sand was shown. Within the scope of research of the physical model tests was the impact of the cyclic load ratio and the initial relative density on the ratcheting evolution. The experiments proved the feasibility of the fibre optic strain gauges to detect the axial cyclic pile response, providing additional data to supplement the recorded load-displacement response. Thus, measurements with fibre optic strain gauges can contribute to a comprehensive description of the cyclic axial pile-bearing behaviour and pile-soil interaction, shedding light on the mechanisms involved in the pile response to axial cyclic loading (first research question).
- Comparing the effect of different cyclic load ratios on the axial pile response revealed a qualitatively similar ratcheting evolution in medium dense and loose over dense sand, indicating that partial two-way cyclic loading leads to greater ratcheting than one-way cyclic loading to the same maximum load. Pile capacity increases in compression and is either maintained or increases in tension following cyclic loading in water-saturated sand. Thus, a significantly stiffer post-cyclic response was found compared to the monotonic loading, potentially enhancing the trust in the bearing capacity of cyclic axial loaded piles.
- This thesis examined the validity of Miner's rule in high cyclic direct simple shear experiments on fine silica sand. The tests, which involved 100,000 load cycles at both a constant and varying mean load and amplitude, investigated the effect of ordering of different cycle packages on the cyclic strain accumulation. The experimental results

indicate a significant effect of the ordering of cycle packages on the accumulated volumetric strain. However, reasonable simplifications of irregular natural loads through classification methods are necessary and required in the design process. Thus, and given the soil spatial variability, the application of Miner's rule is considered acceptable when providing an overall conservative design (second research question).

- The data and evaluations reported in this thesis highlight the strong influence of the loading history on the ratcheting reponse. The ratcheting is mainly affected by the maximum load applied to the soil and its previous loading history. In addition, the key role of the peak loads was evident from the irregular cyclic load tests.
- Conclusively, an approach to model the pile response to cyclic and dynamic loading, which is based on the p-y method was presented. In order to accurately model the cyclic and dynamic pile-bearing behaviour, it is essential to appropriately describe the interaction at the interfaces between wave-pile and pile-soil. Such an approach has been developed as part of this work (third research question).
- A foundation model for high cyclic lateral loading and dynamic analysis of monopile-based OWTs was developed successfully. The model follows the subgrade reaction approach and applies the concept of hypoplasticity to reproduce key characteristics of the surrounding soil and includes geometric and material damping. The basic features of the model were described, and its limitations discussed. The performance of the subgrade reaction model was demonstrated for selected load cases and various offshore-related applications and verified against current standards. The verification indicated that the subgrade reaction model can simulate the monopile response with good agreement to current standards, but in addition, it enables for simulating the response of an entire OWT being exposed to hydrodynamic loading with a considerable reduction in computational effort. Hence, the model combines aspects of cyclic and dynamic loading analysis, providing a promising and efficient approach to assess cyclic and dynamic pile-bearing behaviour.

In summary, this thesis presents new knowledge about the cyclic and dynamic pile-bearing behaviour and pile-soil interaction. The research conducted contrasts the response of pile and soil to both hydrodynamic loading and design load cases. A p-y model that combines cyclic deformation accumulation and dynamic analysis of offshore monopiles was presented and developed.

Outlook

This thesis discusses future potentials in offshore wind turbine design practice and provides a promising and efficient approach to assessing the cyclic and dynamic pile-bearing behaviour. However, different research questions remain that relate either directly to the contents of this thesis or address future research in offshore geotechnical engineering:

- The physical model test results shed light on the cyclic axial pile-bearing behaviour and pile-soil interaction and provide a database to inform development and aid validation of numerical models. The results can encourage progress in further research activities on this topic and related areas, e.g. the effect of load amplitude in terms of the drivability of offshore piles.
- Within this thesis, numerical modelling and physical model tests were applied to investigate the cyclic and dynamic soil and pile response. All of these investigations were conducted on a macroscopic scale. Monitoring particle rearrangements during repetitive loading on a microscopic scale, using CT-imaging could provide significantly improved information and further clarify the underlying mechanisms.
- This thesis focuses on monopiles in sand. Likewise, the approach for a single pile can be transferred to pile groups. Incorporating the pile group geometry in the framework of the p-y model is necessary for this. In addition, studying set-up effects can improve the understanding of the long-term bearing behaviour of pile foundations. The developed model formulation is expected to apply to both of these problems.
- Finally, a comprehensive validation of the developed p-y model on field data needs to be performed. Based on this, the model formulation of the soil-structure interaction can be improved to ensure an adequate description of the cyclic and dynamic pile and soil response. If this can be resolved in future investigations, the approach has great potential to contribute to an effective and accurate offshore pile design.

Bibliography

Aasen, S., A. M. Page, K. Skjolden Skau, and T. A. Nygaard (2017). 'Effect of foundation modelling on the fatigue lifetime of a monopile-based offshore wind turbine'. In: *Wind Energy Science* 2.2, pp. 361–376. DOI: 10.5194/wes-2-361-2017.

Abadie, C. N., B. W. Byrne, and S. Levy-Paing (2015). 'Model pile response to multi-amplitude cyclic lateral loading in cohesionless soils'. In: *Frontiers in offshore geotechnics III*. Ed. by V. Meyer, pp. 681–686. DOI: 10.17863/CAM.40861.

Achmus, M., Y.-S. Kuo, and A. Abdel-Rahman (2008). 'Zur Bemessung von Monopiles für zyklische Lasten'. In: *Bauingenieur* 83, pp. 303–311.

Achmus, M., K. Abdel-Rahman, Y.-S. Kuo, and P. Peralta (2007). 'Untersuchungen zum Tragverhalten von Monopilegründungen unter zyklischer Belastung'. In: *Mitteilungen des Instituts für Grundbau und Bodenmechanik, Technische Universität Braunschweig, Pfahl-Symposium*. Vol. 84, pp. 95–114.

American Petroleum Institute (2000). *Recommended Practice for Planning, Designing, and Constructing Fixed Offshore Platforms-Working Stress Design: Upstream Segment. API Recommended Practice 2A-WSD (RP 2A-WSD): Errata and Supplement 1, December 2002*. American Petroleum Institute.

Arshad, M. and B. C. O'Kelly (2017). 'Model studies on monopile behavior under long-term repeated lateral loading'. In: *International Journal of Geomechanics* 17.1. DOI: 10.1061/(ASCE)GM.1943-5622.0000679.

Bauer, E. (1996). 'Calibration of a comprehensive hypoplastic model for granular materials'. In: *Soils and foundations* 36.1, pp. 13–26. DOI: 10.3208/sandf.36.13.

Bayton, S. M., J. A. Black, and R. T. Klinkvort (2018). 'Centrifuge modelling of long term cyclic lateral loading on monopiles'. In: *Physical Modelling in Geotechnics, Volume 1*. CRC Press, pp. 689–694.

Biarez, J. and P. Y. Hicher (1993). *Elementary mechanics of soil behaviour: saturated remoulded soils*. A.A. Balkema, Rotterdam, Brookfield.

Bienen, B., S. Fan, M. Schröder, and M. F. Randolph (2021). 'Effect of the installation process on monopile lateral response'. In: *Proceedings of the Institution of Civil Engineers-Geotechnical Engineering* 174.5, pp. 530–548. DOI: 10.1680/jgeen.20.00219.

Briaud, J. L., T. O. Smith, and B. J. Meyer (1983). 'Using the pressuremeter curve to design laterally loaded piles'. In: *Offshore Technology Conference*. OTC. DOI: 10.4043/4501-MS.

Briaud, J.-L., T. Smith, and B. Meyer (1984). 'Laterally loaded piles and the pressuremeter: comparison of existing methods'. In: *Laterally loaded deep foundations: Analysis and performance*. ASTM International. DOI: 10.1520/STP36815S.

Burd, H. J., W. J. A. P. Beuckelaers, B. W. Byrne, K. G. Gavin, G. T. Houlsby, D. J. P. Igoe, R. J. Jardine, C. M. Martin, R. A. McAdam, A. Muir Wood, D. M. Potts, J. Skov Gretlund, D. M. G. Taborda, and L. Zdravković (2020). 'New data analysis methods for instrumented medium-scale monopile field tests'. In: *Géotechnique* 70.11, pp. 961–969. DOI: 10.1680/jgeot.18.PISA.002.

Byrne, B. W., G. T. Houlsby, H. J. Burd, K. G. Gavin, D. J. P. Igoe, R. J. Jardine, C. M. Martin, R. A. McAdam, D. M. Potts, D. M. G. Taborda, and L. Zdravković (2020). 'PISA design model for monopiles for offshore wind turbines: application to a stiff glacial clay till'. In: *Géotechnique* 70.11, pp. 1030–1047. DOI: 10.1680/jgeot.18.P.255.

Byrne, B. W., R. McAdam, H. Burd, G. T. Houlsby, C. Martin, W. Beuckelaers, L. Zdravković, D. M. G. Taborda, D. Potts, and R. Jardine (2017). 'PISA: new design methods for offshore wind turbine monopiles'. In: *Offshore Site Investigation Geotechnics 8th International Conference Proceedings*. Society for Underwater Technology, pp. 142–161.

Byrne, B. W., R. A. McAdam, H. J. Burd, W. J. A. P. Beuckelaers, K. G. Gavin, G. T. Houlsby, D. J. P. Igoe, R. J. Jardine, C. M. Martin, A. Muir Wood, D. M. Potts, J. Skow Gretlund, D. M. G. Taborda, and L. Zdravković (2020). 'Monotonic laterally loaded pile testing in a stiff glacial clay till at Cowden'. In: *Géotechnique* 70.11, pp. 970–985. DOI: 10.1680/jgeot.18.PISA.003.

Byrne, B. W., R. A. McAdam, H. J. Burd, G. T. Houlsby, C. M. Martin, L. Zdravković, D. M. G. Taborda, D. M. Potts, R. J. Jardine, M. Sideri, F. C. Schroeder, K. Gavin, P. Doherty, D. Igoe, A. Muir Wood, D. Kallehave, and J. Skov Gretlund (2015). 'New design methods for large diameter piles under lateral loading for offshore wind applications'. In: *Frontiers in offshore geotechnics III*, pp. 705–710.

Carstensen, A., T. Pucker, and J. Grabe (2018). 'Numerical model to predict the displacement of piles under cyclic lateral loading using a new hypoplastic spring element'. In: *Computers and Geotechnics* 101, pp. 217–223. DOI: 10.1016/j.compgeo.2018.05.001.

Chow, S., A. Roy, M. Herduin, E. Heins, L. King, B. Bienen, C. O'Loughlin, C. Gaudin, and M. Cassidy (Sept. 2019). *Characterisation of UWA superfine silica sand*. English. DOI: 10.26182/5d8c185bcd366.

Dafalias, Y. F. and M. T. Manzari (2004). 'Simple plasticity sand model accounting for fabric change effects'. In: *Journal of Engineering mechanics* 130.6, pp. 622–634. DOI: 10.1061/(ASCE)0733-9399(2004)130:6(622).

Dafalias, Y. F., A. G. Papadimitriou, and X. S. Li (2004). 'Sand plasticity model accounting for inherent fabric anisotropy'. In: *Journal of Engineering Mechanics* 130.11, pp. 1319–1333. DOI: 10.1061/(ASCE)0733-9399(2004)130:11(1319).

De Nicola, A. and M. F. Randolph (1997). 'The plugging behaviour of driven and jacked piles in sand'. In: *Géotechnique* 47.4, pp. 841–856. DOI: 10.1680/geot.1997.47.4.841.

Det Norske Veritas (2014). 'Design of Offshore Wind Turbine Structures'. In: *Offshore Standard DNV-OS-J101*.

Deutsche Gesellschaft für Geotechnik e.V. (Ed.) (2018). *Empfehlungen des Arbeitskreises "Baugrunddynamik"*. Ernst & Sohn.

Directorate, N. P. (1977). 'Regulations for the structural design of fixed structures on the Norwegian continental shelf'. In: *Norwegian Petroleum Directorate*.

Doherty, P. and K. Gavin (2012). 'Laterally loaded monopile design for offshore wind farms'. In: *Proceedings of the institution of civil engineers-energy* 165.1, pp. 7–17. DOI: 10.1680/ener.11.00003.

Dührkop, J. (2010). *Zum Einfluss von Aufweitungen und zyklischen Lasten auf das Verformungsverhalten lateral beanspruchter Pfähle in Sand*. Dissertation. Veröffentlichungen des Instituts für Geotechnik und Baubetrieb der Technischen Universität Hamburg-Harburg, Heft 20.

Dührkop, J. and J. Grabe (2008). 'Monopilegründungen von Offshore-Windenergieanlagen–Zum Einfluss einer veränderlichen zyklischen Lastangriffsrichtung'. In: *Bautechnik* 85.5, pp. 317–321. DOI: 10.1002/bate.200810024.

Duque, J., M. Yang, W. Fuentes, D. Mašín, and M. Taiebat (2021). 'Characteristic limitations of advanced plasticity and hypoplasticity models for cyclic loading of sands'. In: *Acta Geotechnica*, pp. 1–23. DOI: 10.1007/s11440-021-01418-z.

Fan, S., B. Bienen, and M. F. Randolph (2021). 'Effects of monopile installation on subsequent lateral response in sand. II: Lateral loading'. In: *Journal of Geotechnical and Geoenvironmental Engineering* 147.5. DOI: 10.1061/(ASCE)GT.1943-5606.0002504.

Fleming, K., A. Weltman, M. Randolph, and K. Elson (2008). *Piling engineering*. CRC press.

Fuentes, W. (2014). 'Contributions in mechanical modelling of fill materials'. In: *Schriftenreihe des Institutes für Bodenmechanik und Felsmechanik des Karlsruher Institut für Technologie* 179.

Fuentes, W., T. Wichtmann, M. Gil, and C. Lascarro (2020). 'ISA-Hypoplasticity accounting for cyclic mobility effects for liquefaction analysis'. In: *Acta Geotechnica* 15, pp. 1513–1531. DOI: 10.1007/s11440-019-00846-2.

Gazetas, G. (1991). 'Foundation vibrations'. In: *Foundation engineering handbook*. Springer, pp. 553–593.

Gazetas, G. and R. Dobry (1984). 'Horizontal response of piles in layered soils'. In: *Journal of Geotechnical engineering* 110.1, pp. 20–40. DOI: 10.1061/(ASCE)0733-9410(1984)110:1(20).

Glasenapp, R. (2016). *Das Verhalten von Sand unter zyklischer irregulärer Belastung*. Dissertation. Technische Universität Berlin. DOI: 10.14279/DEPOSITONCE-5402.

Goldscheider, M. and G. Gudehus (1976). 'Einige Bodenmechanische Probleme bei Küsten- und Offshore-Bauwerken'. In: *Vorträge der Baugrundtagung; Deutsche Gesellschaft für Erd-und Grundbau: Nurnberg, Germany*, pp. 507–522.

Hagemann, A. and J. Grabe (2019). 'Schwingungsverhalten einer Offshore-Windenergieanlage unter dynamischer Anregung'. In: *Tagungsband zur Fachsektionstagung Geotechnik 2019 in Würzburg*. Deutsche Gesellschaft für Geotechnik e. V. (Hrsg.), pp. 352–357.

Heins, E. (2018). *Numerical based identification of pile-soil interaction in terms of the axial pile bearing capacity*. Dissertation. Veröffentlichungen des Instituts für Geotechnik und Baubetrieb der Technischen Universität Hamburg-Harburg, Heft 44.

Herle, I. (1997). *Hypoplastizität und granulometrie einfacher korngerüste*. Dissertation. Veröffentlichungen des Instituts für Bodenmechanik und Felsmechanik der Universität Fridericiana in Karlsruhe, Heft 142.

Hettler, A. (1981). *Verschiebung starrer Gründungskörper in Sand bei monotoner und zyklischer Belastung*. Dissertation. Veröffentlichungen des Instituts für Bodenmechanik und Felsmechanik der Universität Fridericiana in Karlsruhe, Heft 9.

Houlsby, G. T., C. N. Abadie, W. J. A. P. Beuckelaers, and B. W. Byrne (2017). 'A model for nonlinear hysteretic and ratcheting behaviour'. In: *International Journal of Solids and Structures* 120, pp. 67–80. DOI: 10.1016/j.ijsolstr.2017.04.031.

Jardine, R., A. Puech, and K. H. Andersen (2012). 'Keynote Address: Cyclic Loading of Offshore Piles: Potential Effects And Practical Design'. In: *Offshore Site Investigation and Geotechnics: Integrated Technologies-Present and Future*.

Jardine, R. J. (2020). 'Geotechnics, energy and climate change: the 56th Rankine Lecture'. In: *Géotechnique* 70.1, pp. 3–59. DOI: 10.1680/jgeot.18.RL.001.

Jeromin, A., B. Boesche, H. Jacobsen, and R. Patz (Nov. 2014). 'Schwingungsmessung auf der Offshore-Forschungsplattform FINO3'. In: *5. VDI-Fachtagung Schwingungen an Windenergieanlagen 2014*. VDI-Berichte 2220. Bremen, Germany: VDI Wissensforum GmbH.

Kallehave, D., C. LeBlanc Thilsted, and M. A. Liingaard (2012). 'Modification of the API py formulation of initial stiffness of sand'. In: *Proceedings of the 7th International Conference on Offshore Site Investigation and Geotechnics*. Royal Geographical Society, pp. 465–472.

Kallehave, D., B. W. Byrne, C. LeBlanc Thilsted, and K. K. Mikkelsen (2015). 'Optimization of monopiles for offshore wind turbines'. In: *Philosophical Transactions of the Royal Society A: Mathematical, Physical and Engineering Sciences* 373.2035. DOI: 10.1098/rsta.2014.0100.

Kallehave, D., C. LeBlanc Thilsted, and A. Troya (2015). 'Observed variations of monopile foundation stiffness'. In: *Frontiers in Offshore Geotechnics III: Proceedings of the 3rd International Symposium on Frontiers in Offshore Geotechnics (ISFOG 2015)*. Vol. 1. Taylor & Francis Books Ltd, pp. 717–722.

Katsikogiannis, G., E. E. Bachynski, and A. M. Page (2019). 'Fatigue sensitivity to foundation modelling in different operational states for the DTU 10MW monopile-based offshore wind turbine'. In: *Journal of Physics: Conference Series*. Vol. 1356. 1. IOP Publishing. DOI: 10.1088/1742-6596/1356/1/012019.

Kelm, M. (2004). *Numerische Simulation der Verdichtung rolliger Böden mittels Vibrationswalzen*. Dissertation. Veröffentlichungen des Instituts für Geotechnik und Baubetrieb der Technischen Universität Hamburg-Harburg, Heft 6.

Kementzetzidis, E., S. Corciulo, W. G. Versteijlen, and F. Pisanò (2019). 'Geotechnical aspects of offshore wind turbine dynamics from 3D non-linear soil-structure simulations'. In: *Soil Dynamics and Earthquake Engineering* 120, pp. 181–199. DOI: 10.1016/j.soildyn.2019.01.037.

Kementzetzidis, E., A. V. Metrikine, W. G. Versteijlen, and F. Pisanò (2021). 'Frequency effects in the dynamic lateral stiffness of monopiles in sand: insight from field tests and 3D FE modelling'. In: *Géotechnique* 71.9, pp. 812–825. DOI: 10.1680/jgeot.19.TI.024.

Klinkvort, R. T. and O. Hededal (2010). 'Centrifuge modelling of offshore monopile foundation'. In: *Frontiers in offshore geotechnics II*, pp. 581–586. DOI: 10.1201/b10132.

Künzel, A. (2016). *Parameteridentifikation auf Basis faseroptisch gemessener quasikontinuierlicher Dehnungssignale*. Dissertation. Technische Universität Berlin. DOI: 10.14279/depositonce-5558.

Le, V. H. (2015). *Zum Verhalten von Sand unter zyklischer Beanspruchung mit Polarisationswechsel im Einfachscherversuch*. Dissertation. Technische Universität Berlin. DOI: 10.14279/depositonce-4896.

Le, V. H., R. Glasenapp, and F. Rackwitz (2022). 'Untersuchungen zur Zellenkonstruktion und Auswertung von monotonen Einfachscherversuchen mit Sand'. In: *geotechnik* 45.4, pp. 224–240.

LeBlanc, C., B. W. Byrne, and G. T. Houlsby (2010). 'Response of stiff piles to random two-way lateral loading'. In: *Géotechnique* 60.9, pp. 715–721. DOI: 10.1680/geot.09.T.011.

LeBlanc, C., G. T. Houlsby, and B. W. Byrne (2010). 'Response of stiff piles in sand to long-term cyclic lateral loading'. In: *Géotechnique* 60.2, pp. 79–90. DOI: 10.1680/geot.7.00196.

Lin, S.-S. and J.-C. Liao (1999). 'Permanent strains of piles in sand due to cyclic lateral loads'. In: *Journal of geotechnical and geoenvironmental engineering* 125.9, pp. 798–802. DOI: 10.1061/(ASCE)1090-0241(1999)125:9(798).

Little, R. L. and J.-L. Briaud (1988). *Full scale cyclic lateral load tests on six single piles in sand*. Tech. rep. Texas A and M Univ College Station Dept of Civil Engineering.

Liu, H., A. Diambra, J. A. Abell, and F. Pisanó (2020). 'Memory-enhanced plasticity modeling of sand behavior under undrained cyclic loading'. In: *Journal of Geotechnical and Geoenvironmental Engineering* 146.11. DOI: 10.1061/(ASCE)GT.1943-5606.0002362.

Liu, H., F. Pisanò, H. P. Jostad, and N. Sivasithamparam (2022). 'Impact of cyclic strain accumulation on the tilting behaviour of monopiles in sand: An assessment of the Miner's rule based on SANISAND-MS 3D FE modelling'. In: *Ocean Engineering* 250. DOI: 10.1016/j.oceaneng.2022.110579.

Liu, H. Y., J. A. Abell, A. Diambra, and F. Pisanò (2019). 'Modelling the cyclic ratcheting of sands through memory-enhanced bounding surface plasticity'. In: *Géotechnique* 69.9, pp. 783–800. DOI: 10.1680/jgeot.17.P.307.

Liu, H. Y. and F. Pisanó (2019). 'Prediction of oedometer terminal densities through a memory-enhanced cyclic model for sand'. In: *Géotechnique Letters* 9.2, pp. 81–88. DOI: 10.1680/jgele.18.00187.

Long, J. H. and L. C. Reese (1984). 'Testing and analysis of two offshore drilled shafts subjected to lateral loads'. In: *Laterally Loaded Deep Foundations: Analysis and Performance*. ASTM International. DOI: 10.1520/STP36823S.

Long, J. H. and G. Vanneste (1994). 'Effects of cyclic lateral loads on piles in sand'. In: *Journal of Geotechnical Engineering* 120.1, pp. 225–244. DOI: 10.1061/(ASCE)0733-9410(1994)120:1(225).

Luo, L., C. D. O'Loughlin, B. Bienen, Y. Wang, M. J. Cassidy, and N. Morgan (2020). 'Effect of the ordering of cyclic loading on the response of suction caissons in sand'. In: *Géotechnique letters* 10.2, pp. 303–310. DOI: 10.1680/jgele.19.00031.

McAdam, R. A., B. W. Byrne, G. T. Houlsby, W. J. A. P. Beuckelaers, H. J. Burd, K. G. Gavin, D. J. P. Igoe, R. J. Jardine, C. M. Martin, A. Muir Wood, D. M. Potts, J. Skov Gretlund, D. M. G. Taborda, and L. Zdravković (2020). 'Monotonic laterally loaded pile testing in a dense marine sand at Dunkirk'. In: *Géotechnique* 70.11, pp. 986–998. DOI: 10.1680/jgeot.18.PISA.004.

Miner, M. A. (1945). 'Cumulative damage in fatigue'. In: *Journal of Applied Mechanics* 12.3, A159–A164. DOI: 10.1115/1.4009458.

Möller, T., T. S. da Silva Burke, X. Xu, G. Della Ragione, E. Bilotta, and C. N. Abadie (2022). 'Distributed fibre optic sensing for sinkhole early warning: experimental study'. In: *Géotechnique* 73.8, pp. 701–715. DOI: 10.1680/jgeot.21.00154.

Newmark, N. M. (1959). 'A method of computation for structural dynamics'. In: *Journal of the engineering mechanics division* 85.3, pp. 67–94. DOI: 10.1061/JMCEA3.0000098.

Nicolai, G. and L. B. Ibsen (2014). 'Small-scale testing of cyclic laterally loaded monopiles in dense saturated sand'. In: *Journal of Ocean and Wind Energy* 1.4, pp. 240–245.

Niemunis, A. and I. Herle (1997). 'Hypoplastic model for cohesionless soils with elastic strain range'. In: *Mechanics of Cohesive-frictional Materials: An International Journal on Experiments, Modelling and Computation of Materials and Structures* 2.4, pp. 279–299. DOI: 10.1002/(SICI)1099-1484(199710)2:4<279::AID-CFM29>3.0.CO;2-8.

Niemunis, A., T. Wichtmann, and T. Triantafyllidis (2005). 'A high-cycle accumulation model for sand'. In: *Computers and geotechnics* 32.4, pp. 245–263. DOI: 10.1016/j.compgeo.2005.03.002.

Page, A. M., G. Grimstad, G. R. Eiksund, and H. P. Jostad (2018). 'A macro-element pile foundation model for integrated analyses of monopile-based offshore wind turbines'. In: *Ocean Engineering* 167, pp. 23–35. DOI: 10.1016/j.oceaneng.2018.08.019.

Peacock, W. H. and H. B. Seed (1968). 'Sand liquefaction under cyclic loading simple shear conditions'. In: *Journal of the Soil Mechanics and Foundations Division* 94.3, pp. 689–708. DOI: 10.1061/JSFEAQ.0001135.

Pörtner, H.-O., D. C. Roberts, V. Masson-Delmotte, P. Zhai, M. Tignor, E. Poloczanska, and N. M. Weyer (2019). 'The ocean and cryosphere in a changing climate'. In: *IPCC Special Report on the Ocean and Cryosphere in a Changing Climate*. DOI: 10.1017/9781009157964.

Prange, B. and G. Huber (1983). 'Oberflächenwellenfelder zur Bestimmung der dynamischen Untergrundparameter'. In: *Symposium Meßtechnik im Erd-und Grund-bau*, pp. 63–69.

Pucker, T., B. Bienen, and S. Henke (2013). 'CPT based prediction of foundation penetration in siliceous sand'. In: *Applied Ocean Research* 41, pp. 9–18. DOI: 10.1016/j.apor.2013.01.005.

Randolph, M. F. (2003). *RATZ-Load transfer analysis of axially loaded piles*. User Manual, University of Western Australia, Perth.

Randolph, M. F. and S. Gourvenec (2011). *Offshore Geotechnical Engineering (1st ed.)* CRC Press. DOI: https://doi.org/10.1201/9781315272474.

Randolph, M. F., R. J. Jewell, K. J. L. Stone, and T. A. Brown (1991). 'Establishing a new centrifuge facility'. In: *Proceedings of International Conference on Centrifuge Modelling*. Vol. 91, pp. 3–9.

Reese, L. C., W. R. Cox, and F. D. Koop (1974). 'Analysis of laterally loaded piles in sand'. In: *Proceedings of the Offshore Technology Conference*. Paper No. OTC 2080. Houston, Texas. DOI: 10.4043/2080-MS.

Reese, L. C. and H. Matlock (1956). 'Non-dimensional solutions for laterally loaded piles with soil modulus assumed proportional to depth'. In: *Proceedings of the 8th Texas Conference on Soil Mechanics and Foundation Engineering*. Austin, Texas, pp. 1–41.

Richards, I. A., B. W. Byrne, and G. T. Houlsby (2020). 'Monopile rotation under complex cyclic lateral loading in sand'. In: *Géotechnique* 70.10, pp. 916–930. DOI: 10.1680/jgeot.18.P.302.

Rudolph, C., J. Grabe, and I. Albrecht (2014). 'Simple shear tests with a varying shearing direction during cyclic shearing'. In: *Géotechnique Letters* 4.2, pp. 102–107. DOI: 10.1680/geolett.13.00088.

Rudolph, C. (2015). *Untersuchungen zur Drift von Pfählen unter zyklischer, lateraler Last aus veränderlicher Richtung*. Dissertation. Veröffentlichungen des Instituts für Geotechnik und Baubetrieb der Technischen Universität Hamburg-Harburg, Heft 32.

Rudolph, C., B. Bienen, and J. Grabe (2014). 'Effect of variation of the loading direction on the displacement accumulation of large-diameter piles under cyclic lateral loading in sand'. In: *Canadian geotechnical journal* 51.10, pp. 1196–1206. DOI: 10.1139/cgj-2013-0438.

Sawicki, A. and W. Swidzinski (1989). 'Mechanics of a sandy subsoil subjected to cyclic loadings'. In: *International Journal for Numerical and Analytical Methods in Geomechanics* 13.5, pp. 511–529. DOI: 10.1002/nag.1610130505.

Schneider, J. and B. Lehane (2006). 'Effects of width for square centrifuge displacement piles in sand'. In: *Effects of width for square centrifuge displacement piles in sand*. Taylor & Francis, pp. 867–873.

Silver, M. L. and H. B. Seed (1971). 'Volume changes in sands during cyclic loading'. In: *Journal of the Soil Mechanics and Foundations Division* 97.9, pp. 1171–1182. DOI: 10.1061/JSFEAQ.0001658.

Sørensen, S. P. H. (2012). *Soil-structure interaction for nonslender, large-diameter offshore monopiles*. PhD thesis. Department of Civil Engineering, Aalborg University, Issue No. 37.

Sørensen, S. P. H., L. B. Ibsen, and A. H. Augustesen (2010). 'Effects of diameter on initial stiffness of py curves for large-diameter piles in sand'. In: *Numerical Methods in Geotechnical Engineering*, pp. 907–912. DOI: 10.1201/b10551-163.

Standard DNV-ST-0126 (2021). *Support structures for wind turbines*. Det Norske Veritas: DNV.

Stark, A., S. Breidenstein, and J. Grabe (2022). 'On the validity of Miner's rule and its application in Offshore pile design practice'. In: *Proceeding of 41th International Conference on Offshore Mechanics and Arctic Engineering (OMAE) 2022 in Hamburg*. Paper No. OMAE2022-81150. American Society of Mechanical Engineers. DOI: https://doi.org/10.1115/OMAE2022-81150.

Stark, A. and J. Grabe (2021). 'Zur bodendynamischen Strukturdämpfung von Offshore-Windenergieanlagen'. In: *Bautechnik* 98.12, pp. 921–929. DOI: 10.1002/bate.202000109.

Stark, A. and J. Grabe (2022). 'Ein Bettungsmodell zur Prognose des Langzeitverhaltens von Monopiles in Sand'. In: *Tagungsband zur Workshop Numerische Methoden in der Geotechnik 2022 in Hamburg, Heft 53*. Veröffentlichungen des Instituts für Geotechnik und Baubetrieb der Technischen Universität Hamburg, pp. 57–75.

Stark, A. and J. Grabe (2023). 'Zur numerischen Modellierung des zyklischen und dynamischen Tragverhaltens von Offshore-Monopfählen'. In: *Tagungsband zum Pfahl-Symposium 2023 in Braunschweig*. Mitteilung des Instituts für Geomechanik und Geotechnik der Technischen Universität Braunschweig, Heft 113, pp. 149–160.

Staubach, P., J. Machaček, M. C. Moscoso, and T. Wichtmann (2020). 'Impact of the installation on the long-term cyclic behaviour of piles in sand: A numerical study'. In: *Soil Dynamics and Earthquake Engineering* 138. DOI: 10.1016/j.soildyn.2020.106223.

Staubach, P. and T. Wichtmann (2020). 'Long-term deformations of monopile foundations for offshore wind turbines studied with a high-cycle accumulation model'. In: *Computers and Geotechnics* 124. DOI: 10.1016/j.compgeo.2020.103553.

Staubach, P., J. Machaček, B. Bienen, and T. Wichtmann (2022). 'Long-term response of piles to cyclic lateral loading following vibratory and impact driving in water-saturated sand'. In: *Journal of Geotechnical and Geoenvironmental Engineering* 148.11. DOI: 10.1061/(ASCE)GT.1943-5606.0002906.

Taborda, D. M. G., L. Zdravković, D. M. Potts, H. J. Burd, B. W. Byrne, K. G. Gavin, G. T. Houlsby, R. J. Jardine, T. Liu, C. M. Martin, and R. A. McAdam (2020). 'Finite-element modelling of laterally loaded piles in a dense marine sand at Dunkirk'. In: *Géotechnique* 70.11, pp. 1014–1029. DOI: 10.1680/jgeot.18.PISA.006.

Tafili, M., J. Duque, M. Ochmański, D. Mašín, and T. Wichtmann (2023). 'Numerical inspection of Miner's rule and drained cyclic preloading effects on fine-grained soils'. In: *Computers and Geotechnics* 156. DOI: 10.1016/j.compgeo.2023.105310.

Taşan, E., F. Rackwitz, and R. Glasenapp (2011). 'Ein Bemessungsmodell für Monopilegründungen unter zyklischen Horizontallasten'. In: *Bautechnik* 88.5, pp. 301–318. DOI: 10.1002/bate.201101463.

Tatsuoka, F., S. Maeda, K. Ochi, and S. Fujii (1986). 'Prediction of cyclic undrained strength of sand subjected to irregular loadings'. In: *Soils and Foundations* 26.2, pp. 73–90. DOI: 10.3208/sandf1972.26.2_73.

Tatsuoka, F., S. Toki, S. Miura, H. Kato, M. Okamoto, S.-i. Yamada, S. Yasuda, and F. Tanizawa (1986). 'Some factors affecting cyclic undrained triaxial strength of sand'. In: *Soils and foundations* 26.3, pp. 99–116. DOI: 10.3208/sandf1972.26.3_99.

Taylor, R. N. (2018). 'Centrifuges in modelling: principles and scale effects'. In: *Geotechnical centrifuge technology*. CRC Press, pp. 19–33. DOI: 10.1201/9781482269321.

Tran, M. N. and M. F. Randolph (2008). 'Variation of suction pressure during caisson installation in sand'. In: *Géotechnique* 58.1, pp. 1–11. DOI: 10.1680/geot.2008.58.1.1.

Triantafyllidis, T. and S. Chrisopoulos (2016). 'Ein Modell zur Berechnung des Verformungsverhaltens von horizontal hochzyklisch beanspruchten Pfählen'. In: *Bautechnik* 93.9, pp. 605–627. DOI: 10.1002/bate.201600036.

Truong, P., B. M. Lehane, V. Zania, and R. T. Klinkvort (2019). 'Empirical approach based on centrifuge testing for cyclic deformations of laterally loaded piles in sand'. In: *Géotechnique* 69.2, pp. 133–145. DOI: 10.1680/jgeot.17.P.203.

Von Wolffersdorff, P.-A. (1996). 'A hypoplastic relation for granular materials with a predefined limit state surface'. In: *Mechanics of Cohesive-frictional Materials: An International Journal on Experiments, Modelling and Computation of Materials and Struc-*

tures 1.3, pp. 251–271. DOI: 10.1002/(SICI)1099-1484(199607)1:3<251::AID-CFM13>3.0.CO;2-3.

Wichtmann, T. (2005). *Explicit accumulation model for non-cohesive soils under cyclic loading*. Dissertation. Publications of the Institute of Soil Mechanics and Foundation Engineering, Ruhr-University Bochum, Issue No. 38.

Wichtmann, T., W. Fuentes, and T. Triantafyllidis (2019). 'Inspection of three sophisticated constitutive models based on monotonic and cyclic tests on fine sand: Hypoplasticity vs. Sanisand vs. ISA'. In: *Soil Dynamics and Earthquake Engineering* 124, pp. 172–183. DOI: 10.1016/j.soildyn.2019.05.001.

Wichtmann, T., A. Niemunis, and T. Triantafyllidis (2010). 'Strain accumulation in sand due to drained cyclic loading: on the effect of monotonic and cyclic preloading (Miner's rule)'. In: *Soil Dynamics and Earthquake Engineering* 30.8, pp. 736–745. DOI: 10.1016/j.soildyn.2010.03.004.

Wichtmann, T. and T. Triantafyllidis (2017). 'Strain accumulation due to packages of cycles with varying amplitude and/or average stress–On the bundling of cycles and the loss of the cyclic preloading memory'. In: *Soil Dynamics and Earthquake Engineering* 101, pp. 250–263. DOI: 10.1016/j.soildyn.2017.07.012.

Wichtmann, T. (2016). *Soil behaviour under cyclic loading-experimental observations, constitutive description and applications*. Habilitation.

Wichtmann, T., A. Niemunis, and T. Triantafyllidis (2006). 'Gilt die Minersche Regel für Sand?' In: *Bautechnik* 83.5, pp. 341–350. DOI: 10.1002/bate.200610029.

Wichtmann, T., T. Sonntag, and T. Triantafyllidis (2001). 'Über das Erinnerungsvermögen von Sand unter zyklischer Belastung'. In: *Bautechnik* 78.12, pp. 852–865. DOI: 10.1002/bate.200105950.

Winkler, E. (1867). *Die Lehre von der Elasticitaet und Festigkeit: mit besonderer Rücksicht auf ihre Anwendung in der Technik, für polytechnische Schulen, Bauakademien, Ingenieure, Maschinenbauer, Architecten, etc.* H. Dominicus.

Yoshimi, Y. and H. Oh-oka (1975). 'Influence of degree of shear stress reversal on the liquefaction potential of saturated sand'. In: *Soils and foundations* 15.3, pp. 27–40. DOI: 10.3208/sandf1972.15.3_27.

Youd, T. L. (1972). 'Compaction of sands by repeated shear straining'. In: *Journal of the Soil Mechanics and Foundations Division* 98.7, pp. 709–725. DOI: 10.1061/JSFEAQ.0001762.

Zachert, H. and T. Wichtmann (2020). 'Approaches for the Design of Foundations for Offshore Wind Turbines: A Review Based on Comparisons with HCA-Based Models'. In: *Recent developments of soil mechanics and geotechnics in theory and practice*, pp. 113–135. DOI: 10.1007/978-3-030-28516-6_7.

Zdravković, L., R. J. Jardine, D. M. G. Taborda, D. Abadias, H. J. Burd, B. W. Byrne, K. G. Gavin, G. T. Houlsby, D. J. P. Igoe, T. Liu, C. M. Martin, R. A. McAdam, A. Muir Wood, D. M. Potts, J. Skov Gretlund, and E. Ushev (2020). 'Ground characterisation for PISA

pile testing and analysis'. In: *Géotechnique* 70.11, pp. 945–960. DOI: 10.1680/jgeot.18.PISA.001.

Zdravković, L., D. M. G. Taborda, D. M. Potts, D. Abadias, H. J. Burd, B. W. Byrne, K. G. Gavin, G. T. Houlsby, R. J. Jardine, C. M. Martin, R. A. McAdam, and E. Ushev (2020). 'Finite-element modelling of laterally loaded piles in a stiff glacial clay till at Cowden'. In: *Géotechnique* 70.11, pp. 999–1013. DOI: 10.1680/jgeot.18.PISA.005.

A Laboratory test results on very fine silica sand

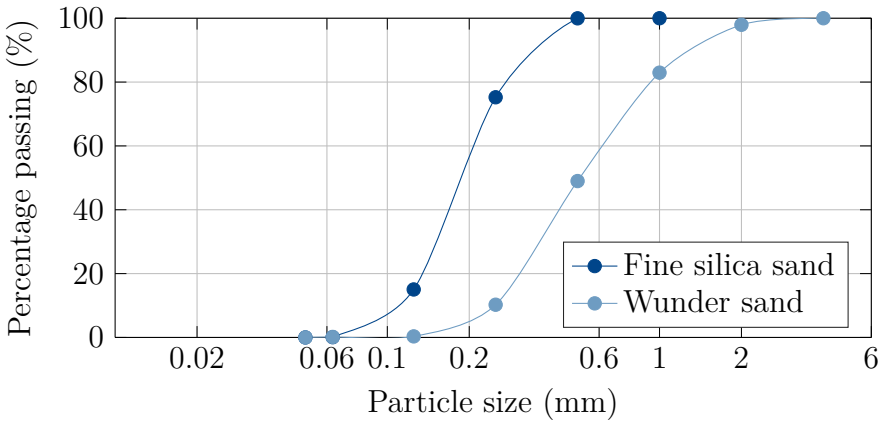

Figure A.1: Particle size distribution fine silica sand and wunder sand.

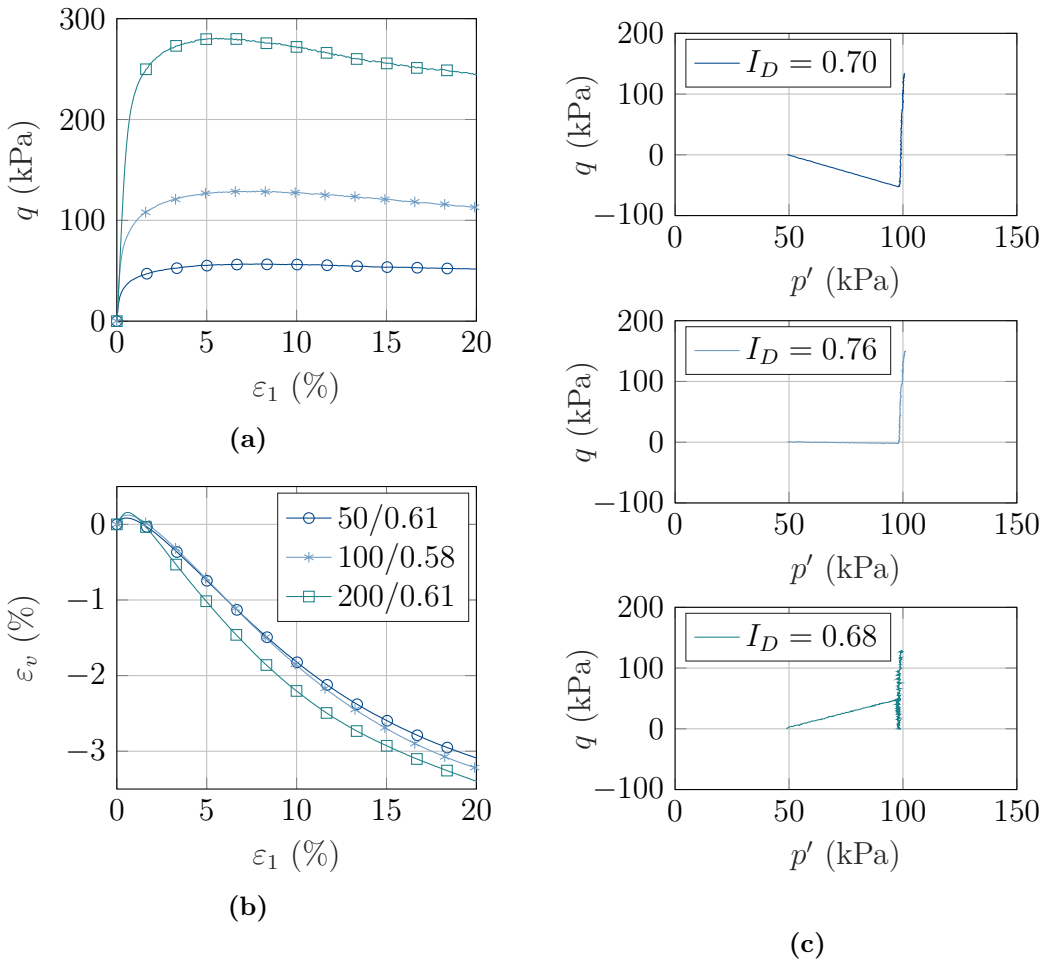

Figure A.2: Results of triaxial tests for very fine silica sand on a medium dense sample with three different reference pressures: a) stress-strain behaviour, b) course of volumetric strain. c) Results of stress path controlled triaxial tests on very fine silica sand.

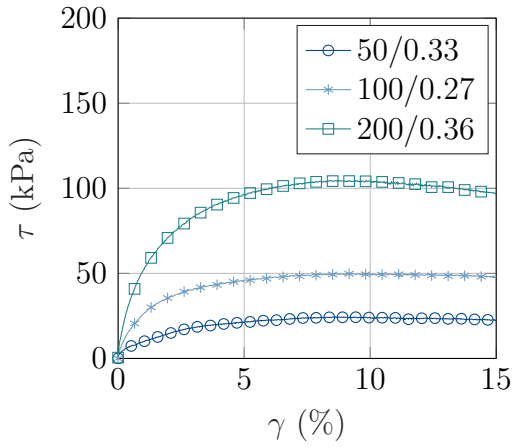

(a)

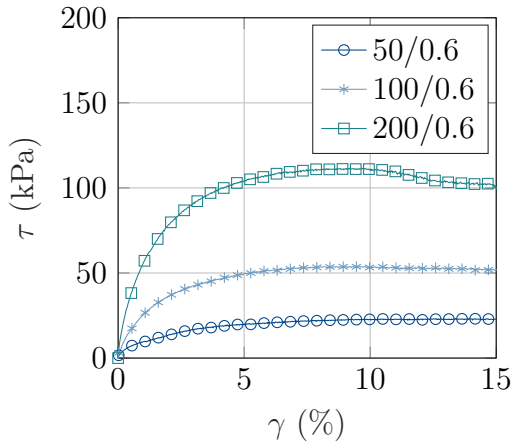

(b)

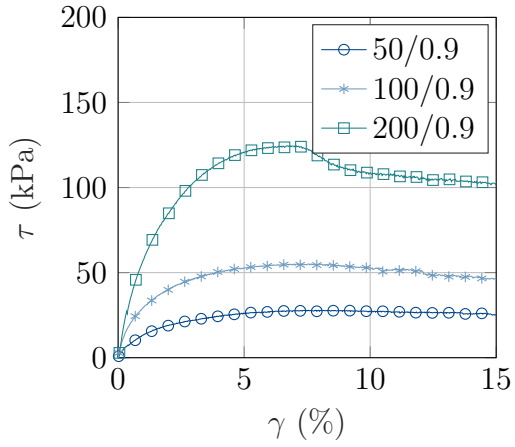

(c)

Figure A.3: Results of monotonic direct simple shear tests for very fine silica sand with three different axial stresses and initial relative densities: a) loose, b) medium dense and c) dense sand.

B Material parameters

Table B.1: Hypoplastic material parameters for Wunder sand taken from (Carstensen et al., 2018)

Parameter	Value	Description (Unit)
φ_c	31.5	critical state friction angle (°)
h_s	10^7	granular hardness (MPa)
n	0.25	exponent
e_{d0}	0.45	minimum void ratio at $p' = 0$
e_{c0}	0.7	critical void ratio at $p' = 0$
e_{i0}	0.84	maximum void ratio at $p' = 0$
a	0.16	empirical factor
b	0.5	exponent
d	3	exponent
φ_{ref}	34.5	reference friction angle (°)
e_{ref}	0.46	reference void ratio
γ'	11.0	submerged unit weight (N/m^3)